Politecnico di Torino

FACOLTÀ DI INGEGNERIA

Corso di Laurea in Ingegneria matematica


Tesi di laurea magistrale

# A continuum mechanical model to predict the growth of Glioblastoma Multiforme and the deformation of white matter tracts


Candidato:

**Francesca Ballatore**

**Matricola s276097**

Relatore:

**Prof.ssa Chiara Giverso**

Correlatori:

**Prof. Andrea Borio**

**Giulio Lucci**



**Anno Accademico 2020-2021**

# Acknowledgements

Ho deciso di dedicare questo spazio a chi, con dedizione e pazienza, ha contribuito alla realizzazione dell'elaborato.

In primo luogo vorrei ringraziare la mia relatrice, la Professoressa Chiara Giverso, per l'attenta presenza e l'aiuto costante durante tutti questi mesi. Ringrazio inoltre il Professor Andrea Borio e Giulio Lucci per il loro supporto e il loro contributo alla realizzazione di tale lavoro.

Un grazie particolare va ai miei genitori Antonio e Stefania, per essermi sempre stati accanto e non avermi mai fatto mancare il loro sostegno in questi anni, a mia sorella Anna, per essere stata presente in ogni scelta importante e aver vissuto con me questi mesi di lockdown, che senza di lei sarebbero stati insopportabili, a nonna Maria e nonna Carla, per il loro amore e il loro appoggio.

Grazie a Gianluca, per aver condiviso ogni giorno con me gioie, sacrifici e successi e per avermi donato nuove prospettive, standomi accanto durante le interminabili giornate di studio e spronandomi in ogni momento a non abbattermi e a superare i miei limiti.

Un ringraziamento speciale va ai miei amici, i quali mi hanno dato tutta la forza necessaria per affrontare gli ostacoli che ho incontrato in questo cammino, avendo così un peso determinante nel conseguimento di questo risultato. In particolar modo vorrei ringraziare Benedetta, da sempre la mia persona, che non mi lascia mai sola in ogni istante della mia vita, consigliandomi nei momenti più difficili e brindando con me ai traguardi più importanti, Diletta e Giulia, coinquiline per pochi mesi o per anni, che mi hanno accompagnato in ogni passo di questo percorso, non smettendo mai di incoraggiandomi, ed infine Giorgia e Serena, che nonostante i tanti chilometri che spesso ci separano, ci sono sempre e mi fanno sentire in ogni istante la loro vicinanza.

Dedico questo traguardo anche ai miei compagni di corso, le persone con cui ho condiviso attimi di gioia e di tristezza, con il rammarico di non aver potuto concludere insieme gli ultimi semestri del nostro percorso.

Ed infine ci tengo a ringraziare il Politecnico di Torino, mia seconda casa in questi cinque anni, per avermi fatto capire cosa significa impegnarsi per ottenere un risultato ed aver contribuito a farmi diventare la donna che sono adesso.

# Contents

# List of Figures

# List of Tables

# Abstract

Glioblastoma Multiforme (GBM) is one of the most malignant types of brain cancer and it exhibits a strong resistance to common therapies. Therefore, it is crucial to investigate its progression, in order to acquire more details about its anisotropic nature, which follows the orientation of surrounding white matter tracts. Mathematical models of cerebral tumour growth can help in understanding the physiology and the progression of this disease, for the purpose of predicting the evolution of tumour shape and volume and quantifying its aggressiveness.

The aim of the present work is to reproduce the evolution of this highly malignant brain tumour evaluating its mechanical impact on the surrounding healthy tissue. A mathematical multiphase model for GBM, based on Continuum Mechanics, is developed, where both the healthy and the diseased regions are treated as a saturated biphasic mixture, comprising a solid and a fluid phase. Moreover, it is considered the region occupied by the tumour as separated from the host tissue by a sharp moving interface. The cell phase is supposed to behave as a Mooney-Rivlin hyperelastic solid, with different material parameters between the healthy and the diseased zone. Instead, the liquid phase is considered constitutively as an ideal fluid. With the aim to describe the mechanical effect of tumour growth onto tissue deformation, theory for materials with evolving natural configurations and the multiplicative decomposition of the deformation gradient tensor are employed. For what concerns the growth tensor, which appears in this decomposition, we focus on its anisotropic evolution, in order to enforce the different cases of monodirectional, planar and spherical growth. Furthermore, it is necessary to introduce in the model an equation describing the evolution of nutrients in the domain, since their amount affects the cells capability to duplicate. The preferential directions for nutrient diffusion and cancer cell motion and growth are obtained, at the initial time step, through DTI imaging. Then, in order to take into account the modification of the preferred directions according to the brain tissue deformation, a push-forward of the corresponding Lagrangian tensor is performed.

After having set the mechanical model for Glioblastoma growth, we solve it through numerical simulations. For this purpose, the Lagrangian formulation is derived from the Eulerian model. Later, a weak formulation of the Lagrangian model is obtained in order to numerically solve the model using FEniCS, a Python-based PDE finite element solver. At the beginning, the code is tested on a simplified geometry in order to verify its stability and effectiveness. Afterwards, the numerical simulations on the real three-dimensional brain geometry are performed, using available data from MRI and DTI to build the computational domain and account for patient-specific anisotropy. From a numerical point of view, the obtained algorithm is stable and it allows to represent discontinuous deformation

gradients, through the use of a mesh conforming to the material host-tumour interface. On the other hand, from a modelling point of view, with respect to available models in the literature, the anisotropy has also been included in tumour growth and the model is able to describe how the brain tracts are modified due to the tumour mass expansion.

# Chapter 1

# Biological background

In this chapter, a biological background of the problem at hand is provided. For this reason, in the first section the most important features of cancer and carcinogenesis are described. After this introduction, we focus on brain tumours and in particular on Glioblastoma Multiforme, which is the main subject of our study.

## 1.1 Cancer Basics

### 1.1.1 Cancer classification

Cancer remains the number two cause of death in the world, second only to heart disease. It describes an enormous spectrum of diseases, which all originate from uncontrolled cellular growth. Commonly divided into benign tumours (unable to metastasize) or malignant tumours (able to invade normal tissues), cancers are further defined and classified by their cell type, tissue or organ of origin. Following this last partition, four main types of cancer to mention are [**1**]:

- *Carcinomas.* A carcinoma originates in the skin or the tissue that covers the surface of internal organs and glands. Carcinomas are the most common type of cancer and they usually form solid tumours.
- *Sarcomas.* A sarcoma originates in the tissues that support and connect the body. A sarcoma can develop in fat, muscles, nerves, tendons, joints, blood vessels, lymph vessels, cartilage or bone.
- *Leukemias.* Leukemia is a cancer of the blood. Leukemia begins when healthy blood cells change and grow uncontrollably.
- *Lymphomas.* Lymphoma is a cancer that begins in the lymphatic system, i.e. a network of vessels and glands that help fight infection.

### 1.1.2 Cancer biology

It is important now to understand which is the process leading to tumour formation.
Cells are the basic units that make up the human body. Cells grow and divide to make new cells as the body needs them. Usually, cells die when they get too old or damaged. After this organic process, new cells take their place [**1**].

Tumour development begins when some cell within a normal population sustains a genetic mutation that increases its propensy to proliferate, especially when it would normally rest. The altered cell and its descendand continue to appear normal, but they reproduce so quickly. This condition is called *hyperplasia*. After years, one in a million of these cells suffers another mutation and so it further loosens control on cell growth. In this new phase, the offspring of this cell appear abnormal in shape and in orientation. The tissue is now said to exhibit *dysplasia*. The affected cells become increasingly abnormal in growth and appearance. If the tumour has not yet broken through any boundaries between tissues, it is called *in situ cancer*. This tumour may remain contained indefinitely [**2**].

Although not all solid tumours share the same features, two common macro-stages are usually identified [**2**, **3**]: an avascular and a vascular phase. During the former, which has been described above, the tumour remains localized with dimensions of a few millimeters in diameter and it can only receive nutrients by diffusion. At this stage, tumours form three-dimensional avascular nodules called *multicell spheroids*, in which an external layer of proliferating cells surrounds a region composed of quiescent cells. Meanwhile, cells located at the centre of the spheroid begin to die and progressively form a necrotic core, because they are deprived of vital nutrients and oxygen. During the avascular phase, tumour cells have not yet spread to other tissues.

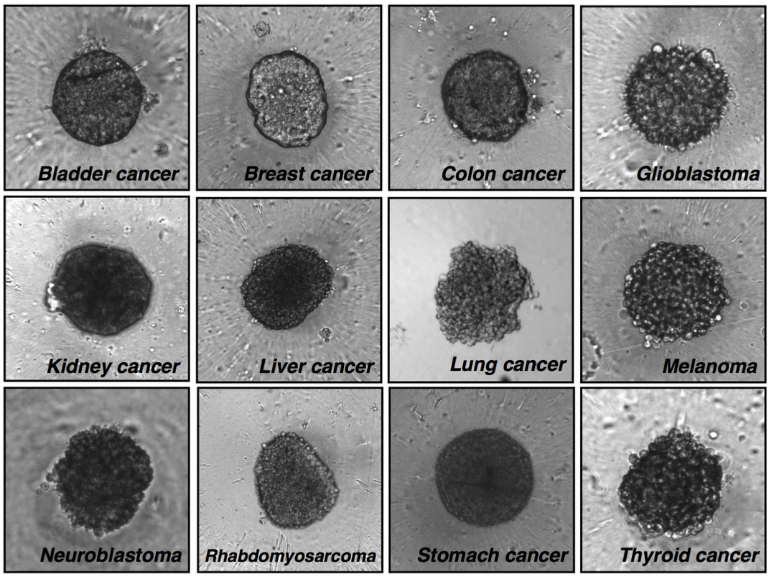


Figure 1.1: Different type of spheroids [**4**]

The vascular phase starts when cancer cells begin to spread from the place where they originally formed to other parts of the body. At first, the neoplasm starts to break the healthy host tissue and to drive angiogenesis. Angiogenesis is the formation of new blood vessels from existing capillaries and it is normally a physiological mechanism because oxygen and nutrients are crucial for cell function and survival. However, angiogenesis becomes a pathological phenomenon when exploited by a growing tumoural mass suffering from hypoxia, i.e. a lack of oxygen. In this way the tumour induces new blood vessels from the surrounding tissue to sprout towards itself, with the aim to provide itself an adequate nutrient supply. Going into detail, tumour cell hypoxia triggers the secretion by tumour cells of a number of chemicals, collectively called Tumour Angiogenic Factors (TAFs), among which the Vascular Endothelial Growth Factor (VEGF) plays a fundamental role. TAFs diffuse through the surrounding tissue until they reach the nearby vasculature. In response to these stimuli, nearby endothelial cells (EC) of blood vessels proliferate and migrate following the chemical gradient towards the tumour. Later, angioproteins promote the migration of muscle cells that form the intermediate layer around the new endothelial one, leading to the complete formation of a new vessel. The process continues with the formation of additional sprouts and loops until the development of a new vascular network which penetrates the tumour, providing it a supply of oxygen and nutrients [**5**].

One of the most relevant and simultaneously most dangerous consequences of tumour vascularization is the occurrence of *metastases*, i.e. secondary tumours arising from the primary mass at distant locations. Once it has become malignant, cancer spreads out and invades other tissues exploiting the vasculature. One of the first places a cancer often spreads is to the lymph nodes. Lymph nodes are tiny and bean-shaped organs that help fight infection. They are located in clusters in different parts of the body, such as the neck and groin area. Cancer may also spread through the bloodstream to distant parts of the body. These parts may include the bones, liver, lungs or brain. Even if the cancer spreads, it is still named for the area where it began [**1**].
To sum up, metastatic progression of solid tumours can be divided into five major steps [**6**]:

1. invasion of the basement membrane and cell migration;
2. intravasation into the surrounding vasculature or lymphatic system;
3. survival in the circulation;
4. extravasation from vasculature to secondary tissue;
5. colonization at secondary tumour sites

Each stage of metastasis imposes harsh conditions and energetically taxing challenges for the cancer cells to complete.

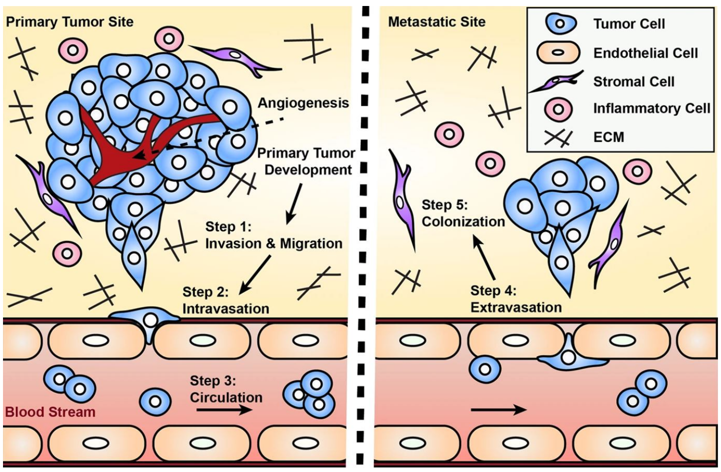


Figure 1.2: Metastatic progression of solid tumours [**6**]

Metastatic cancer is a signal that the malignant tumour has become invasive: as a consequence, its complete removal or cure becomes harder.

### 1.1.3 Hallmarks of cancer

The hallmarks of cancer comprise six biological capabilities acquired during the multistep development of human tumours. The idea was coined by Douglas Hanahan and Robert Weinberg in their paper *The Hallmarks of Cancer* [**7**]. They continue to provide a solid foundation for understanding the biology of cancer. It is suggested that the vast catalog of cancer cell genotypes is a manifestation of six essential alterations in cell physiology that collectively dictate malignant growth:

- *Self-sufficiency in growth signals.* Typically, cells of the body require hormones and other molecules that act as signals for them to grow and divide. Instead, cancer cells have the ability to grow without these external signals. There are multiple ways in which cancer cells can do this: by producing these signals themselves (this is known as autocrine signalling), by permanently activating the signalling pathways that respond to these signals or by destroying 'off switches' that prevents excessive growth from these signals (negative feedback).

- *Insensitivity to anti-growth signals.* Within a normal tissue, growth-inhibitory signals act to maintain cellular quiescence and homeostasis. These processes are orchestrated by proteins known as tumour suppressor genes. However, cancerous cells develop the ability to circumvent such signals. As a consequence they continue to grow and divide, regardless of their surroundings.

- *Evasion of programmed cell death.* Cells have the ability to 'self-destruct', a process also known as apoptosis. This is required for organisms to grow and develop properly and for maintaining tissues of the body. It is also initiated when a cell is damaged or infected. Cancer cells, however, lose this ability. In fact, even though cells may become grossly abnormal, they do not undergo apoptosis.

- *Limitless replicative potential.* Cells of the body have not the ability to divide indefinitely. They have indeed a limited number of divisions before the cells become unable to divide (senescence) or die (crisis). Cancer cells escape this limit and are apparently capable of indefinite growth and division. However, those immortal cells have damaged chromosomes, which can become cancerous.

- *Sustained angiogenesis.* Normal tissues of the body have blood vessel going through them in order to provide oxygen from the lungs. Cells should be near these vessels to get sufficient oxygen for them to survive. An extending tumour requires new blood vessels to deliver adequate oxygen to its cells and subsequently takes advantage of this typical physiological process for its advantage.

- *Tissue invasion and metastasis.* The ability to create distant settlements and invade other tissues is a peculiarity of a malignant tumour, as mentioned before.

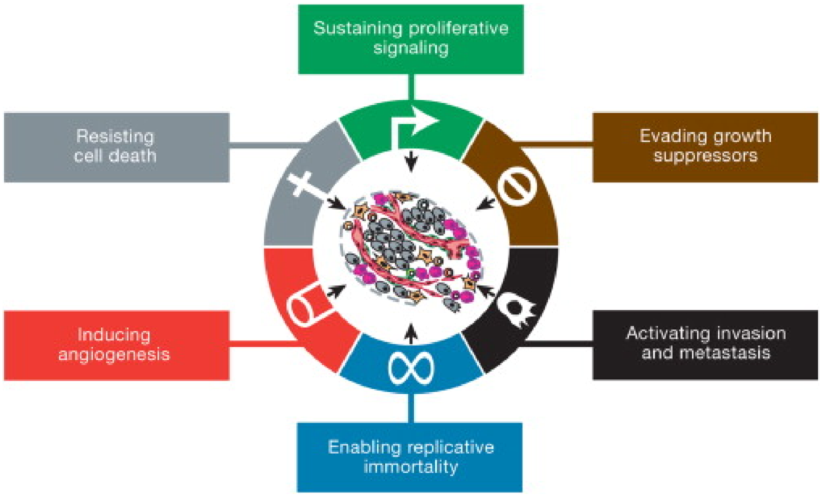


Figure 1.3: Hallmarks of cancer [7]

In 2011, two additional hallmarks have been identified [8]:

- *Reprogramming of energy metabolism.* Most cancer cells use alternative metabolic pathways to generate energy. In fact they modify their metabolism in order to sustain uncontrolled proliferation.

- *Ability of evading immune destruction.* Despite cancer cells cause increased inflammation and angiogenesis, they also appear to be able to avoid interaction with the body's immune system.

## 1.2 Brain Tumours and Glioblastoma Multiforme

### 1.2.1 Brain anatomy and functions

The human brain is the most complex organ in the human body. It is made up of billions of neurons and it also has a number of specialized parts that are involved in important functions. Understanding the anatomy and the composition of the brain can help give a better idea of how disease and damage may affect its ability to function.
The brain is made up of many specialized areas that work together [9]:

- The *cortex* is the outermost layer of the brain. Thinking and voluntary movements start in the cortex.

- The *brain stem* is between the spinal cord and the rest of the brain. Basic functions like breathing and sleep are controlled here.

- The *basal ganglia* are a cluster of structures in the center of the brain. The basal ganglia coordinate messages between other brain areas.

- The *cerebellum* is at the base and the back of the brain. The cerebellum is responsible for coordination and balance.

The brain is also divided into several lobes:

- The *frontal lobes* are responsible for problem solving and judgment and motor function.

- The *parietal lobes* manage sensation, handwriting and body position.
- The *temporal lobes* are involved with memory and hearing.
- The *occipital lobes* contain the brain's visual processing system.

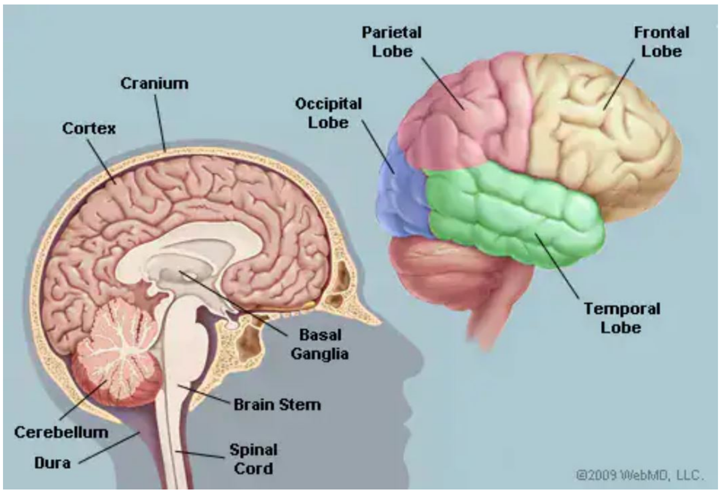


Figure 1.4: Different parts of the brain [**9**]

To look instead at the smaller components that make up the human brain, they are called *neurons*. The neuron is one of two basic types of cells in the nervous system. The other type is the *neuroglial cell* [**10**].
Neurons are electrically excitable cells that are the main functional units of the nervous system. Their function is to transmit nerve impulses. Most neurons consist of a soma, which corresponds to the cell body and contains the nucleus, and many dendrites branching from the soma. The dendrites receive and transmit information to and from other neurons through the synapses. The information read out at the origin of the axon, the portion of the nerve cell specialized for signal conduction to the next site of synaptic interaction. It is a long and slender tube which carries the action potential, a brief electrochemical impulse that permits communication between nerve cells.

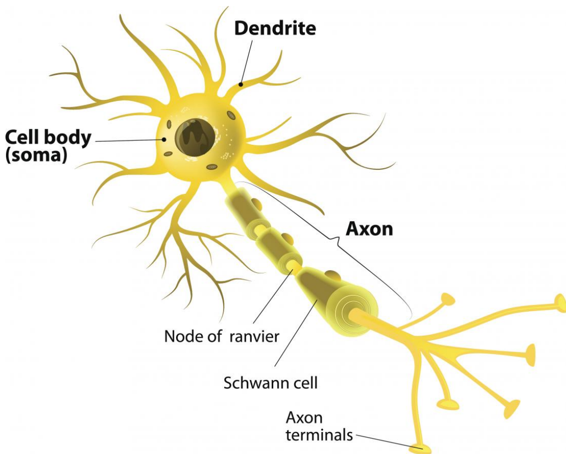


Figure 1.5: The structure of a typical neuron [**10**]

In addition to neurons, nervous tissues also consist of neuroglia, also called glial cells. There are several different types of neuroglia, each with a different function. In general, neuroglia provide support for neurons and help them carry out the basic function of nervous tissues, which is to transmit nerve impulses. There are several types of glial cells: the most important ones in the central nervous system are astrocytes, oligodendrocytes, microglia and ependymal cells. *Astrocytes* are star-shaped cells which provide physical support and nourishment to neurons. They also control the chemical composition of the fluid surrounding the neurons by taking up or releasing substances whose concentration must be kept within critical levels.
The principal function of *oligodendrocytes* is to provide support to axons and to produce the myelin sheath, which surrounds and insulates axons from one another. *Microglia cells* act as cleaners of the nervous system, removing dead and dying neurons. They protect the brain from invading micro-organisms and they are also responsible for the inflammatory reaction in response to brain damage.
Finally, *ependymal cells* take part in the production of the cerebrospinal fluid and promote its circulation.

### 1.2.2 Types of brain tumours

A brain tumour occurs when abnormal cells form within the brain. The brain and nervous system tumours constitute about 1.6% of all new cases of cancer diagnosed every year. They also cause 2% of all deaths from cancer [**11**].
A first classification splits them into two major groups: primary and secondary tumours [**12**]:

- *Primary brain cancer* refers to malignant tumours that form either in the brain or in the nerves originating in the brain. Brain cancer does not frequently metastasize to outside of the central nervous system (CNS).
- *Secondary brain cancer* refers to malignant tumours that originated elsewhere but have spread to the brain. Secondary brain cancer is more common than primary brain cancer.

There are over 100 types of cancer that can affect the central nervous system (CNS). It is necessary to remember that cancers that arise in other locations (breast, lung, etc.) and spread to the brain are still treated as the cancers of the original site. So it becomes important to discuss primary brain cancers and their classification [**13**]:

- *Gliomas*: they are the most common and deadly brain cancers. They originate in the glial cells of the central nervous system (CNS). Gliomas can be divided into 3 main categories:
  - *Astrocytomas*: they develop in astrocytes and are found in the cerebrum and the cerebellum. Astrocytomas make up approximately 50% of all primary brain tumours. It is significant to stress that Glioblastoma multiforme is an astryocytoma subtype.
  - *Oligodendrogliomas*: they are tumours that develop in oligodendrocytes, i.e. glial cells that produce myelin, a component of the brain that increases impulse speed.

- *Ependymomas*: they are tumours that develop in the ependymal cells, i.e. the cells in the brain where ceribrospinal fluid (CSF) is created and stored. Ependymoma tumours are usually found in ventricle linings, the spinal cord or the regions near the cerebellum.

- *Nongliomas*: they are tumours that do not arise from glial cells. More prevalent examples of nongliomas are:
  - *Meningiomas*: they are tumours that develop in the meninges, membranes covering the brain and spinal cord. Meningioma tumours are frequently formed from arachnoid cells. These cells are responsible for the absorption of the cerebrospinal fluid (CSF). Most meningiomas are benign as malignant meningiomas are extremely rare.
  - *Medulloblastomas*: they arise in the posterior fossa, i.e. a specific region of the space inside the intracranial cavity that contains the brainstem and the cerebellum.

Furthermore, WHO (World Health Organization) classify gliomas also by their behaviour and malignity [**14**]:

- *Grade I*: circumscribed tumours with low proliferative potential, biologically benign and often curable through surgical resection alone;
- *Grade II*: low-grade malignancies that may follow long clinical courses, but the early diffuse infiltration of the surrounding brain makes them incurable by only surgery;
- *Grade III*: tumours that are malignant and present abnormal cells. They are very likely to spread into nearby tissues and tend to come back;
- *Grade IV*: the most malignant tumours, they spread very quickly and show both pathological angiogenesis and necrosis. They are invasive and resistant to common therapies.

### 1.2.3 Glioblastoma Multiforme

Glioblastoma Multiforme (GBM), also referred to as a grade IV astrocytoma, is a fast-growing and aggressive brain tumour. It invades the nearby brain tissue but generally does not spread to distant organs. Glioblastoma Multiforme accounts for 47.7% of all malignant brain tumours [**15**]. Glioblastoma has an incidence of 3.21 per 100 000 population. Median age of diagnosis is 64 years and it is more common in men as compared to women. Survival is poor with approximately 40% survival in the first year post diagnosis and 17% in the second year. In fact, GBM can result in death in less than six months, if untreated.
In adults, GBM occurs most frequently within the cerebral hemispheres, especially in the frontal and temporal lobes of the brain. It presents unique treatment challenges due to:

- Localization of tumours in the brain
- Inherent resistance to conventional therapy
- Limited capacity of the brain to repair itself

- Migration of malignant cells into adjacent brain tissue
- The variably disrupted tumour blood supply, which inhibits effective drug delivery
- Tumour capillary leakage, resulting in an accumulation of fluid around the tumour and intracranial hypertension
- Tumour-induced seizures
- The resultant neurotoxicity of treatments directed at gliomas

The first recorded reports of this malignant glioma were given in British scientific reports, by Berns in 1800 and by Abernety in 1804 [**16**]. After, the first comprehensive histomorphological description was given in 1865 by Rudolf Virchow. For many years it was known as *spongioblastoma multiforme*, until Bailey and Cushing in 1926 proposed the name Glioblastoma Multiforme. Between 1934 and 1941 the most prolific researcher in glioma research was Hans-Joachim Scherer, who postulated some of the clinico-morphological aspects of GBM. Only with the introduction of molecular and genetic tests the true multifomity of GBM has been established, as it shows different genotypes bearing the same histomorphological and it may appear very different from an individual to another.

As far as treatment care, brain tumours and GBM in particular are extremely resistant to therapies. The standard of treatment for a GBM is neurosurgery. However, complete removal is almost impossible because of infiltration, so this type of cancer is very likely to appear again. The surgery is followed by daily radiation and oral chemotherapy for six and a half weeks, then a six-month regimen of oral chemotherapy given five days a month. Even with this complete treatment, almost all patients experience tumour progression with nearly universal mortality and a median survival of less than 16 months.

## 1.3 Imaging techniques used in brain tumour detection

In this section, a description of the characteristics of the main imaging techniques used in brain tumour detection, namely Magnetic Resonance Imaging (MRI) and Diffusion Tensor Imaging (DTI), is presented. Medical images obtained through these techniques are employed to provide a computational reconstruction of the brain, helping to build a realistic geometry and to account for anisotropy of the brain environment. A more detailed description of imaging physics is reported in [**17**, **18**].
Magnetic Resonance Imaging (MRI) is a non-invasive imaging technology that produces three dimensional detailed anatomical images. It is often used for disease detection, diagnosis and treatment monitoring. It works through the detection of magnetic dipoles in the atomic nuclei of the organism. More specifically, protons placed into a static magnetic field $\mathbf{B}$ behave like spinning magnets and tend to align to this field in spite of their thermal motion. However, since protons possess an intrinsic magnetic dipole moment due to their spin, the combination of the external field with the spin results in a precession around the direction of $\mathbf{B}$, increasing the magnetization $\mathbf{M}$ of the tissue which, under normal conditions, will be a vector aligned with the external magnetic field. The magnetization is said to

be fully longitudinal, i.e. directed as the magnetic field, while the transverse magnetization, i.e. the one in the direction orthogonal to the magnetic field, is null. However, if an electromagnetic radiation with a specific frequency is directed to the tissue irradiated by the magnetic field, some protons can absorb energy thanks to the resonance phenomenon and rotate their spin of 90 degrees. In this way, the protons come into phase with the external electromagnetic pulse, and therefore into phase with each other. This results in a decrease in the longitudinal magnetization, with a simultaneous increase in the transverse magnetization, which is not null anymore. At the time when the pulse is switched off, the protons will gradually recover their original configuration and it is postulated to happen exponentially and to be governed by two characteristic time constants [**17**]:

$$M_1(t) = M_0 \left(1 - e^{-t/T_1}\right) \tag{1.1}$$

$$M_2(t) = M_0 e^{-t/T_2} \tag{1.2}$$

where $M_1$ denotes the magnitude of the longitudinal magnetization and $M_2$ the magnitude of the transverse magnetization, assuming that the magnetization vector was rotated by 90° at $t = 0$. The time constant $T_1$ is called *longitudinal relaxation time* and quantifies the time required for $M_1$ to recover, while $T_2$ is known as *transverse relaxation time*, related to the time that the transverse magnetization needs to disappear. By exploiting the differences in $T_1$ and $T_2$ into different tissues, it is possible to acquire signals from the $M_1$ and $M_2$ curves. Furthermore, two more parameters called Time to Recover, i.e. the time between two consecutive pulses, and Time to Echo, i.e. the time between the pulse and the acquisition of the signal, allow to associate the magnetization intensity to a colour, obtaining an MRI image.
The main problem of MRI is that it does not provide any information concerning the direction of the fibers. A possible way to overcome this limitation is to use Diffusion Weighted Imaging (DWI), and in particular Diffusion Tensor Imaging (DTI). DWI is a form of MRI imaging based upon measuring the random Brownian motion of water molecules within a voxel of tissue. If we apply a pulsed field gradient to a uniform magnetic field in MRI, it will cause a phase shift in protons which depends on the position of protons themselves. However, if another pulse with the same magnitude but opposite direction is applied, phase alignment between protons should be recovered, and the original signal should be captured again. If this does not happen, it means that some molecules have moved during the time interval between the two opposite gradients due to diffusion. In this way the diffusion coefficient of water molecules in a specific region of the brain can be estimated. Stejskal and Tanner [**19**] proposed an equation in order to quantify the signal loss due to diffusion in a zone:

$$S = S_0 e^{-bD} \tag{1.3}$$

where $S_0$ is the MRI signal intensity when no diffusion-field gradient is imposed, $D$ is the diffusion coefficient and $b$ is a parameter, called diffusion weighting factor, that includes all the quantities characterizing the field gradient. From equation (1.3) we want to evaluate $D$: this can be made carrying out two measurements, one with $b = 0$ and the other one with $b \neq 0$, and calculating the signal intensities:

$$D = -\frac{1}{b} \ln \frac{S}{S_0} \tag{1.4}$$

In this way, we can assign values of $D$ to each portion of the image, building a map of diffusion coefficients inside the brain. It is important to underline that what we have measured by doing so is not properly the diffusion coefficient, since it depends on many other factors, for this reason it is often more correctly referred to as *apparent diffusion coefficient* (ADC).
If a certain tissue is isotropic and so there are not preferential directions in it, the quantification of the ADC fully describes diffusion properties. On the other hand, if we consider anisotropic tissues like white matter, where preferential directions are present, a single measurement of the ADC along a certain direction does not completely characterize diffusion. Actually, performing measurements with different directions of the field gradient leads to different results. In order to overcome this problem, Diffusion Tensor Imaging (DTI) is employed. Using this technique, we do not characterize diffusion by a single coefficient but rather by a second-order symmetric tensor, called *diffusion tensor*:

$$\mathbb{D}_0 = \begin{pmatrix} D_{xx} & D_{xy} & D_{xz} \\ D_{xy} & D_{yy} & D_{yz} \\ D_{xz} & D_{yz} & D_{zz} \end{pmatrix} \tag{1.5}$$

In this way, we can modify equation (1.3) as follows:

$$S = S_0 e^{-\mathbb{B}:\mathbb{D}_0} \tag{1.6}$$

where the diffusion-weighting factor $\mathbb{B}$ is a tensor as well. As a consequence, in order to estimate the components of the diffusion tensor seven measurements are now requested: one in order to obtain $S_0$ and six for the independent components of $\mathbb{D}_0$. The Figure 1.6 shows an example of a representation of the diffusion tensor (DTI).

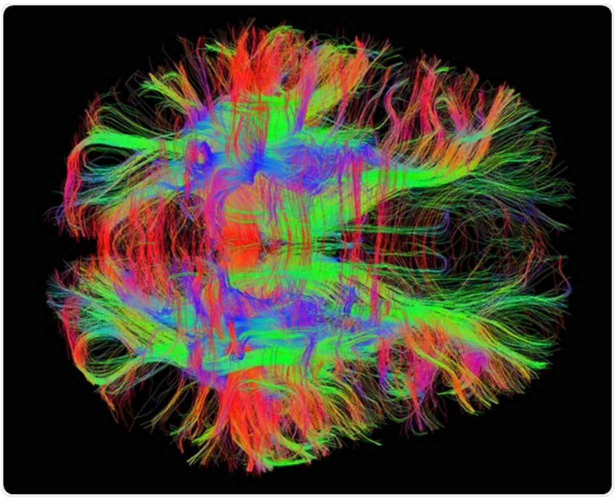

Figure 1.6: Diffusion tensor imaging **[20]**

# Chapter 2

# Brain mechanics

The human brain is still a subject of extensive investigation aimed at understanding its behavior and function. Today it is known that mechanical factors play an important role in regulating brain activity. Unfortunately researchers are far from having a deep knowledge of them because the mechanical behavior of brain tissue is one of the most demanding and complicated to model. Nonetheless, the last decade has seen fundamental advances in different areas of brain mechanics, since a more detailed understanding of brain tissue mechanics is required to develop proper constitutive models.
In this chapter firstly the basic concept of kinematics and dynamics of continua are exposed. In a second moment the theory of mixtures is introduced. After that it is summarized how tissue growth could be mechanically described, by means of a multiplicative decomposition of the deformation gradient. Then a mechanical characterization of brain tissue is presented, where the main characteristics that have to be taken into consideration when constructing a mechanical model are highligthed. Lastly a list of used constitutional models is reported, specifying the advantages and disadvantages of each of them.

## 2.1 Continuum mechanics background

In this section it is reported a summary of important concepts of continuum mechanics which are used in the following. These notions are mainly taken from [**21**] and [**22**].
A finite deformation $\chi(\mathbf{X}, t)$ assigns to each material point $\mathbf{X} \in \mathcal{B}_*$ its position $\mathbf{x}$ in three-dimensional Euclidean space $\mathcal{E}$:

$$\mathcal{B}_* \ni \mathbf{X} \longrightarrow \mathbf{x} = \chi(\mathbf{X}, t) \in \mathcal{E}$$

The image of $\mathcal{B}_*$ through deformation $\chi(\mathbf{X}, t)$ is called a *deformed configuration*, and it is indicated by $\mathcal{B}$. It is assumed that $\chi(\mathbf{X}, t)$ is a diffeomorphism, meaning that it is $C^1$, globally invertible and its inverse is $C^1$.
The tensor field

$$\mathbb{F} := \text{Grad}\ \chi, \quad F_i^L = \frac{\partial \chi_i}{\partial X^L}$$

is called *deformation gradient*. Its determinant, also called *Jacobian*, is denoted by $J := \det\mathbb{F}$ and it needs to be strictly positive in order to avoid unphysical effects.

The deformation gradient and its determinant allow to describe how vectors, area and volume elements deforms from the initial configuration to the deformed one:

$$d\mathbf{x} = \mathbb{F} d\mathbf{X} \tag{2.1}$$

$$d\boldsymbol{\Sigma} = J\mathbb{F}^{-T} d\boldsymbol{\Sigma}_* \tag{2.2}$$

$$dV = JdV_* \tag{2.3}$$

where $d\boldsymbol{\Sigma}_*$ and $dV_*$ are an element of area and an element of volume in the reference configuration $\mathcal{B}_*$, respectively, and $d\boldsymbol{\Sigma}$ and $dV$ are the corresponding elements in $\mathcal{B}$.
The deformation of a continuum from the reference configuration $\mathcal{B}_*$ to the deformed one $\mathcal{B}$ can be described using the *displacement field* $\mathbf{u}(\mathbf{X})$, defined through:

$$\mathbf{x}(\mathbf{X}) = \mathbf{X} + \mathbf{u}(\mathbf{X})$$

Differentiating the previous equation with respect to the material coordinates, we obtain the relation:

$$\mathbb{F} = \mathbb{I} + \text{Grad } \mathbf{u} \tag{2.4}$$

where $\mathbb{I}$ is the second order identity tensor and

$$\text{Grad } \mathbf{u} := \frac{\partial \mathbf{u}}{\partial \mathbf{X}}, \quad (\text{Grad } \mathbf{u})_{ij} := \frac{\partial u_i}{\partial X_j}$$

We now introduce some other useful quantities that will be used in the model.
The right Cauchy-Green deformation tensor is the symmetric tensor defined as:

$$\mathbb{C} := \mathbb{F}^T \mathbb{F}$$

It is usually referred to as the *displacement gradient.* It is also useful to define the left Cauchy-Green deformation tensor:

$$\mathbb{B} := \mathbb{F}\mathbb{F}^T$$

It is possible to note that $\mathbb{C}$ operates from the configuration of reference $\mathcal{B}_*$ in itself, while $\mathbb{B}$ operates from $\mathcal{B}$ in itself. Furthermore the two tensors are symmetric and positive definite and they have the same eigenvalues $\lambda_i$, $i = 1, 2, 3$.
The first, second and third principal invariant of $\mathbb{C}$ are defined as:

$$I_C = tr\mathbb{C} = \lambda_1 + \lambda_2 + \lambda_3$$

$$II_C = \frac{1}{2}\left[(tr\mathbb{C})^2 - tr\mathbb{C}^2\right] = \lambda_1\lambda_2 + \lambda_1\lambda_3 + \lambda_2\lambda_3$$

$$III_C = det\mathbb{C} = \lambda_1\lambda_2\lambda_3$$

The three invariants of $\mathbb{C}$ coincide with the ones of $\mathbb{B}$.

It is important to focus on the *kinematics* of a continuum body. To do that it is considered a reference configuration $\mathcal{B}_*$ and the coordinates in this configuration are called *material or lagrangian coordinates.* The set of positions $\mathcal{B}_t$ occupied by the body at time $t$ is the actual configuration of the body and the coordinates in this configuration are called *spatial or eulerian coordinates.* Each variable $q$ associated with the motion of the body can be expressed in Lagrangian form or in Eulerian form depending on whether it is expressed in variables $(\mathbf{X}, t)$ or $(\mathbf{x}, t)$:

$$q = \tilde{q}(\mathbf{X}, t) = q(\mathbf{x}, t)$$
$$q(\mathbf{x}, t) = \tilde{q}(\chi^{-1}(\mathbf{x}; t), t)$$

The variation of $\tilde{q}$ in time keep the material point fixed, while $\frac{\partial q}{\partial t}(\mathbf{x}, t)$ keeps the spatial coordinate fixed. To link these two quantities:

$$\begin{aligned}\frac{dq}{dt}(\mathbf{x}(t), t) &= \frac{\partial q}{\partial t}(\mathbf{x}(t), t) + \frac{\partial q}{\partial x^j}(\mathbf{x}(t), t)\frac{dx^j}{dt}(\mathbf{x}(t), t) \\ &= \frac{\partial q}{\partial t}(\mathbf{x}(t), t) + \mathbf{v}(\mathbf{x}(t), t) \cdot \nabla q(\mathbf{x}(t), t)\end{aligned}$$

where

$$\mathbf{v} := \frac{\partial \mathbf{x}}{\partial t}(\mathbf{X}, t)$$

is the velocity. In this way we define the acceleration (in Lagrangian form):

$$\mathbf{a}(\mathbf{X}, t) := \frac{\partial^2 \mathbf{x}}{\partial t^2}(\mathbf{X}, t)$$

while the acceleration in Eulerian form:

$$\mathbf{a}(\mathbf{x}, t) = \frac{\partial \mathbf{v}}{\partial t}(\mathbf{x}(t), t) + \mathbf{v}(\mathbf{x}(t), t) \cdot \nabla \mathbf{v}(\mathbf{x}(t), t)$$

It is important to remark now some important theorems widely employed in Continuum Mechanics.
The *Reynolds' transport theorem* plays a fundamental role: if $V_t$ is a spatial volume that convects with the body and $\psi$ is a scalar field of class $C^1$ then

$$\frac{d}{dt}\int_{V_t} \psi dV = \int_{V_t} \left(\frac{\partial \psi}{\partial t} + \nabla \cdot (\psi \mathbf{v})\right) dV \tag{2.5}$$

If the set $V_t$ is not convecting, Reynolds' relation needs to be modified considering the velocity of the boundary $\partial V_t$, $\mathbf{v}_{\boldsymbol{\Sigma}}$, relative to the boundary of the body $\mathbf{v}$, i.e. $w_n := (\mathbf{v}_{\boldsymbol{\Sigma}} - \mathbf{v}) \cdot \mathbf{n}$

$$\frac{d}{dt}\int_{V_t} \psi dV = \int_{V_t} \left(\frac{\partial \psi}{\partial t} + \nabla \cdot (\psi \mathbf{v})\right) dV + \int_{\partial V_t} \psi w_n d\Sigma \tag{2.6}$$

Another very important theorem is the *Cauchy's theorem*: if $\mathbf{t}$ denotes the traction per unit area of the body, there exists a tensor field $\mathbb{T}$, called Cauchy's stress tensor, such that:

$$\mathbf{t}(\mathbf{n}) = \mathbb{T}\mathbf{n}$$

At this point it is possible to introduce the *mass balance equation*. If $\rho(\mathbf{x}, t)$ represents the mass density and mass conservation principle is assumed, it takes the following integral form:

$$\frac{d}{dt}\int_{V_t} \rho(\mathbf{x}, t) dV = 0$$

that is equivalent to this system of local conditions:

$$\frac{\partial \rho}{\partial t} + \nabla \cdot (\rho \mathbf{v}) = 0 \qquad \text{in } \mathcal{B}_t \setminus \mathcal{S}_t$$

$$[|\rho w_n|] = 0 \qquad \text{su } \mathcal{S}_t$$

where $\mathcal{S}_t$ is the boundary of the actual configuration $\mathcal{B}_t$.
It is exposed now the *momentum balance equation*:

$$\frac{d}{dt}\int_{V_t} \rho \mathbf{v} dV = \int_{V_t} \mathbf{b} dV + \int_{\partial V_t} \mathbf{t} d\Sigma$$

where $\mathbf{b}$ represents the resultant of all forces which act on volume elements of material and $\mathbf{t}$ denotes the traction per unit area of the body, as said above. In local form is:

$$\rho\left(\frac{\partial \mathbf{v}}{\partial t} + \mathbf{v}\cdot\nabla\mathbf{v}\right) = \nabla\cdot\mathbb{T} + \mathbf{b}$$

*Balance laws for angular momentum* leads instaed to the symmetry of Cauchy's stress tensor: $\mathbb{T} = \mathbb{T}^T$

### 2.1.1 Constitutive equations and hyperelasticity

It is important here to remark some concept that will be useful in the following. The previously mentioned mass, momentum and angular momentum balance equation are quite general and they are common to any continuous system, independently of the material of which it is constituted. It is therefore necessary to introduce into the mechanics of the continuous systems the notion of response of a body to external stresses for the purpose of take into account the nature of the material of which it is composed.
In this section the main results related to hyperelasticity are presented. A continuum is said to be hyperelastic if there exists a function $\sigma(\mathbb{F})$ such that:

$$\mathbb{T}(\mathbb{F}) = \rho\frac{\partial\sigma}{\partial\mathbb{F}}\mathbb{F}^T$$

where $\mathbb{T}$ is the Cauchy stress tensor, $\rho$ is the material density and $\mathbb{F}$ is the deformation gradient. This condition can be expressed also in another way. In fact a continuum is hyperelastic if there exists a strain energy density function $\mathcal{W}(\mathbb{F})$ such that:

$$\mathbb{T}(\mathbb{F}) = \frac{1}{J}\frac{\partial\mathcal{W}}{\partial\mathbb{F}}\mathbb{F}^T$$

where $J = \det\mathbb{F}$. These two conditions presented are equivalent. Moreover, in order to satisfy the objectivity axiom, the constitutive equation for the tensor $\mathbb{T}$ must be independent of the rigid reference adopted. In hyperelsticity this is equivalent to saying that :

$$\sigma(\mathbb{F}) = \hat{\sigma}(\mathbb{C})$$

Furthermore a solid is isotropic hyperelastic and its constitutive equation satisfies the principle of objectivity if and only if with respect to the natural configuration it results:

$$\sigma(\mathbb{F}) = \hat{\sigma}(\mathbb{C}) = \tilde{\sigma}(I_B, II_B, III_B)$$

In conclusion it is valid the following relation:

$$\hat{\mathbb{T}}(\mathbb{B}) = 2\rho\frac{\partial\tilde{\sigma}(I_B, II_B, III_B)}{\partial\mathbb{B}}\mathbb{B}$$

that is:

$$\hat{\mathbb{T}}(\mathbb{B}) = 2\rho\frac{\partial\tilde{\sigma}}{\partial I_B}\mathbb{B} + 2\rho\frac{\partial\tilde{\sigma}}{\partial II_B}(I_B\mathbb{I} - \mathbb{B})\mathbb{B} + 2\rho\frac{\partial\tilde{\sigma}}{\partial III_B}(\mathbb{B}^2 - I_B\mathbb{B} + II_B\mathbb{I})\mathbb{B}$$

using Cayley-Hamilton theorem, this is equivalent to

$$\hat{\mathbb{T}}(\mathbb{B}) = 2\rho III_B \frac{\partial \tilde{\sigma}}{\partial III_B} \mathbb{I} + 2\rho \left( \frac{\partial \tilde{\sigma}}{\partial I_B} + \frac{\partial \tilde{\sigma}}{\partial II_B} I_B \right) \mathbb{B} - 2\rho \frac{\partial \tilde{\sigma}}{\partial II_B} \mathbb{B}^2$$

## 2.2 Mixture theory

Mixture theory allows to describe mathematically a continuum composed by an arbitrary number of phases interacting with each other. A fundamental assumption in the theory of mixtures is that each point in the space occupied by the mixture is filled by a particle belonging to each constituent. Thus, in essence, the space occupied by the mixture is made of several co-existent continua. In this way it is possible to generalize the basic concepts of a unique continuum to several co-existent continua. For contents of this section, refer to [**23**].
It is considered a mixture of $n$ constituents. It is denoted by $\mathbf{X}_\alpha$, $\alpha = 1, ..., n$, a typical particle belonging to each constituent in the reference state. At time $t$, these typical particles occupy the position:

$$\mathbf{x} = \chi_\alpha(\mathbf{X}_\alpha, t) \qquad \alpha = 1, ..., n$$

The velocity of each of these particles is given by

$$\mathbf{v}_\alpha = \frac{\partial \chi_\alpha}{\partial t} \qquad \alpha = 1, ..., n$$

In order to define the mean velocity of the mixture, let denote as $\rho_\alpha$ the mass density of the $\alpha-$th constituent in the mixed state, that is the ratio between the mass of the $\alpha$-th component and the total volume. The total mass density of the mixture is so defined as:

$$\rho = \sum_{\alpha=1}^{n} \rho_\alpha$$

and so the mean velocity is given by:

$$\mathbf{v} = \frac{1}{\rho} \sum_{\alpha=1}^{n} \rho_\alpha \mathbf{v}_\alpha$$

The deformation gradient $\mathbb{F}_\alpha$ associated with the $\alpha$-th constituent is given by:

$$\mathbb{F}_\alpha := \text{Grad } \chi_\alpha \qquad \alpha = 1, ..., n$$

So it is possible to define also the right and left Cauchy-Green stress tensor:

$$\mathbb{C}_\alpha = (\mathbb{F}_\alpha)^T \mathbb{F}_\alpha, \qquad \mathbb{B}_\alpha = \mathbb{F}_\alpha (\mathbb{F}_\alpha)^T$$

and their principal invariants:

$$I_{C_\alpha} = tr\mathbb{C}_\alpha, \qquad II_{C_\alpha} = \frac{1}{2} \left[ (tr\mathbb{C}_\alpha)^2 - tr(\mathbb{C}_\alpha)^2 \right], \qquad III_{C_\alpha} = det\mathbb{C}_\alpha$$

Let $q$ be any quantity (scalar, vector or tensor) defined at the point $\mathbf{x}$ in the mixture at time t. Thus

$$\frac{d^{(\alpha)} q}{dt} = \frac{\partial}{\partial t} q(\mathbf{x}, t) + \mathbf{v}^\alpha(\mathbf{x}, t) \cdot \nabla q(\mathbf{x}, t)$$

So it is possible to define the variation of $q$ with respect to time as noted by an observer at $\mathbf{x}$ moving with the mean velocity of the mixture:

$$\frac{d^{(\alpha)}q}{dt} = \frac{\partial}{\partial t}q(\mathbf{x},t) + \mathbf{v}(\mathbf{x},t) \cdot \nabla q(\mathbf{x},t)$$

The acceleration $\mathbf{a}_\alpha$ of the $\alpha$-th constituent is defined through

$$\mathbf{a}_\alpha = \frac{\partial^2 \chi_\alpha}{\partial t^2}$$

For what concerns Cauchy's stress tensor:

$$\mathbf{t}_\alpha(\mathbf{n}) = \mathbb{T}_\alpha \mathbf{n}$$

and

$$\mathbf{t} = \sum_{\alpha=1}^{n} \mathbf{t}_\alpha, \qquad \mathbb{T} = \sum_{\alpha=1}^{n} \mathbb{T}_i$$

so it is still valid the following:

$$\mathbf{t}(\mathbf{n}) = \mathbb{T}\mathbf{n}$$

The theory of mixtures takes into account the possible transformation of mass due to thermal interactions or chemical reactions between the constituents. So $\Gamma_\alpha$ represents the production of the $\alpha$-th constituent due to these actions. If $V$ is any fixed volume in the mixture, *the balance of mass* of a component requires that:

$$\frac{d}{dt}\int_V \rho_\alpha dV = \int_V \Gamma_\alpha dV$$

In this way the local form is:

$$\frac{\partial \rho_\alpha}{\partial t} + \nabla \cdot (\rho_\alpha \mathbf{v}_\alpha) = \Gamma_\alpha$$

The balance of mass for the mixture as a whole should have the same form as that for a single constituent continuum. In order to have that it is requested that:

$$\sum_{\alpha=1}^{n} \Gamma_\alpha = 0$$

which states that there is no net production of mass.
It is important to define now the concept of *volume fraction*, that is, the volume occupied by the $\alpha$-th constituent over the total volume:

$$\phi_\alpha(\mathbf{x},t) := \frac{V_\alpha(\mathbf{x},t)}{V(\mathbf{x},t)}$$

In the case of a *saturated medium*, the constraint

$$\sum_{\alpha=1}^{n} \phi_\alpha = 0$$

has to hold. Furthermore it is defined the *true mass density* for the $\alpha$-th phase $\gamma_\alpha$ as the ratio between the mass of the $\alpha$-th component and its volume (not the total volume), so that $\rho_\alpha = \phi_\alpha \gamma_\alpha$. By inserting it in the mass balance equation and assuming that all phases are incompressible, that is $\frac{d\gamma_\alpha}{dt} = 0$, it becomes:

$$\frac{\partial \phi_\alpha}{\partial t} + \nabla \cdot (\phi_\alpha \mathbf{v}_\alpha) = \frac{\Gamma_\alpha}{\gamma_\alpha}$$

Moreover each component of a mixture must satisfy its own *momentum balance equation*:

$$\rho_\alpha \left( \frac{\partial \mathbf{v}_\alpha}{\partial t} + \mathbf{v}_\alpha \cdot \nabla \mathbf{v}_\alpha \right) = \nabla \cdot \mathbb{T}_\alpha + \rho_\alpha \mathbf{b}_\alpha + \mathbf{m}_\alpha$$

where $\mathbb{T}_\alpha$ is the partial Cauchy stress tensor of the $\alpha$-th phase, $\mathbf{b}_\alpha$ is the body force acting on the $\alpha$-th constituent and the term $\mathbf{m}_\alpha$ is the momentum supply that accounts for the interaction between different phases [**24**].

## 2.3 Multiplicative decomposition of the deformation gradient

In classical Continuum Mechanics a body is seen as a collection of particles [**25**]. Each particle should have its counterpart in a certain reference configuration of the body. One way of describing the growth of a body is to imagine that new particles appear even if they were not present in the original configuration. Clearly an approach like this has the problem that it is impossible to define a motion that maps the original configuration onto the current one. A possible way to overcome this difficulty is to consider as an increase of the mass of the already existing particles. In such a case it is possible to define a motion that connects all these configurations because the number of particles does not change. However the total mass of the body in going from the original to the current configuration may change because the mass of the particles may have changed.
Let a body be in the configuration $\mathcal{B}_0$ at time $t = 0$. Suppose that the body has undergone growth or resorption together with the possible application of loads, so that at current time $t$ the configuration is $\mathcal{B}_t$.
In the scientific papers [**25**, **26**, **27**, **28**, **29**, **30**] it is presented how to decompose the deformation assuming multiple natural configurations. The concept of evolving natural configurations consists in splitting the evolution in pure elastic deformations and deformations subsequent to anelastic distortions, such as growth and remodelling. Following the modelling background proposed in [**25**, **28**], in this section it is summarized how this multiplicative decomposition of the deformation gradient can be done. It is assumed to cut a generic particle out of the body and to relieve its state of stress while keeping its mass constant. In this way the body will reach a state that is in general different from the one it had in $\mathcal{B}_0$ and also from the one achieved in $\mathcal{B}_t$. This is the natural state of that particle at time $t$, while the *natural configuration of the body at time t* is the collection of all the particles in their natural states at time $t$ and it is indicated by $\mathcal{B}_g$. In this way it is possible to measure the deformation from the natural configuration $\mathcal{B}_g$ through the tensor $\mathbb{F}_e$, which is connected to the stress response of the material, while the path from $\mathcal{B}_0$ to the natural configuration is described by the tensor $\mathbb{F}_g$, which is directly connected to growth and it is therefore named *growth tensor*. This decomposition is graphically shown in Figure 2.1. The deformation gradient $\mathbb{F}$ indicates how the body is deforming locally in going from $\mathcal{B}_0$ to $\mathcal{B}_t$, while, in an analogous way, $\mathbb{F}_e$ tells how the body is deforming locally in going from the

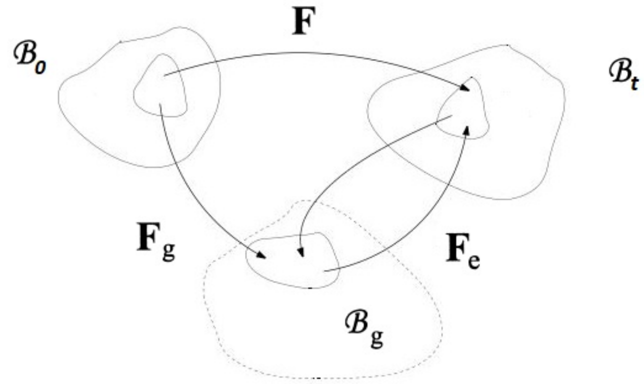


Figure 2.1: Multiplicative decomposition of the deformation gradient (from Lubarda, 2004 [**30**] and Ambrosi and Mollica, 2002 [**25**]).

natural configuration $\mathcal{B}_g$ to $\mathcal{B}_t$, while $\mathbb{F}_g$ tells how the body is growing locally. It is valid this relation:

$$\mathbb{F} = \mathbb{F}_e \mathbb{F}_g$$

Furthermore, since the deformation gradient $\mathbb{F}$ is invertible, it follows that $\mathbb{F}_e$ and $\mathbb{F}_g$ are invertible too. Moreover the determinant of the deformation gradient is expressed as:

$$J = J_e \cdot J_g$$

If $J_g > 1$ the body is subject to growth, on the contrary if $J_g < 1$ the body is subject to resorption.
It is necessary then to prescribe a constitutive equation for the path $\mathcal{B}_g$ to $\mathcal{B}_t$, and independently, an evolution equation for the path $\mathcal{B}_0$ to $\mathcal{B}_g$. It is important to remark that, if necessary, these parts can then be subdivided further, in this way the constitutive model can be constructed from multiple building blocks that represent the key physical features of the tissue. For example in [**26**] it is multiplicatively decomposed the deformation gradient $\mathbb{F}$ into an elastic part $\mathbb{F}_e$ and a viscous part $\mathbb{F}_v$. In [**27**] the deformation gradient of the cellular population $\mathbb{F}_c$ is decomposed as

$$\mathbb{F}_c = \mathbb{F}_e \mathbb{F}_p \mathbb{F}_g$$

where $\mathbb{F}_e$ is the purely elastic contribution to the overall deformation gradient, whereas $\mathbb{F}_g$ and $\mathbb{F}_p$ represent the inelastic distortions related to growth and to the plastic reorganisation of the tissue's internal structure.

## 2.4 Mechanical characterization of brain tissue

It is now presented the continuum of interest: the brain tissue. It is fundamental to characterize it in order to construct a model as accurate as possible.
Brain tissue consists of gray and white matter and is covered with the thin layer of pia and arachnoid membranes. The gray matter is made up of neuronal cell

bodies, which are distributed at the surface of the cerebral cortex which does not seem to have any directional preference, while the white matter is composed of bundles of myelinated nerve cell processes (or axons), that can be highly oriented. However, the analysis made by Budday et al. (2017) reported in [**32**] has established that the microstructural anisotropy due to the alignment of nerve fibers in the tissue does not result in an anisotropic elastic response. Therefore in a first moment it is neglected a possible anisotropic response in the elastic part of the deformation and it is assumed that brain tissue is isotropic. On the other hand, the anisotropic orientation of fibers highly influence anelastic distortions, such as growth and remodelling.
Another important issue could be whether the brain tissue should be treated as solid or as fluid. An answer arrives from [**33**], which reports that brain tissue samples, immersed in saline, return to a clearly defined shape after being deformed, which indicates a need for a solid model. But, viewed as a solid, the brain is extremely soft and its mechanical response is heavily influenced by the fluid phase. Therefore a mechanical analysis requires a coupled multi-field theory. Nevertheless it is important to underline that, as reported in [**26**], most constitutive models for the brain tissue only consider the solid phase, i.e. they are monophasic, either purely elastic or viscoelastic. Biphasic and triphasic models are used when the effects of the other phases are non-negligible.
Moreover the issue of compressibility of brain tissue warrants careful investigation because the tissue may behave incompressibly in impact situations while it may be effectively compressible in long duration processes, as reported in [**34**]. So the choice should be done depending on the situation one wants to study.
Furthermore the vast majority of experimental results agree upon the nonlinear and viscous nature of brain tissue. It is evident also in the experiments made in [**35**, **36**, **37**] which subject the brain to compression, tension or shear. Moreover experiments on brain samples under multiaxial loading have shown that human brain tissue is characterized by a peculiar elastic response under combined shear and compression/tension: there is a significant increase in shear stress with increasing axial compression compared to a moderate increase with increasing axial tension. So it is extremely important to derive constitutive models that manage to capture this characteristic response.

## 2.5 Constitutive models for human brain tissue

Computational simulations are a powerful tool to predict the mechanical behavior of the human brain in health and disease. Of course the success of these simulations depends critically on the underlying constitutive model and on the reliable identification of its material parameters. Constitutive modeling consists in considering and choosing families of models with desirable properties. In fact it is important to find a functional form that both enforces particular properties of the considered material and is general enough to be adapted for specific systems. In order to do this is fundamental to have deeply understood the defining characteristics of brain tissue. Moreover it has to be said that the mechanical behavior of brain tissue may be modeled in different ways based on the specific conditions of interest and in particular on the magnitude of the strain rate. Hence, different constitutive relations may be needed for the same material depending on the particular condition.

In **[26]** the authors categorize the different features of existing models into time-independent, time-dependent, and history-dependent contributions. To model the time-independent and elastic behavior of the brain tissue, most existing models adopt a hyperelastic approach. To model the time-dependent response, most models either use a convolution integral approach or a multiplicative decomposition of the deformation gradient. In the following some models of each type are presented.
An important fact that is taken into consideration is the viscoelastic response of brain tissue. The data shows clearly that the response of brain tissue has a viscous component indicated by a different response in loading and unloading. Constitutive relations for viscoelastic materials consist of a time-independent elastic contribution and a time-dependent viscous contribution. In **[38]** the authors prove that the non-linear viscoelastic model, based on the strain energy function in polynomial form with time-dependent coefficients, is suitable for description of brain tissue deformation behaviour under compression, typical for surgical procedures. The strain energy function of the following form is used:

$$\mathcal{W} = \int_0^t \left\{ \sum_{i+j=1}^{N} C_{ij}(t-\tau) \cdot \frac{d}{d\tau} \left[ \frac{\partial}{\partial \lambda_z} ((I_1 - 3)^i (I_2 - 3)^j) \right] \right\} d\tau$$

where $I_1$,$I_2$ and $I_3$ are strain invariants and $\lambda_z$ is a stretch in vertical direction. In **[39]** it is developed a finite deformation, linear viscoelastic model of brain tissue by the same authors. The polynomial strain energy function of the hyperelastic, linear viscoelastic medium is written in the following form:

$$\mathcal{W} = \int_0^t \left\{ \sum_{i+j=1}^{N} \left[ C_{ij0} \left( 1 - \sum_{k=1}^{n} g_k \left( 1 - e^{-\frac{t-\tau}{\tau_k}} \right) \right) \right] \frac{d}{d\tau} \left[ (I_1 - 3)^i (I_2 - 3)^j \right] \right\} d\tau$$

where $\tau_k$ are characteristic times, $g_k$ are relaxation coefficients and $N$ is the order of polynomial in strain invariants. The model developed here has a number of advantages over the previously proposed. Firstly it requires only four material parameters to be identified. Furthermore it is known that the major deficiency of most of the models is the fact that they were identified using experimental data obtained in vitro and there is no certainty whether they can be applied in the realistic in vivo setting. In **[40]** it is shown that the previously proposed model can be applied in finite element simulation of brain deformation in vivo for moderate strain rates, and consequently, to neurosurgical simulation.
However it is also important to focus on the tissue's effective elastic response under small strain rate. Following what was made in **[32]**, this response is obtained as the average between the loading and the unloading paths, assuming that this corresponds to the case when the strain rate approaches zero. The attention is so restricted to hyperelastic isotropic materials, that fall into the category of time-independent models. One of the first models that have been found in good agreement with the experimental data, both in single and multiaxial loading, is Ogden-type hyperelastic incompressible isotropic models **[41]**:

$$\mathcal{W}^{Ogd}(\mathbb{C}) = \sum_{i=1}^{N} \frac{\mu_i}{\alpha_i} (\lambda_1^{\alpha_i} + \lambda_2^{\alpha_i} + \lambda_3^{\alpha_i} - 3)$$

where $N$, $\mu_i$ and $\alpha_i$ are the material parameters. In **[32]** it is shown that the models with higher order terms (i.e. high values of $N$) are more successful in

approximating the data than the ones with lower order terms. Unfortunately the fact that a relatively large number of parameters may be required to approximate the data to the desired accuracy makes them less attractive to users.
In [**32**, **35**, **36**, **37**] it is shown that the isotropic modified one-term Ogden model is suitable to represent the hyperelastic behavior under combined shear, compression, and tension loadings. The strain energy density function is:

$$\mathcal{W}^{Ogd}(\mathbb{C}) = 2\frac{\mu}{\alpha^2}(\lambda_1^\alpha + \lambda_2^\alpha + \lambda_3^\alpha - 3)$$

where $\mu = \frac{1}{2}\mu_1\alpha_1$ corresponds to the classical shear modulus and $\alpha_1 = \alpha$ is able to capture the compression-tension asymmetry and the elastic behaviour of the brain with multiple loading modes simultaneously. It is also emphasized that the parameter $\alpha$ needs to adopt a negative value to represent the effect that stresses are higher in compression than in tension. A positive value for a would yield the opposite trend, which is inappropriate for brain tissue. The strength of this model consist in the fact that less parameters are involved. On the other hand in [**42**] is underlined that this constitutive model fails to simultaneously capture the constitutive response of brain tissue at different stretch levels when using the calibration approach. To overcome this problem it is presented a new model by combining the Mooney–Rivlin model with the one-term Ogden model.
The Mooney-Rivlin model has the following form:

$$\mathcal{W}^{MR}(\lambda_1, \lambda_2, \lambda_3) = \frac{c_1}{2}(\lambda_1^2 + \lambda_2^2 + \lambda_3^2 - 3) + \frac{c_2}{2}(\lambda_1^{-2} + \lambda_2^{-2} + \lambda_3^{-2} - 3)$$

where $c_1$ and $c_2$ are constant parameters. The final model takes on the form:

$$\mathcal{W}(\lambda_1, \lambda_2, \lambda_3) = \frac{c_0}{2\alpha}(\lambda_1^{2\alpha}+\lambda_2^{2\alpha}+\lambda_3^{2\alpha}-3)+\frac{\bar{c_1}}{2}(\lambda_1^2+\lambda_2^2+\lambda_3^2-3)+\frac{\bar{c_2}}{2}(\lambda_1^{-2}+\lambda_2^{-2}+\lambda_3^{-2}-3)$$

in terms of four global parameters. This proposed model is an hyperelastic model to date calibrated simultaneously to experimental data for brain tissue under finite simple shear superposed on varying axial tension or compression.
Since it will be the one used in our model, it is useful to rewrite the Mooney-Rivlin model taking into account the notions of frame indifference and isotropy:

$$\widehat{\mathcal{W}}_{\text{sn}}(\mathbb{C}_\text{e}) = \frac{1}{2}\mu_1 (\text{I}_{\mathbb{C}_\text{e}} - 3) + \frac{1}{2}\mu_2 (\text{II}_{\mathbb{C}_\text{e}} - 3) \tag{2.7}$$

where $\text{I}_{\mathbb{C}_\text{e}}$ and $\text{II}_{\mathbb{C}_\text{e}}$ are, respectively, the first and the second invariant of $\mathbb{C}_\text{e}$.
Lastly there are also history-dependent models of brain tissue. Various experiments have shown that preconditioning has a significant effect on the mechanical properties of brain tissue, which implies that the tissue response depends critically on the loading history. One example of this type of models can be the Franceschini model, described in [**26**].

# Chapter 3

# Mathematical models for Glioblastoma

Mathematical models for cerebral tumour growth can help in understanding the physiology of tumour growth, in order to predict future tumour shape and volume and to quantify its aggressiveness. Furthermore they can be useful to study the response of the tumour to therapy. During the last decade theoreticians have developed a great variety of tumour models covering various morphological and functional aspects of tumour growth. In this chapter the most popular brain tumour models are summarized, analyzing the results that have been obtained so far in this field. Lastly it is presented the mathematical model taken into account.

## 3.1 Overview on mathematical models of brain tumour

Tumour growth models can be divided according to what level they focus their study: microscopic or macroscopic levels. As it is reported in [**43**] the former models study the observations at microscopic level by describing the interactions between healthy tissues and tumour cells. These models study tumour growth at different levels: avascular, angiogenesis and vascular. On the contrary, the latter models utilize medical imaging techniques and mathematical formulae to simulate the tumour cells diffusion, proliferation and the induced mass effect.

### 3.1.1 Microscopic models

The microscopic scale refers to phenomena that occur at the sub-cellular level and to the activities that take place within the cell. These types of models keep track of the single cell behaviour and its interactions with other agents. As stated in [**44**], microscopic models of brain tumour proliferation mainly fulfill two objectives: the first is to reproduce the early growth of gliomas at the very beginning, when the tumour is still in its avascular phase, the second is to investigate the cancer invasive behaviour.
The used models are mostly cellular automata (CA), cellular Potts model (CPM) or agent-based models (ABMs). A cellular automaton (CA) consists of a regular grid of cells, each in one of a finite number of states. The grid can be in any finite number of dimensions. For each cell, a set of cells called its neighborhood is defined relative to the specified cell. An initial state is selected by assigning a state for each cell. A new generation is created (advancing $t$ by 1), according to

some fixed rule that determines the new state of each cell in terms of the current state of the cell and the states of the cells in its neighborhood. On the other hand, cellular Potts model (CPM) is a computational model of cells and tissues. It is used to simulate individual and collective cell behavior, tissue morphogenesis and cancer development. CPM describes cells as deformable objects with a certain volume, that can adhere to each other and to the medium in which they live. The formalism can be extended to include cell behaviours such as cell migration, growth and division, and cell signalling. Finally, agent-based models (ABMs) are a class of microscopical models for simulating the actions and interactions of autonomous agents with a view to assessing their effects on the system as a whole. ABMs differ from cellular automata in the fact that they are usually lattice-free, so that cells are allowed to move and change their orientation, providing a more realistic description of the phenomenon.

Concerning early glioma tumour growth, Sander et al. [**46**] formulate a chemotaxis model (the evolution of the system is affected by the gradient of nutrient concentration) for the GBMs complex growth patterns in vitro, in which invasive cells organize in tenuous branches. The work of Kansal et al. [**47**] models the 3D evolution of gliomas by developing a cellular automaton. The system is firstly iniziated with an initial distribution of about 1000 cells and then one can follow the evolution to a fully developed tumour of $10^{11}$ cells. Furthermore Mansury et al. [**48**] use an agent-based model in order to realistically simulate early avascular GBM growth.

Wurzel et al. [**49**] presented a model that is developed simulating the invasion, proliferation and death of tumour cells. This model aims to investigate the effect of brain structure inhomogeneity, in fact it is modelled as an orientation gradient field parallel to the white matter fiber tracts, which facilitates invasion/migration of the tumour cells. Glioma cell migration on a substrate of collagen was investigated by Aubert et al. [**50**]. They propose a 2D CA model which indicates that chemotaxis or cell–cell communication through gap junctions is necessary to reproduce experimental density profiles of glioma cell distributions in tumour spheroids. In another study, migration patterns of glioma cells in the presence of astrocytes were studied by Aubert et al. [**51**]. An extended version of the model proposed in [**50**] was used and it suggests that the interactions between glioma cells and astrocytes play an important role in glioma invasion, due to the effect of heterotypic (between glioma cells and surrounding astrocytes) gap junction inhibition which dominates that of homotypic (between glioma cells) inhibition. Finally, to explore the influence of the ECM on glioma cell migration, Szabò et al. [**52**] considered not only cell–cell adhesion but also cell–ECM interactions. The interplay between haptotaxis, matrix degradation and active cell movement was investigated by means of a 2D CPM.

### 3.1.2 Macroscopic models

Continuum-based models focus on the evolution of cancer cell density over time. The macroscopic models can be either diffusive or biomechanical, as reported in [**43**]. Diffusive models are able to simulate the cancerous cells' diffusion into healthy tissues and their corresponding proliferation using the reaction-diffusion model. On the other side, biomechanical ones mainly target studying the mass effect of tumour bulk on the other anatomical structures of the brain using stress and strain relationship. They focus their studies on deformation and structure changes (mass effect) of the brain tissue which is usually considered as elastic, viscoelastic or hyperelastic material.

### Diffusive models

The diffusive models are firstly presented. They mainly use of the reaction-diffusion equation proposed in [**53**, **54**, **55**]:

$$\frac{\partial c(x,t)}{\partial t} = \nabla \cdot (D\nabla c(x,t)) + f(c(x,t)) \tag{3.1}$$

The proliferation term $f(c(x,t))$ could be estimated by either exponential [**53**, **54**, **55**], logistic [**43**] or Gompertz terms [**56**]. The model formulation is completed by boundary conditions which impose initial conditions $c(x,0) = c_0(x)$ where $c_0(x)$ defines the initial spatial distribution of malignant cells and no migration of cells beyond the brain boundary:

$$D\nabla c \cdot \mathbf{n}_{\partial\Omega} = 0$$

The diffusion coefficient is considered a constant if an isotropic growth is assumed. However there are also other possibilities: in [**54**] is presented a mathematical formulation of the model which involves spatially varying diffusion $D(x)$, where $D(x) = D_G$, a constant, for $x$ in grey matter and $D(x) = D_W$, another constant, for $x$ in white matter. It has been observed that tumoral cells diffuse more rapidly in white matter than in gray matter so it holds $D_W > D_G$. Furthermore in [**57**] it is proposed to further generalize this model to take into account not only the heterogeneity of the brain tissue but also its anisotropy, dealing with the fact that glioma cell migration is facilitated in the direction of white matter fibers. In this case $\mathbf{D}$ is a $3 \times 3$ symmetric positive definite matrix that models the local anisotropy.
This model is also used to estimate the effects of treatments to which patients are usually subjected, that can be either chemotherapy or radiotherapy. Typically, these effects are expressed as loss (negative) terms in (3.1). In [**54**] it is shown how (3.1) can be expanded to allow for chemotherapy. If $G(t)$ defines the temporal profile of the chemotherapy treatments, then, assuming a loss proportional to the strength or amount of therapy at a given time, the equation model (3.1) can be rewritten as:

$$\frac{\partial c(x,t)}{\partial t} = \nabla \cdot (D\nabla c(x,t)) + f(c(x,t)) - G(t)c(x,t)$$

In [**43**] it is presented a model that can estimate the effect of radiation therapy doses by calculating the cells survival probability after radiation dose. The survival probability is defined as:

$$S = e^{-(\alpha d_i(c,t) + \beta d_i(c,t)^2)}$$

where $d_i(c,t)$ is the radiotherapy dose number $i$ in the radiotherapy course over time while $\alpha$ and $\beta$ are, respectively, the linear and quadratic radiobiology parameters. The loss of tumour cells can be calculated using:

$$r(c,t,d_i) = \begin{cases} 0 & \text{no radiation} \\ 1 - S(\alpha, \beta, d_i(c,t)) & \text{radiation} \end{cases}$$

The model equation (3.1) can be modified adding the term:

$$R(x,t) = c(x,t)(1 - c(x,t))r(x,t,d_i)$$

Furthermore in [**54**] it is shown that (3.1) can be used also to simulate surgical resection. In order to do this the tumour cell density is set to zero inside the resection bed. This model supports the concept that gliomas infiltrate so diffusely that they cannot be cured by resection alone, but, increasing the size of resection, does increase life expectancy.
In [**58**] it is instead presented a mathematical model for glioma and the immune system interactions, in order to find an effective immunotherapy. In this case it consists of a system of ODEs rather than PDEs.

#### Biomechanical models

The introduction of a mechanical framework allows to deal with several important problems such as the description of the stress field inside the growing spheroid and at the interface with the external tissues. Biomechanical models consist of deriving mass and momentum balance equations for each cell population. When developing the momentum balance equations, consideration of cell-to-cell mechanical interactions is required and constitutive laws must be employed to describe such interactions. The very first difficulty that is encountered is the necessity to take into account a quite large number of cell types as well as biological effects. Earlier models of this type, assumed the brain to consist of a single solid phase and modeled its mechanical response using an external force proportional to the concentration gradient of cancer cells. More comprehensive biomechanical models have also been developed that address the biphasic (i.e. fluid and solid phase) nature of the brain.

Ambrosi and Preziosi in [**59**] assume that the ensemble of cells live in a liquid environment in which some chemical factors diffuse. The correct mechanical framework for a system of this type is the theory of multicomponent continua; namely, the authors treat tumours as deformable porous media. This description allows in principle to determine how the tumour uncontrolled growth may cause compression, necrosis, collapse, or rupture of the surrounding tissues and, in particular, collapse of immature blood vessels and infiltration and rupture of ducts and capsules. In turn, the models allow to determine how the stresses inside the tumour related to the compression of the external tissues can interfere with tumour growth. Focusing on the evolution of tumour cells and of the extracellular liquid one can write the mass and momentum balance equations in the form prevously discussed in Section 2.2:

$$\frac{\partial \phi_T}{\partial t} + \nabla \cdot (\phi_T \mathbf{v}_T) = \Gamma_T$$

$$\frac{\partial \phi_l}{\partial t} + \nabla \cdot (\phi_l \mathbf{v}_l) = \Gamma_l$$

$$\rho_T \phi_T \left( \frac{\partial \mathbf{v}_T}{\partial t} + \mathbf{v}_T \cdot \nabla \mathbf{v}_T \right) - \nabla \mathbb{T}_T = \mathbf{m}_T$$

$$\rho_l \phi_l \left( \frac{\partial \mathbf{v}_l}{\partial t} + \mathbf{v}_l \cdot \nabla \mathbf{v}_l \right) - \nabla \mathbb{T}_l = \mathbf{m}_l$$

where $\Gamma_T$, $\Gamma_l$ are the production rates of cells and liquid, respectively, $\mathbb{T}_T$ ,$\mathbb{T}_l$ are the partial stress tensor of the tumour and liquid, respectively. The momentum supply $\mathbf{m}_l$, $\mathbf{m}_T$ of the $i$-th constituent, contain both the drag due to the local interaction between the components and the Fickian diffusion of the single constituent. It has to be added the saturation assumption and, since there are no external sources, conservation conditions for mass and momentum are to be satisfied:

$$\phi_T + \phi_l = 1$$

$$\rho_T \Gamma_T + \rho_l \Gamma_l = 0$$

$$\mathbf{m}_T + \mathbf{m}_l + \rho_T \Gamma_T \mathbf{v}_T + \rho_l \Gamma_l \mathbf{v}_l = 0$$

Furthermore the concentration $u_i$ of some chemicals satisfy advection–diffusion equations:

$$\frac{\partial u_i}{\partial t} + \nabla \cdot (u_i \mathbf{v}) = \nabla \cdot (Q_i \nabla u_i) + G_i - D_i u_i \qquad i = 1, ..., m$$

The role of the extracellular matrix is also taken into account as a development of the basic model.
Also in [**60**] Byrne and Preziosi develop a model for multicell spheroids as deformable porous media in the theory of mixtures. They assume that the tumour comprises two constituents only: a solid phase and a liquid phase. In addition, the motion of the cells and the intercellular fluid is so slow that inertial terms can be neglected. The governing equations were supplemented by constitutive laws that enable the internal stresses and, in particular, the stress at the interface between the tumour and its surroundings to be calculated.
In [**61**] Angeli et al. developed a biphasic (tumour's solid and fluid phases) tissue growth theory incorporating the effects of radiotherapy. The model was developed to account for the kinematics of the growth of a spherical tumour seed surrounded by healthy tissue. It is based on the decomposition of the total deformation gradient tensor $\mathbb{F} = \mathbb{F}_e \mathbb{F}_g$, where $\mathbb{F}_e$ is the elastic component of $\mathbb{F}$ used to account for interactions with the normal tissue, and $\mathbb{F}_g$ was assumed to be an isotropic tensor that accounts for tumour growth due to cancer cell proliferation. The calculation of the survival fraction $S_f$ of cancer cells post-irradiation is based on the linear–quadratic model also expressed in [**43**] and the transport of oxygen is modeled by taking into account the convection and diffusion mechanisms that deliver oxygen in the tissue, the oxygen entering the tissue from the blood vessels and the amount of oxygen consumed by cells.
The previous model was also used in [**62**] in order to take into account the infiltration and distant invasion of cancer cells to the surrounding tissues. This model model incorporates the tumour biomechanical response at the tissue level and accounts for cellular events by modeling cancer cell proliferation, infiltration to surrounding tissues and invasion to distant locations.

As reported in [**63**], recently developed approach for Glioblastoma Multiforme modeling employs multiphase diffuse interface models of Cahn-Hilliard type. From a physical viewpoint, sharp interfaces are replaced by transition layers: this is made by introducing a fourth-order nonlinear advection-reaction-diffusion equation analogous to the phase-field model of Cahn and Hilliard [**64**]. This kind of approach avoids the need to impose interface conditions between the tumour

and the host tissue and eliminates the necessity of tracking the interface motion explicitely.
This approach is used in [**65**], where it is developed a mathematical model of tumour growth in a dynamic microenvironments with deformable membranes. Using a diffuse domain approach, the complex domain is captured implicitly using an auxiliary function and the governing equations are appropriately modified, extended and solved in a larger, regular domain.
Focusing on the Glioblastoma, Colombo et al. [**66**] presented a diffuse interface model for the GBM, in which no boundary conditions at the interface between the normal and the diseased region are required. Despite the diffused nature of the interface, the model is purely mechanical, in fact the tumour lesion and the surrounding environment are described though incompressible binary mixture model.
An advancement with respect to the state-of-the-art GBM models is presented by Agosti et al. in [**67**, **68**]. In their works it is developed a continuum multiphase diffuse-interface model of GBM accounting both for its growth and its response to therapies. It is certainly a further step towards the ambitious goal to provide a computational tool that support medical doctors in clinical practice.
It is necessary to point out that a drawback of diffuse-interface models is that it is difficult to incorporate deformations. We cannot use constitutive equations typical of solids, at least for how the problem is defined today. For this reason the solid phase is described with an elastic liquid. It is a subject that is still to be studied.

## 3.2 Eulerian model derivation

In this section a continuum, multiphase model for Glioblastoma Multiforme growth and proliferation is presented, starting from the model derived in [**63**] and removing or modifying some assumptions that had been made.
The hyphothesis made is that the region occupied by the tumour (denoted by $\Omega_t(t)$) is completely separated from the healthy host tissue (denoted by $\Omega_h(t)$), so that the boundary between the tumour and the surrounding environment can be described by a moving interface. Furthermore, both of these regions are treated as saturated domains consisting of two distinct phases, which represent the cell population (labelled with subscript "s") and the interstitial fluid (labelled with subscript "$\ell$"). The cell phase is supposed to behave as an hyperelastic solid, while the liquid phase is instead considered constitutively as an ideal fluid.
In this description, we assume that the cellular phase includes healthy, diseased and necrotic cells, while the fluid phase resumes interstitial brain fluid, blood and nutrients; the distinction between cancer and host tissue is then realized through the use of a separating interface rather than through the introduction of different phases for tumorous and healthy cells.
The multiphase approach employed to describe tumour growth is based on the theory of mixtures. Indeed it consists of a set of mass and momentum balance

equations:

$$\frac{\partial \phi_{\mathrm{s}}}{\partial t} + \nabla \cdot (\phi_{\mathrm{s}} \mathbf{v}_{\mathrm{s}}) = \Gamma_{\mathrm{s}} \tag{3.2}$$

$$\frac{\partial \phi_{\ell}}{\partial t} + \nabla \cdot (\phi_{\ell} \mathbf{v}_{\ell}) = \Gamma_{\ell} \tag{3.3}$$

$$\rho \phi_{\mathrm{s}} \left( \frac{\partial \mathbf{v}_{\mathrm{s}}}{\partial t} + \mathbf{v}_{\mathrm{s}} \cdot \nabla \mathbf{v}_{\mathrm{s}} \right) = \nabla \cdot \widetilde{\mathbb{T}}_{\mathrm{s}} + \rho \phi_{\mathrm{s}} \mathbf{b}_{\mathrm{s}} + \widetilde{\mathbf{m}}_{\mathrm{s}} \tag{3.4}$$

$$\rho \phi_{\ell} \left( \frac{\partial \mathbf{v}_{\ell}}{\partial t} + \mathbf{v}_{\ell} \cdot \nabla \mathbf{v}_{\ell} \right) = \nabla \cdot \widetilde{\mathbb{T}}_{\ell} + \rho \phi_{\ell} \mathbf{b}_{\ell} + \widetilde{\mathbf{m}}_{\ell} \tag{3.5}$$

Both the phases are assumed to be intrinsically incompressible and external body forces (such as the gravitational force) as well as inertial effects are negligible. These assumptions are made in agreement with **[24]**, which states that they are reasonable when dealing with biological problems, since the motion of cells and interstitial fluid is very slow. Thus, equations (3.4) and (3.5) become:

$$\nabla \cdot \widetilde{\mathbb{T}}_{s} + \widetilde{\mathbf{m}}_{s} = 0 \tag{3.6}$$

$$\nabla \cdot \widetilde{\mathbb{T}}_{\ell} + \widetilde{\mathbf{m}}_{\ell} = 0 \tag{3.7}$$

For each phase ($\alpha = s, \ell$), $\phi_\alpha$ denotes the volumetric fraction, $\mathbf{v}_\alpha$ is the velocity, $\widetilde{\mathbb{T}}_\alpha$ is the partial Cauchy stress tensor, $\Gamma_\alpha$ is the mass growth rate and $\widetilde{\mathbf{m}}_\alpha$ represents the rate at which the $\alpha$-th phase exchanges momentum with the other phase. Since we made the saturation assumption, the following has to hold:

$$\phi_s + \phi_\ell = 1 \tag{3.8}$$

Summing equations (3.2) and (3.3) over both phases, using (3.8) and assuming the mixture to be closed with respect to mass (i.e. assuming mass exchanges occur only among the constituents taken into account) yields:

$$\nabla \cdot (\phi_{\mathrm{s}} \mathbf{v}_{\mathrm{s}} + \phi_{\ell} \mathbf{v}_{\ell}) = \Gamma_{\mathrm{s}} + \Gamma_{\ell} = 0 \tag{3.9}$$

The term $\widetilde{\mathbf{m}}_\alpha$ with $\alpha = s, \ell$ in equations (3.6) and (3.7) contains all forces acting on the $\alpha$-th phase due to its interactions with the only other present phase. In **[27]** it is shown, using thermodynamics arguments, that it is given by a dissipative and a non-dissipative part:

$$\widetilde{\mathbf{m}}_\alpha = \widetilde{\mathbf{m}}_\alpha^{(\mathrm{d})} + p \nabla \phi_\alpha \tag{3.10}$$

where $p$ is the pressure of the interstitial fluid. Furthermore, the dissipative part can be expressed as:

$$\widetilde{\mathbf{m}}_\alpha^{(\mathrm{d})} = \overline{\mathbf{m}}_{\alpha\beta} \tag{3.11}$$

where the term $\overline{\mathbf{m}}_{\alpha\beta}$ represents the force acting on the $\alpha$-th phase due to the other phase, denoted by subscript $\beta$. By invoking the action-reaction principle, in our case it holds that:

$$\widetilde{\mathbf{m}}_{\mathrm{s}}^{(\mathrm{d})} = \overline{\mathbf{m}}_{\mathrm{s}\ell} = -\overline{\mathbf{m}}_{\ell\mathrm{s}} = -\widetilde{\mathbf{m}}_{\ell}^{(\mathrm{d})} \tag{3.12}$$

Furthermore, from the theory of mixtures, we know that the Cauchy stress associated with the $\alpha$-th phase of the mixture can be written as a sum of a purely hydrostatic contribution, which indicates the amount of pressure sustained by the $\alpha$-th phase, and an effective stress:

$$\widetilde{\mathbb{T}}_\alpha = -\phi_\alpha p \mathbb{I} + \mathbb{T}_\alpha \tag{3.13}$$

**Mass and momentum balance laws in $\Omega_{\mathrm{t}}(t)$** Firstly, we focus on the region occupied by the tumour. We assume that, in this region, cells proliferate since the tumour is growing: from the closed mixture assumption, it follows that the mass exchange in the cellular phase happens at the expense of the liquid phase. So the mass balance equations become:

$$\frac{\partial \phi_{\mathrm{s}}}{\partial t} + \nabla \cdot (\phi_{\mathrm{s}} \mathbf{v}_{\mathrm{s}}) = \Gamma_{\mathrm{s}} \tag{3.14}$$

$$\frac{\partial \phi_{\ell}}{\partial t} + \nabla \cdot (\phi_{\ell} \mathbf{v}_{\ell}) = -\Gamma_{\mathrm{s}} \tag{3.15}$$

We focus now on the momentum balance equation. Using what we highlighted in (3.10) and (3.13), equations (3.6) and (3.7) become:

$$-\phi_{\mathrm{s}} \nabla p + \nabla \cdot \mathbb{T}_{\mathrm{s}} + \overline{\mathbf{m}}_{s\ell} = \mathbf{0} \tag{3.16}$$

$$-\phi_{\ell} \nabla p + \nabla \cdot \mathbb{T}_{\ell} + \overline{\mathbf{m}}_{\ell s} = \mathbf{0} \tag{3.17}$$

Moreover we require that the effective stress of the fluid phase $\mathbb{T}_{\ell}$ is negligible with respect to the pressure gradient and to the interaction forces between fluid and solid phase. Furthermore, we made the hypothesis:

$$\overline{\mathbf{m}}_{\ell s} = -\mu \phi_{\ell}^2 \mathbb{K}\left(\phi_{\ell}\right)^{-1} \left(\mathbf{v}_{\ell} - \mathbf{v_s}\right) \tag{3.18}$$

As a consequence, we derive from (3.17) the famous Darcy's law as a momentum balance for the fluid phase:

$$\mathbf{v}_{\ell} = \mathbf{v_s} - \frac{\mathbb{K}\left(\phi_{\ell}\right)}{\mu \phi_{\ell}} \nabla p \tag{3.19}$$

where $\mathbf{v}_{\ell}$ is the velocity of the fluid, $\mathbf{v}_s$ is the velocity of the cellular phase, $\mu$ is the dynamic viscosity of the fluid component and $\mathbb{K}\left(\phi_{\ell}\right)$ is the permeability tensor. To account for the anisotropy in the fluid motion due to the presence of white and gray matter fibers in the brain tissue, we can take the permeability tensor as:

$$\mathbb{K}\left(\phi_{\ell}\right) = K\left(\phi_{\ell}\right) \mathbb{A} \tag{3.20}$$

where $\mathbb{A}$ denotes the Eulerian preferential directions tensor. $K\left(\phi_{\ell}\right)$, that for the saturation condition (3.8) could be expressed as a function of $\phi_{\mathrm{s}}$, can take different forms. In order to simplify the model, it could be also considered as a constant term, i.e. $K\left(\phi_{\ell}\right) = k_p$.

On the other hand we will discuss in Section 3.2.4 how it is possible to derive the tensor of preferential directions.

The momentum balance for the mixture can then be obtained by summing (3.16) and (3.17), recalling the saturation condition (3.8) and the action-reaction principle (3.11):

$$-\nabla p + \nabla \cdot \mathbb{T}_{\mathrm{s}} = \mathbf{0} \tag{3.21}$$

**Mass and momentum balance laws in $\Omega_{\mathrm{h}}(t)$** In the domain occupied by the healthy tissue we assume that the proliferation of cells is compensated by natural cell death, so that the rate of growth $\Gamma_{\mathrm{s}}$ is equal to 0. The closed mixture assumption implies that also the source term $\Gamma_{\ell}$ must be null. Hence, the mass balances in the healthy region can be written as:

$$\frac{\partial \phi_{\mathrm{s}}}{\partial t} + \nabla \cdot (\phi_{\mathrm{s}} \mathbf{v}_{\mathrm{s}}) = 0 \tag{3.22}$$

$$\frac{\partial \phi_{\ell}}{\partial t} + \nabla \cdot (\phi_{\ell} \mathbf{v}_{\ell}) = 0 \tag{3.23}$$

As regards momentum balance equations, they are the same as in the region occupied by the tumour, that means equations (3.21) and (3.19).

### 3.2.1 Stress tensor and constitutive equations

In order to close the system of mass and momentum balance equations and to understand how Glioblastoma Multiforme growth influences mechanically the surrounding tissues, we have to determine an appropriate evolution law for the effective part of the Cauchy stress tensor $\mathbb{T}_{\mathrm{s}}$, associated with the cellular tumour population, both in the diseased and in the healthy region. The definition of a realistic constitutive equation for brain tissue is summarized in Subsection 2.1.1 and Section 2.5. Here we derive stress-deformations relationships employing the evolving natural configurations framework [**25**], which are resumed in Section 2.3.

**Effective stress tensor in $\Omega_{\mathrm{t}}(t)$** As we pointed out before we employ a multiplicative decomposition of the deformation gradient:

$$\mathbb{F}_{\mathrm{s}} = \mathbb{F}_{\mathrm{e}} \mathbb{F}_{\mathrm{g}} \tag{3.24}$$

where $\mathbb{F}_{\mathrm{e}}$ represents the elastic contribution while $\mathbb{F}_{\mathrm{g}}$ is the part associated to growth. A consequence of equation (3.24) is that the volumetric part of the deformation gradient, $J_{\mathrm{s}} = \det \mathbb{F}_{\mathrm{s}}$, can be written as:

$$J_{\mathrm{s}} = J_{\mathrm{e}} J_{\mathrm{g}} \tag{3.25}$$

where $J_{\mathrm{e}} = \det \mathbb{F}_{\mathrm{e}}$ and $J_{\mathrm{g}} = \det \mathbb{F}_{\mathrm{g}}$. Since the overall deformation gradient $\mathbb{F}_{\mathrm{s}}$ is assumed to be non singular, from (3.25) it follows that each tensor introduced in (3.24) is non singular as well.

In analogy with [**25**], we assume that the mechanical response is hyperelastic from the natural configuration, in order that the tumour is going to be modelled as a hyperelastic material that is capable of growing. Of course, this is often a simplification of the behavior of the material, which would be better approximated employing a viscoelastic constitutive equation. Nevertheless, in the case of tumour growth, which is a very slow process, the rate dependent response can be neglected without introducing significant errors.
The assumption we made is that the strain energy density $\mathcal{W}_{\mathrm{sn}}$ is of Mooney-Rivlin type, described from equation (2.7). Since the solid phase is considered as an approximately incompressible elastic material, it is better to use the theory developed in [**21**], which is also based on the multiplicative decomposition of the deformation gradient $\mathbb{F}_{\mathrm{s}}$. Let $\overline{\mathbb{C}}_{\mathrm{e}} := J^{-\frac{2}{3}} \mathbb{C}_{\mathrm{e}}$ be the isochoric part of the elastic right Cauchy-Green deformation tensor. We define the strain energy density per unit volume of the natural configuration as a function of the invariants of $\overline{\mathbb{C}}_{\mathrm{e}}$:

$$\widehat{\mathcal{W}}_{\mathrm{sn}} \left( \overline{\mathbb{C}}_{\mathrm{e}} \right) = \frac{1}{2} \mu_{1\mathrm{t}} \left( \mathrm{I}_{\overline{\mathbb{C}}_{\mathrm{e}}} - 3 \right) + \frac{1}{2} \mu_{2\mathrm{t}} \left( \mathrm{II}_{\overline{\mathbb{C}}_{\mathrm{e}}} - 3 \right) \tag{3.26}$$

where

$$\mathrm{I}_{\overline{\mathbb{C}}_\mathrm{e}} = \mathrm{tr}\left(\overline{\mathbb{C}}_\mathrm{e}\right) \tag{3.27}$$

$$\mathrm{II}_{\overline{\mathbb{C}}_\mathrm{e}} = \frac{1}{2}\left[\left(\mathrm{tr}\,\overline{\mathbb{C}}_\mathrm{e}\right)^2 - \mathrm{tr}\left(\overline{\mathbb{C}}_\mathrm{e}^2\right)\right] \tag{3.28}$$

and $\mu_{1\mathrm{t}}$ and $\mu_{2\mathrm{t}}$ are the material parameters of the tumour. As we pointed out in Subsection 2.1.1, if we know the elastic energy $\sigma_\mathrm{s}(\mathbb{F}_\mathrm{e})$ we can express the Cauchy stress tensor of the cellular phase as:

$$\mathbb{T}_\mathrm{s} = \rho_\mathrm{s}\frac{\partial \sigma_\mathrm{s}}{\partial \mathbb{F}_\mathrm{e}}\mathbb{F}_\mathrm{e}^T \tag{3.29}$$

Furthermore, the elastic energy must depend only on the right Cauchy-Green tensor $\mathbb{C}_\mathrm{e} = \mathbb{F}_\mathrm{e}^T\mathbb{F}_\mathrm{e}$ in order to satisfy the material indifference principle, that means:

$$\mathbb{T}_\mathrm{s} = 2\rho_\mathrm{s}\mathbb{F}_\mathrm{e}\frac{\partial \widehat{\sigma}_\mathrm{s}}{\partial \mathbb{C}_\mathrm{e}}\mathbb{F}_\mathrm{e}^T \tag{3.30}$$

During the pure elastic deformation defined by $\mathbb{F}_\mathrm{e}$, the typical assumption is that the mass is preserved, so it is possible to relate the energy function to the strain energy density function as follows:

$$\widehat{\mathcal{W}}_\mathrm{sn} = \widehat{\sigma}_\mathrm{s}\rho_\mathrm{sn} = \widehat{\sigma}_\mathrm{s}\rho_\mathrm{s}J_\mathrm{e} = \widehat{\sigma}_\mathrm{s}\rho_\mathrm{s}\phi_\mathrm{s}^{-1}\phi_\mathrm{sn} = \widehat{\sigma}_\mathrm{s}\widehat{\rho}_\mathrm{s}\phi_\mathrm{sn} \tag{3.31}$$

where $\widehat{\rho}_\mathrm{s}$ denotes the true mass density of the solid phase, $\rho_\mathrm{s} = \widehat{\rho}_\mathrm{s}\phi_\mathrm{s}$ is the apparent mass density and $\phi_\mathrm{sn}$ is the volumetric fraction of the cell phase in the natural state. In (3.31) we have imposed mass conservation between the natural and the current configuration in the following way:

$$\rho_\mathrm{sn} = J_\mathrm{e}\rho_\mathrm{s} \tag{3.32}$$

Then, we made the hypothesis that the solid phase is incompressible, that means $\widehat{\rho}_\mathrm{s}$ is a constant. In this way it is possible to rewrite (3.32) as:

$$\phi_\mathrm{sn} = J_\mathrm{e}\phi_\mathrm{s} \tag{3.33}$$

Finally, using (3.30), (3.31) and (3.33), we can derive the expression for the Cauchy stress of the solid phase:

$$\begin{aligned}
\mathbb{T}_\mathrm{s} &= 2\rho_\mathrm{s}\mathbb{F}_\mathrm{e}\frac{\partial \widehat{\sigma}_\mathrm{S}}{\partial \mathbb{C}_\mathrm{e}}\mathbb{F}_\mathrm{e}^T \\
&= 2\frac{\widehat{\rho}_\mathrm{s}\phi_\mathrm{s}}{\widehat{\rho}_\mathrm{s}\phi_\mathrm{sn}}\mathbb{F}_\mathrm{e}\frac{\partial \widehat{\mathcal{W}}_\mathrm{sn}}{\partial \mathbb{C}_\mathrm{e}}\mathbb{F}_\mathrm{e}^T \\
&= 2\frac{\phi_\mathrm{s}}{\phi_\mathrm{sn}}\mathbb{F}_\mathrm{e}\frac{\partial \widehat{\mathcal{W}}_\mathrm{sn}}{\partial \mathbb{C}_\mathrm{e}}\mathbb{F}_\mathrm{e}^T \\
&= 2J_\mathrm{e}^{-1}\mathbb{F}_\mathrm{e}\frac{\partial \widehat{\mathcal{W}}_\mathrm{sn}}{\partial \mathbb{C}_\mathrm{e}}\mathbb{F}_\mathrm{e}^T
\end{aligned}$$

So we obtain that the constitutive expression of the Cauchy stress tensor $\mathbb{T}_\mathrm{s}$:

$$\mathbb{T}_\mathrm{s} = 2J_\mathrm{e}^{-1}\mathbb{F}_\mathrm{e}\frac{\partial \widehat{\mathcal{W}}_\mathrm{sn}}{\partial \mathbb{C}_\mathrm{e}}\mathbb{F}_\mathrm{e}^T \quad \text{in } \Omega_\mathrm{t}(t) \tag{3.34}$$

Then, we have to compute:

$$\frac{\partial \widehat{\mathcal{W}}_{\mathrm{sn}}\left(\overline{\mathbb{C}}_{\mathrm{e}}\right)}{\partial \mathbb{C}_{\mathrm{e}}} = \frac{\partial \overline{\mathbb{C}}_{\mathrm{e}}}{\partial \mathbb{C}_{\mathrm{e}}} \frac{\partial \widehat{\mathcal{W}}_{\mathrm{sn}}}{\partial \overline{\mathbb{C}}_{\mathrm{e}}} \tag{3.35}$$

We first use some tensor algebra to calculate the derivative of $\overline{\mathbb{C}}_{\mathrm{e}}$ with respect to $\mathbb{C}_{\mathrm{e}}$:

$$\begin{aligned}\frac{\partial \overline{\mathbb{C}}_{\mathrm{e}}}{\partial \mathbb{C}_{\mathrm{e}}} &= \frac{\partial}{\partial \mathbb{C}_{\mathrm{e}}}\left(J_{\mathrm{e}}^{-2/3}\mathbb{C}_{\mathrm{e}}\right) \\ &= J_{\mathrm{e}}^{-2/3}\frac{\partial \mathbb{C}_{\mathrm{e}}}{\partial \mathbb{C}_{\mathrm{e}}} + \mathbb{C}_{\mathrm{e}} \otimes \frac{\partial}{\partial \mathbb{C}_{\mathrm{e}}}\left(J_{\mathrm{e}}^{-2/3}\right) \\ &= J_{\mathrm{e}}^{-2/3}\underline{\underline{\mathbb{I}}} - \frac{1}{3}J_{\mathrm{e}}^{-8/3}\mathbb{C}_{\mathrm{e}} \otimes \frac{\partial\left(\det \mathbb{C}_{\mathrm{e}}\right)}{\partial \mathbb{C}_{\mathrm{e}}}\end{aligned} \tag{3.36}$$

where in the last passage we have denoted by $\underline{\underline{\mathbb{I}}}$ the fourth-order identity tensor and used the fact that:

$$\begin{aligned}\frac{\partial J_{\mathrm{e}}^{-2/3}}{\partial \mathbb{C}_{\mathrm{e}}} &= \frac{\partial J_{\mathrm{e}}^{-2/3}}{\partial\left(\det \mathbb{C}_{\mathrm{e}}\right)}\frac{\partial\left(\det \mathbb{C}_{\mathrm{e}}\right)}{\partial \mathbb{C}_{\mathrm{e}}} = \frac{1}{2J_{\mathrm{e}}}\frac{\partial J_{\mathrm{e}}^{-2/3}}{\partial J_{\mathrm{e}}}\frac{\partial\left(\det \mathbb{C}_{\mathrm{e}}\right)}{\partial \mathbb{C}_{\mathrm{e}}} \\ &= \frac{1}{2J_{\mathrm{e}}}\left(-\frac{2}{3}J_{\mathrm{e}}^{-5/3}\right)\frac{\partial\left(\det \mathbb{C}_{\mathrm{e}}\right)}{\partial \mathbb{C}_{\mathrm{e}}} \\ &= -\frac{1}{3}J_{\mathrm{e}}^{-8/3}\frac{\partial\left(\det \mathbb{C}_{\mathrm{e}}\right)}{\partial \mathbb{C}_{\mathrm{e}}}\end{aligned}$$

Hence, going on from (3.36), we have:

$$\frac{\partial \overline{\mathbb{C}}_{\mathrm{e}}}{\partial \mathbb{C}_{\mathrm{e}}} = J_{\mathrm{e}}^{-2/3}\underline{\underline{\mathbb{I}}} - \frac{1}{3}J_{\mathrm{e}}^{-2/3}\mathbb{C}_{\mathrm{e}} \otimes \mathbb{C}_{\mathrm{e}}^{-1} \tag{3.37}$$

since

$$\frac{\partial\left(\det \mathbb{C}_{\mathrm{e}}\right)}{\partial \mathbb{C}_{\mathrm{e}}} = \mathbb{C}_{\mathrm{e}}^2 - I_{\mathbb{C}_{\mathrm{e}}}\mathbb{C}_{\mathrm{e}} + II_{\mathbb{C}_{\mathrm{e}}}\mathbb{I}$$

and by the Cayley-Hamilton theorem:

$$\mathbb{C}_{\mathrm{e}}^2 - I_{\mathbb{C}_{\mathrm{e}}}\mathbb{C}_{\mathrm{e}} + II_{\mathbb{C}_{\mathrm{e}}}\mathbb{I} = III_{\mathbb{C}_{\mathrm{e}}}\mathbb{C}_{\mathrm{e}}^{-1} = J_{\mathrm{e}}^2\mathbb{C}_{\mathrm{e}}^{-1}$$

Therefore, we can write:

$$\begin{aligned}\frac{\partial \overline{\mathbb{C}}_{\mathrm{e}}}{\partial \mathbb{C}_{\mathrm{e}}} &= J_{\mathrm{e}}^{-2/3}\left(\underline{\underline{I}} - \frac{1}{3}\mathbb{C}_{\mathrm{e}} \otimes \mathbb{C}_{\mathrm{e}}^{-1}\right) \\ &= J_{\mathrm{e}}^{-2/3}\left(\underline{\underline{I}} - \frac{1}{3}J_{\mathrm{e}}^{2/3}\overline{\mathbb{C}}_{\mathrm{e}} \otimes \mathbb{C}_{\mathrm{e}}^{-1}\right) \\ &= J_{\mathrm{e}}^{-2/3}\left(\underline{\underline{I}} - \frac{1}{3}\overline{\mathbb{C}}_{\mathrm{e}} \otimes \left(J_{\mathrm{e}}^{-2/3}\mathbb{C}_{\mathrm{e}}\right)^{-1}\right) \\ &= J_{\mathrm{e}}^{-2/3}\left(\underline{\underline{I}} - \frac{1}{3}\overline{\mathbb{C}}_{\mathrm{e}} \otimes \overline{\mathbb{C}}_{\mathrm{e}}^{-1}\right)\end{aligned} \tag{3.38}$$

At the end we have:

$$\frac{\partial \widehat{\mathcal{W}}_{\mathrm{sn}}\left(\overline{\mathbb{C}}_{\mathrm{e}}\right)}{\partial \mathbb{C}_{\mathrm{e}}} = J_{\mathrm{e}}^{-2/3}\left(\underline{\underline{I}} - \frac{1}{3}\overline{\mathbb{C}}_{\mathrm{e}}^{-1} \otimes \overline{\mathbb{C}}_{\mathrm{e}}\right)\frac{\partial \widehat{\mathcal{W}}_{\mathrm{sn}}}{\partial \overline{\mathbb{C}}_{\mathrm{e}}} \tag{3.39}$$

For simplicity, we denote by $\mathbb{W}$ the right side of (3.39), i.e.

$$\mathbb{W} := J_{\mathrm{e}}^{-2/3}\left(\underline{\underline{I}} - \frac{1}{3}\overline{\mathbb{C}}_{\mathrm{e}}^{-1} \otimes \overline{\mathbb{C}}_{\mathrm{e}}\right)\frac{\partial \widehat{\mathcal{W}}_{\mathrm{sn}}}{\partial \overline{\mathbb{C}}_{\mathrm{e}}} \tag{3.40}$$

The constitutive expression of the Cauchy stress tensor $\mathbb{T}_{\mathrm{s}}$ is then:

$$\mathbb{T}_{\mathrm{s}} = 2J_{\mathrm{e}}^{-1}\mathbb{F}_{\mathrm{e}}\mathbb{W}\mathbb{F}_{\mathrm{e}}^{T} \quad \text{in } \Omega_{\mathrm{t}}(t) \tag{3.41}$$

The constitutive expression of the Cauchy stress tensor $\mathbb{T}_{\mathrm{s}}$ should be accompanied by equations determining $\mathbb{F}_{\mathrm{s}}$ and $\mathbb{F}_{\mathrm{g}}$. By the way, the tensor $\mathbb{F}_{\mathrm{s}}$ is entirely determined by the motion of the cell phase and for this reason it is not an additional unknown for the model:

$$\dot{\mathbb{F}}_{\mathrm{s}}\mathbb{F}_{\mathrm{s}}^{-1} = \nabla \mathbf{v}_{\mathrm{s}} \tag{3.42}$$

So it remains to determine $\mathbb{F}_{\mathrm{g}}$ by solving appropriate evolution equations. The evolution of $\mathbb{F}_{\mathrm{g}}$ can be obtained through equation (3.14), as suggested in [**27**, **29**]. First of all, we multiply it by $J_s$ and the we rewrite it on the reference configuration as:

$$\overline{J_{\mathrm{s}}\phi_{\mathrm{s}}}^{\,\cdot} = J_{\mathrm{s}}\Gamma_{\mathrm{s}} \tag{3.43}$$

Secondly, we recall that $\widehat{\rho}_\alpha$ denotes the true mass density of each phase and $\rho_\alpha = \widehat{\rho}_\alpha\phi_\alpha$ the apparent mass density; in this way $\rho_{\mathrm{sr}} = J_{\mathrm{s}}\rho_{\mathrm{s}}$ is the mass density of the solid phase in the reference configuration, while $\rho_{\mathrm{sn}} = J_{\mathrm{e}}\rho_{\mathrm{s}}$ is the mass density of the solid phase in the natural configuration. Considering the cell phase incompressible and using (3.25) and (3.33), we obtain:

$$\phi_{\mathrm{sr}} = J_{\mathrm{s}}\phi_{\mathrm{s}} = J_{\mathrm{e}}J_{\mathrm{g}}\phi_{\mathrm{s}} = J_{\mathrm{g}}\phi_{\mathrm{sn}} \tag{3.44}$$

where $\phi_{\mathrm{sr}}$ is the volumetric fraction of the solid phase in the reference configuration. Then, substituting into (3.43) and recalling (3.44), we obtain:

$$\overline{J_{\mathrm{g}}\phi_{\mathrm{sn}}}^{\,\cdot} = J_{\mathrm{s}}\Gamma_{\mathrm{s}} \tag{3.45}$$

$$J_{\mathrm{g}}\dot{\phi}_{\mathrm{sn}} + \phi_{\mathrm{sn}}\dot{J}_{\mathrm{g}} = J_{\mathrm{s}}\Gamma_{\mathrm{s}} \tag{3.46}$$

If we call $\mathbb{L}_{\mathrm{g}}$ the strain rate tensor (or velocity gradient) associated to $\mathbb{F}_{\mathrm{g}}$, i.e.

$$\mathbb{L}_{\mathrm{g}} = \dot{\mathbb{F}}_{\mathrm{g}}\mathbb{F}_{\mathrm{g}}^{-1} \tag{3.47}$$

it holds from standard calculus that

$$\dot{J}_{\mathrm{g}} = J_{\mathrm{g}}\mathrm{tr}\left(\mathbb{L}_{\mathrm{g}}\right) \tag{3.48}$$

If we introduce this result in (3.46), we obtain:

$$\dot{\phi}_{\mathrm{sn}}J_{\mathrm{g}} + J_{\mathrm{g}}\phi_{\mathrm{sn}}\,\mathrm{tr}\left(\mathbb{L}_{\mathrm{g}}\right) = J_{\mathrm{s}}\Gamma_{\mathrm{s}} \tag{3.49}$$

Following what is done in [**25**, **27**, **29**], we make the assumption that the rate of mass change of the solid phase is entirely compensated by the volume change due to growth. This requirement leads to:

$$\phi_{\mathrm{s}}\,\mathrm{tr}\left(\mathbb{L}_{\mathrm{g}}\right) = \Gamma_{\mathrm{s}} \tag{3.50}$$

Multiplying both sides of (3.50) by $J_\mathrm{s}$:

$$J_\mathrm{s}\phi_\mathrm{s}\,\mathrm{tr}\left(\mathbb{L}_\mathrm{g}\right) = J_\mathrm{s}\Gamma_\mathrm{s} \tag{3.51}$$

which, if we recall (3.44), it is equivalent to:

$$J_\mathrm{g}\phi_\mathrm{sn}\,\mathrm{tr}\left(\mathbb{L}_\mathrm{g}\right) = J_\mathrm{s}\Gamma_\mathrm{s} \tag{3.52}$$

Observing (3.49) and (3.52), we can conclude that $\phi_\mathrm{sn}$ is constant in time and it can be assumed known from the outset.

We will discuss in Section 3.2.4 the assumption made for the anisotropic growth tensor $\mathbb{F}_\mathrm{g}$ and consequentely we will derive its evolution, in order to satisfy (3.50).

**Effective stress tensor in $\Omega_\mathrm{h}(t)$** We have said before that in the host healthy tissue, the net source term $\Gamma_\mathrm{s}$ is null, since the death of healthy cells is compensated by proliferation. This implies that the multiplicative decomposition is not needed and so the Cauchy stress tensor for the cell phase can be derived using a plain hyperelastic constitutive equation. We still consider that the host cell population behaves as an approximately incompressible elastic material and we assume a Mooney-Rivlin strain energy density function $\mathcal{W}_\mathrm{s}$ in the healthy region, expressed per unit volume:

$$\widehat{\mathcal{W}}_\mathrm{s}\left(\overline{\mathbb{C}}_\mathrm{e}\right) = \frac{1}{2}\mu_{1\mathrm{h}}\left(\mathrm{I}_{\overline{\mathbb{C}}_\mathrm{e}} - 3\right) + \frac{1}{2}\mu_{2\mathrm{h}}\left(\mathrm{II}_{\overline{\mathbb{C}}_\mathrm{e}} - 3\right) \tag{3.53}$$

where $\mu_{1\mathrm{h}}$, $\mu_{2\mathrm{h}}$ are the material parameters of the host tissue, $\mathbb{F}_\mathrm{e}$ is the elastic deformation gradient tensor of the healthy region and $\overline{\mathbb{C}}_\mathrm{e} = J^{-\frac{2}{3}}\mathbb{C}_\mathrm{e}$ is the isochoric part of elastic right Cauchy-Green deformation tensor.
In conclusion, the Cauchy stress tensor of the solid phase in the healthy domain is given by:

$$\mathbb{T}_\mathrm{s} = \frac{2}{J_\mathrm{e}}\mathbb{F}_\mathrm{e}\frac{\partial\widehat{\mathcal{W}}_\mathrm{s}}{\partial\mathbb{C}_\mathrm{e}}\mathbb{F}_\mathrm{e}^T = \frac{2}{J_\mathrm{e}}\mathbb{F}_\mathrm{e}\mathbb{W}\mathbb{F}_\mathrm{e}^T \quad \text{in } \Omega_\mathrm{h}(t) \tag{3.54}$$

with $\mathbb{W}$ is defined in (3.40).
In principle, the strain energy density function of the healthy tissue might be different from the one describing the elastic behaviour of the tumour tissue, i.e. the material parameters could not be the same.

### 3.2.2 Nutrients

The rate of tumour growth $\Gamma_\mathrm{s}$ is influenced by many different factors, but of course the amount of nutrients plays a fundamental role, because it strongly affects the cells capability to duplicate. Consequently, it is necessary to introduce in the model an equation describing their evolution in the domain. We assume that nutrients are transported by the fluid phase and they can diffuse into it. On the other side, they are taken by the growing tumour and uniformly supplied by the vasculature. We introduce the hypotesis that the nutrients absorbed by the healthy tissue are immediately replaced by the vasculature, whereas the nutrients uptake by the tumour tissue is not negligible. Following these hypothesis we can write the mass balance equation governing the concentration of available nutrients $c_n$ normalized with respect to the physiological concentration, so that $c_n \in [0, 1]$:

$$\frac{\partial}{\partial t}\left(\phi_\ell c_n\right) + \nabla\cdot\left(\phi_\ell c_n \mathbf{v}_\ell\right) = \nabla\cdot\left(\phi_\ell \mathbb{D}\nabla c_n\right) + \Gamma_\ell c_n + G_n \tag{3.55}$$

where $\phi_\ell$ is the volumetric fraction of the fluid phase, $\mathbf{v}_\ell$ is the velocity of the same phase, $\mathbb{D}$ is the Eulerian diffusion tensor and $G_n$ is the source term which accounts for absorption of nutrients by the tumour and increasing in concentration due to incoming nutrients. We will discuss about $\mathbb{D}$ in Section 3.2.4. Using standard calculus techniques, we can rewrite (3.55) as:

$$c_n \frac{\partial \phi_\ell}{\partial t} + \phi_\ell \frac{\partial c_n}{\partial t} + \phi_\ell \mathbf{v}_\ell \cdot \nabla c_n + c_n \nabla \cdot (\phi_\ell \mathbf{v}_\ell) = \nabla \cdot (\phi_\ell \mathbb{D} \nabla c_n) + \Gamma_\ell c_n + G_n \quad (3.56)$$

If we recall the mass balance equation of the fluid phase (3.15), (3.56) can be rephrased as:

$$\frac{\partial c_n}{\partial t} + \mathbf{v}_\ell \cdot \nabla c_n = \frac{1}{\phi_\ell} \nabla \cdot (\phi_\ell \mathbb{D} \nabla c_n) + \frac{G_n}{\phi_\ell} \quad (3.57)$$

In particular, we will consider the following form for the source term:

$$G_n = [-\zeta \phi_{\mathrm{s}} \phi_\ell c_n + S_n (1 - c_n) \phi_\ell] \quad (3.58)$$

This expression is valid only in the tumour domain and it describes the fact that nutrients are consumed by the tumour with a constant rate $\zeta$. Furthermore, nutrients are supplied by the vasculature at a rate $S_n$ as far as their concentration is below the physiological value ($c_n < 1$). The consumption and the delivery of nutrients is also weighted with a factor $\phi_\ell$ to mathematically assert that the more fluid phase is available, the greater uptake or supply of nutrients can be provided. On the other hand, in the healthy region we assume that production and absorption of nutrients are reciprocally balanced, so in that case $G_n = 0$. Considering the formulation of $G_n$ assumed in (3.58), the final equation describing the evolution of normalized nutrients concentration becomes:

$$\frac{\partial c_n}{\partial t} + \mathbf{v}_\ell \cdot \nabla c_n = \frac{1}{\phi_\ell} \nabla \cdot (\phi_\ell \mathbb{D} \nabla c_n) + [-\zeta \phi_{\mathrm{s}} c_n + S_n (1 - c_n)] \qquad \text{in } \Omega_{\mathrm{t}}(t) \quad (3.59)$$

$$\frac{\partial c_n}{\partial t} + \mathbf{v}_\ell \cdot \nabla c_n = \frac{1}{\phi_\ell} \nabla \cdot (\phi_\ell \mathbb{D} \nabla c_n) \qquad \text{in } \Omega_{\mathrm{h}}(t) \quad (3.60)$$

### 3.2.3 Cell net proliferation rate

We can now express the cell net proliferation rate $\Gamma_{\mathrm{s}}$, after having introduced the equation which describes the available nutrients. As first approximation, we assume the following constitutive equation:

$$\Gamma_{\mathrm{s}} = \nu \phi_{\mathrm{s}} (1 - \phi_{\mathrm{s}}) (c_n - c_0)_+ \quad (3.61)$$

where $(\cdot)_+$ denotes the positive part and $\nu$ is a positive coefficient. In this constitutive equation emerges that the proliferation rate depends linearly on the available concentration of nutrients $c_n$, provided that it is greater than a threshold $c_0$: this can be thought of as the hypoxia threshold, below which tumour cells stop duplicating. On the other hand, as long as $c_n > c_0$, the cell phase is allowed to grow and the proliferation is proportional to the difference between the actual nutrients concentration and the hypoxia threshold. Moreover, the growth depends on the fraction of cells that is already present since cell population grows by duplication. At the end, there is a factor $(1 - \phi_{\mathrm{s}})$, that accounts for the phenomenon of contact inhibition, i.e. the proliferation rate is decreased as the cellular phase fills all the available space.

An alternative formulation consists in the introduction of a volumetric fraction threshold $\phi_{\max}$, as follows:

$$\Gamma_{\mathrm{s}} = \nu\phi_{\mathrm{s}}\left(\phi_{\max} - \phi_{\mathrm{s}}\right)\left(c_n - c_0\right)_+ \tag{3.62}$$

Of course more complicate relation exist. One example is reported in **[29]**, which includes explicitly the role of stresses:

$$\Gamma_{\mathrm{s}} = \nu\phi_{\mathrm{s}}\left(\phi_{\max} - \phi_{\mathrm{s}}\right)\left(c_n - c_0\right)_+\left(1 - \delta_1\frac{(\Sigma)_+}{(\Sigma)_+\delta_2}\right) \tag{3.63}$$

where $\delta_1 < 1$, $\delta_2$ are positive constants that account for the role of mechanical stress on cell proliferation and $\Sigma$ can be for example the isotropic part of the Cauchy stress, namely:

$$\Sigma = -\frac{1}{3}\operatorname{tr}\left(\mathbb{T}_{\mathrm{s}}\right) \tag{3.64}$$

This choice is made in order to reproduce growth inhibition due to compression, but other forms are possible.
However, in our model, we consider the cell net proliferation rate $\Gamma_{\mathrm{s}}$ described in (3.62).

### 3.2.4 Diffusion tensor $\mathbb{D}$, preferential directions tensor $\mathbb{A}$ and growth tensor $\mathbb{F}_{\mathrm{g}}$

Assuming known the initial time diffusion tensor $\mathbb{D}_0$, obtained through DTI imaging, we can derive an expression for the diffusion tensor $\mathbb{D}$, the preferential directions tensor $\mathbb{A}$ and the growth tensor $\mathbb{F}_{\mathrm{g}}$.

**Diffusion tensor** If we call $\lambda_1$, $\lambda_2$ and $\lambda_3$ the eigenvalues (considered in decreasing order) of $\mathbb{D}_0$ and $\mathbf{e}_1$, $\mathbf{e}_2$ and $\mathbf{e}_3$ the corresponding undeformed eigenvectors, we can equivalently write $\mathbb{D}_0$ as:

$$\mathbb{D}_0 = \lambda_1\mathbf{e}_1 \otimes \mathbf{e}_1 + \lambda_2\mathbf{e}_2 \otimes \mathbf{e}_2 + \lambda_3\mathbf{e}_3 \otimes \mathbf{e}_3 \tag{3.65}$$

It is important to notice that the eigenvectors $\mathbf{e}_1$, $\mathbf{e}_2$ and $\mathbf{e}_3$ could be supposed orthogonal, since $\mathbb{D}_0$ is symmetric. Over time, the eigenvectors will deform through $\mathbb{F}_{\mathrm{s}}$, i.e. they become $\mathbb{F}_{\mathrm{s}}\mathbf{e}_1$, $\mathbb{F}_{\mathrm{s}}\mathbf{e}_2$ and $\mathbb{F}_{\mathrm{s}}\mathbf{e}_3$. So we obtain the Eulerian diffusion tensor through a push-forward of the Lagrangian $\mathbb{D}_0$:

$$\mathbb{D} = \lambda_1\mathbb{F}_{\mathrm{s}}\mathbf{e}_1\mathbf{e}_1^T\mathbb{F}_{\mathrm{s}}^T + \lambda_2\mathbb{F}_{\mathrm{s}}\mathbf{e}_2\mathbf{e}_2^T\mathbb{F}_{\mathrm{s}}^T + \lambda_3\mathbb{F}_{\mathrm{s}}\mathbf{e}_3\mathbf{e}_3^T\mathbb{F}_{\mathrm{s}}^T = \mathbb{F}_{\mathrm{s}}\mathbb{D}_0\mathbb{F}_{\mathrm{s}}^T \tag{3.66}$$

**Preferential directions tensor** We can define the inital time tensor $\widehat{\mathbb{A}_0}$ as follows:

$$\widehat{\mathbb{A}_0} = a_1(r)\lambda_1\mathbf{e}_1 \otimes \mathbf{e}_1 + a_2(r)\lambda_2\mathbf{e}_2 \otimes \mathbf{e}_2 + a_3(r)\lambda_3\mathbf{e}_3 \otimes \mathbf{e}_3 \tag{3.67}$$

where:

$$\begin{bmatrix} a_1(r) \\ a_2(r) \\ a_3(r) \end{bmatrix} = \begin{bmatrix} r & r & 1 \\ 1 & r & 1 \\ 1 & 1 & 1 \end{bmatrix} \begin{bmatrix} c_l \\ c_p \\ c_s \end{bmatrix} \tag{3.68}$$

The parameter $r \in \mathbb{R}$ is a measure of anisotrophy (if $r > 1$ it gives greater weight to the anisotrophic behaviour), while $c_l$, $c_p$ and $c_s$ are called linear, planar and spherical index, respectively. They are defined as follows:

$$c_l = \frac{\lambda_1 - \lambda_2}{\lambda_1 + \lambda_2 + \lambda_3}, \quad c_p = \frac{2\left(\lambda_2 - \lambda_3\right)}{\lambda_1 + \lambda_2 + \lambda_3}, \quad c_s = \frac{3\lambda_3}{\lambda_1 + \lambda_2 + \lambda_3} \tag{3.69}$$

The meaning of these coefficients can be derived from their definitions: if $c_l \approx 1$ there is only one preferential direction, identified by the first eigenvector of the tensor (monodirectional growth); if $c_p \approx 1$ there are two dominating directions that do not prevail over each other (planar growth); finally, if $c_s \approx 1$, there is no preferential direction at all and the tensor is isotropic (spherical growth). Clearly, it holds the condition $c_l + c_p + c_s = 1$. Finally, we can define the inizial time preferential directions tensor as:

$$\mathbb{A}_0 = \frac{3\widehat{\mathbb{A}_0}}{\mathrm{tr}(\widehat{\mathbb{A}_0})} \tag{3.70}$$

In this way we have that $\mathrm{tr}(\mathbb{A}_0) = 3$. As said before, we obtain the Eulerian tensor through a push-forward of the Lagrangian $\mathbb{A}_0$:

$$\mathbb{A} = a_1(r)\lambda_1\mathbb{F}_\mathrm{s}\mathbf{e}_1\mathbf{e}_1^T\mathbb{F}_\mathrm{s}^T + a_2(r)\lambda_2\mathbb{F}_\mathrm{s}\mathbf{e}_2\mathbf{e}_2^T\mathbb{F}_\mathrm{s}^T + a_3(r)\lambda_3\mathbb{F}_\mathrm{s}\mathbf{e}_3\mathbf{e}_3^T\mathbb{F}_\mathrm{s}^T = \mathbb{F}_\mathrm{s}\mathbb{A}_0\mathbb{F}_\mathrm{s}^T \tag{3.71}$$

**Anisotropic growth tensor** For what concerns the growth tensor $\mathbb{F}_\mathrm{g}$, the condition (3.50) has to hold. Remembering the equality (3.48), it becomes:

$$\frac{\dot{J}_\mathrm{g}}{J_\mathrm{g}} = \frac{\Gamma_\mathrm{s}}{\phi_\mathrm{s}}, \quad \text{where } J_\mathrm{g} = \det \mathbb{F}_\mathrm{g} \tag{3.72}$$

We can express $\mathbb{F}_\mathrm{g}$ in the eigenvectors basis:

$$\mathbb{F}_\mathrm{g} = g_1\mathbf{e}_1 \otimes \mathbf{e}_1 + g_2\mathbf{e}_2 \otimes \mathbf{e}_2 + g_3\mathbf{e}_3 \otimes \mathbf{e}_3 \tag{3.73}$$

Now it is important to define the anisotropic evolution of $g_1$, $g_2$ and $g_3$, in order to respect the different cases of monodirectional, planar and spherical growth. We will take into consideration the following evolution:

$$\frac{\dot{g}_1}{g_1} = \frac{\lambda_1 a_1(r)}{\lambda_1 a_1(r) + \lambda_2 a_2(r) + \lambda_3 a_3(r)}\frac{\Gamma_\mathrm{s}}{\phi_\mathrm{s}}, \qquad \text{with } g_1(0) = 1 \tag{3.74}$$

$$\frac{\dot{g}_2}{g_2} = \frac{\lambda_2 a_2(r)}{\lambda_1 a_1(r) + \lambda_2 a_2(r) + \lambda_3 a_3(r)}\frac{\Gamma_\mathrm{s}}{\phi_\mathrm{s}}, \qquad \text{with } g_2(0) = 1 \tag{3.75}$$

$$\frac{\dot{g}_3}{g_3} = \frac{\lambda_3 a_3(r)}{\lambda_1 a_1(r) + \lambda_2 a_2(r) + \lambda_3 a_3(r)}\frac{\Gamma_\mathrm{s}}{\phi_\mathrm{s}}, \qquad \text{with } g_3(0) = 1 \tag{3.76}$$

We will briefly show that the tensor (3.73), associated with the evolutions (3.74), (3.75) and (3.76), satisfies (3.72). Since the determinant is the product of the eigenvalues, we have:

$$J_\mathrm{g} = g_1 g_2 g_3 \tag{3.77}$$

$$\dot{J}_\mathrm{g} = \dot{g}_1 g_2 g_3 + g_1 \dot{g}_2 g_3 + g_1 g_2 \dot{g}_3 \tag{3.78}$$

By replacing (3.77) and (3.78) in (3.72), we obtain:

$$\frac{\dot{g}_1}{g_1} + \frac{\dot{g}_2}{g_2} + \frac{\dot{g}_3}{g_3} = \frac{\Gamma_\mathrm{s}}{\phi_\mathrm{s}} \tag{3.79}$$

and remembering (3.74), (3.75) and (3.76), we have that (3.72) holds.

### 3.2.5 The complete Eulerian model

In the following, we collect together the equations governing the evolution of the system that we have developed in the previous sections.
The set of equations in the domain $\Omega_{\mathrm{t}}(t)$ is then:

$$\frac{\partial \phi_{\mathrm{s}}}{\partial t} + \nabla \cdot (\phi_{\mathrm{s}} \mathbf{v}_{\mathrm{s}}) = \Gamma_{\mathrm{s}} \tag{3.80a}$$
$$\frac{\partial \phi_{\ell}}{\partial t} + \nabla \cdot (\phi_{\ell} \mathbf{v}_{\ell}) = -\Gamma_{\mathrm{s}} \tag{3.80b}$$
$$\phi_{\ell} + \phi_{\mathrm{s}} = 1 \tag{3.80c}$$
$$-\nabla p + \nabla \cdot \mathbb{T}_{\mathrm{s}} = \mathbf{0} \tag{3.80d}$$
$$\mathbf{v}_{\ell} = \mathbf{v}_{\mathrm{s}} - \frac{\mathbb{K}(\phi_{\ell})}{\mu \phi_{\ell}} \nabla p \tag{3.80e}$$
$$\dot{\mathbb{F}}_{\mathrm{s}} \mathbb{F}_{\mathrm{s}}^{-1} = \nabla \mathbf{v}_{\mathrm{s}} \tag{3.80f}$$
$$\frac{\partial c_n}{\partial t} + \mathbf{v}_{\ell} \cdot \nabla c_n = \frac{1}{\phi_{\ell}} \nabla \cdot (\phi_{\ell} \mathbb{D} \nabla c_n) + \left[-\zeta \phi_{\mathrm{s}} c_n + S_n (1 - c_n)\right] \tag{3.80g}$$

where

$$\mathbb{F}_{\mathrm{e}} = \mathbb{F}_{\mathrm{s}} \mathbb{F}_{\mathrm{g}}^{-1} \tag{3.81a}$$
$$\mathcal{W}_{\mathrm{sn}}\left(\overline{\mathbb{C}}_{\mathrm{e}}\right) = \left[\frac{1}{2}\mu_{1\mathrm{t}}\left(\mathrm{I}_{\overline{\mathbb{C}}_{\mathrm{e}}} - 3\right) + \frac{1}{2}\mu_{2\mathrm{t}}\left(\mathrm{II}_{\overline{\mathbb{C}}_{\mathrm{e}}} - 3\right)\right] \tag{3.81b}$$
$$\mathbb{T}_{\mathrm{s}} = 2 J_{\mathrm{e}}^{-1} \mathbb{F}_{\mathrm{e}} \mathbb{W} \mathbb{F}_{\mathrm{e}}^{T} \tag{3.81c}$$
$$\mathbb{K}(\phi_{\ell}) = K(\phi_{\ell}) \mathbb{A} \tag{3.81d}$$
$$\Gamma_{\mathrm{s}} = \nu \phi_{\mathrm{s}} (\phi_{\max} - \phi_{\mathrm{s}}) (c_n - c_0)_{+} \tag{3.81e}$$

Furthermore, $\mathbb{D}$, $\mathbb{A}$ and $\mathbb{F}_{\mathrm{g}}$ are defined as in Section 3.2.4, with the evolution for $g_1$, $g_2$ and $g_3$ presented in (3.74), (3.75) and (3.76). The tensor $\mathbb{W}$ has the expression reported in (3.40). Furthermore, we will consider $K(\phi_{\ell})$ as a constant, i.e. $K(\phi_{\ell}) = k_p$.
On the other hand, the set of equations in the domain $\Omega_{\mathrm{h}}(t)$ is:

$$\frac{\partial \phi_{\mathrm{s}}}{\partial t} + \nabla \cdot (\phi_{\mathrm{s}} \mathbf{v}_{\mathrm{s}}) = 0 \tag{3.82a}$$
$$\frac{\partial \phi_{\ell}}{\partial t} + \nabla \cdot (\phi_{\ell} \mathbf{v}_{\ell}) = 0 \tag{3.82b}$$
$$\phi_{\ell} + \phi_{\mathrm{s}} = 1 \tag{3.82c}$$
$$-\nabla p + \nabla \cdot \mathbb{T}_{\mathrm{s}} = \mathbf{0} \tag{3.82d}$$
$$\mathbf{v}_{\ell} = \mathbf{v}_{\mathrm{s}} - \frac{\mathbb{K}(\phi_{\ell})}{\mu \phi_{\ell}} \nabla p \tag{3.82e}$$
$$\dot{\mathbb{F}}_{\mathrm{s}} \mathbb{F}_{\mathrm{s}}^{-1} = \nabla \mathbf{v}_{\mathrm{s}} \tag{3.82f}$$
$$\frac{\partial c_n}{\partial t} + \mathbf{v}_{\ell} \cdot \nabla c_n = \frac{1}{\phi_{\ell}} \nabla \cdot (\phi_{\ell} \mathbb{D} \nabla c_n) \tag{3.82g}$$

The constitutive assumptions (3.81) still hold in the healthy domain, remembering that in the healthy region we assume $\mathbb{F}_{\mathrm{g}} = \mathbb{I}$, since there is no growth there, and we possibly change the material parameters by considering $\mu_{1\mathrm{h}}$ and $\mu_{2\mathrm{h}}$.
The system is closed, since it has 22 scalar unknowns (the volumetric fractions $\phi_{\mathrm{s}}$

and $\phi_\ell$, the nine components of the deformation gradient $\mathbb{F}_{\rm s}$, the three components of the velocities $\mathbf{v}_{\rm s}$ and $\mathbf{v}_\ell$, the scalar fields $g_1$, $g_2$, $g_3$, $p$ and $c_n$) in 22 scalar equations. Once the system has been solved, we can obtain the displacement field through the relation (2.4):

$$\mathbb{F} = \mathbb{I} + \mathrm{Grad}\mathbf{u} \tag{3.83}$$

**Interface conditions** Since the material interface $\partial\Omega_{\rm t}(t)$ between the tumour and the healthy tissue moves with the tumour cells with velocity $\mathbf{v}_{\rm s}|_{\partial\Omega_{\rm t}(t)}$, we have to satisfy the following interface conditions on the two sides of the boundary in order to guarantee the continuity of the displacement, stress and flux at the interface:

$$[\![\mathbf{v}_{\rm s}\cdot\mathbf{n}]\!]|_{\partial\Omega_{\rm t}(t)} = 0 \tag{3.84a}$$
$$[\![\phi_\ell\,(\mathbf{v}_\ell-\mathbf{v}_{\rm s})\cdot\mathbf{n}d\Sigma]\!]|_{\partial\Omega_{\rm t}(t)} = 0 \tag{3.84b}$$
$$[\![p]\!]|_{\partial\Omega_{\rm t}(t)} = 0 \tag{3.84c}$$
$$[\![c_n]\!]|_{\partial\Omega_{\rm t}(t)} = 0 \tag{3.84d}$$
$$[\![\mathbb{T}\mathbf{N}d\Sigma]\!]|_{\partial\Omega_{\rm t}(t)} = \mathbf{0} \tag{3.84e}$$
$$[\![(\phi_\ell c_n\,(\mathbf{v}_\ell-\mathbf{v}_{\rm s})-\phi_\ell\mathbb{D}\nabla c_n)\cdot\mathbf{n}d\Sigma]\!]|_{\partial\Omega_{\rm t}(t)} = 0 \tag{3.84f}$$

Furthermore, it is physically reasonable to assume not only the continuity of the velocity $\mathbf{v}_{\rm s}$ along the normal direction, but that there are not breakage and rotations between the tumour and the healthy tissue. This hypothesis leads to the fact that $\mathbf{v}_{\rm s}$ is supposed continuos also along the unit tangential component $\boldsymbol{\tau}$:

$$[\![\mathbf{v}_{\rm s}\cdot\boldsymbol{\tau}]\!]|_{\partial\Omega_{\rm t}(t)} = 0 \tag{3.85}$$

This assumption leads us to say that the displacement field $\mathbf{u}_{\rm s}$ is continuous along $\partial\Omega_{\rm t}(t)$. This condition does not imply that also $\mathbb{F}_{\rm s}$ and $J_{\rm s}$ are continuous, but that the areas deform in the same way at the interface. Remembering the relation:

$$\mathbf{n}d\Sigma = J_{\rm s}\mathbb{F}_{\rm s}^{-T}\mathbf{N}d\Sigma_*$$

this conditions means that $d\Sigma_*^{(1)}$ and $d\Sigma_*^{(2)}$ can be imposed equal in the following equality at the interface:

$$J_{\rm s}^{(1)}\mathbb{F}_{\rm s}^{-1(1)}\mathbf{N}d\Sigma_*^{(1)} = J_{\rm s}^{(2)}\mathbb{F}_{\rm s}^{-1(2)}\mathbf{N}d\Sigma_*^{(2)}$$

and this imply:

$$J_{\rm s}^{(1)}\mathbb{F}_{\rm s}^{-T(1)}\mathbf{N} = J_{\rm s}^{(2)}\mathbb{F}_{\rm s}^{-T(2)}\mathbf{N} \quad\longrightarrow\quad [\![J_{\rm s}\mathbb{F}_{\rm s}^{-T}\mathbf{N}]\!]|_{\partial\Omega_t^*} = 0 \tag{3.86}$$

At the end, removing $d\Sigma$ in (3.84b), (3.84e) and (3.84f) for the assumption made above, the interface conditions that we impose are the following:

$$[\![\mathbf{u}_{\rm s}]\!]|_{\partial\Omega_{\rm t}(t)} = 0 \tag{3.87a}$$
$$[\![\phi_\ell\,(\mathbf{v}_\ell-\mathbf{v}_{\rm s})\cdot\mathbf{n}]\!]|_{\partial\Omega_{\rm t}(t)} = 0 \tag{3.87b}$$
$$[\![p]\!]|_{\partial\Omega_{\rm t}(t)} = 0 \tag{3.87c}$$
$$[\![c_n]\!]|_{\partial\Omega_{\rm t}(t)} = 0 \tag{3.87d}$$
$$[\![\mathbb{T}_{\rm s}\mathbf{N}]\!]|_{\partial\Omega_{\rm t}(t)} = \mathbf{0} \tag{3.87e}$$
$$[\![(\phi_\ell c_n\,(\mathbf{v}_\ell-\mathbf{v}_{\rm s})-\phi_\ell\mathbb{D}\nabla c_n)\cdot\mathbf{n}]\!]|_{\partial\Omega_{\rm t}(t)} = 0 \tag{3.87f}$$

where $\mathbf{n}$ denotes the unit normal vector to $\partial\Omega_{\rm t}(t)$ pointing outwards while $\boldsymbol{\tau}$ represents the unit tangential vector.
We underline that the continuity of the effective stress $\mathbb{T}_{\rm s}$ (3.87e) follows from the continuity of the pressure across the surface (3.87c) and the continuity across the interface of the total stress $\mathbb{T} = -p\mathbb{I} + \mathbb{T}_{\rm s}$ (3.84e).

## 3.3 Lagrangian formulation of the model

Our aim is to rewrite the Eulerian equations, derived in the previous section, using a Lagrangian description of motion. In this way the quantities of interest are considered in terms of material coordinates. We will denote by $\Omega_{\rm t}^*$ the reference configuration of the tumour. Moreover, we will use a superscript $^*$ to denote any material element. We recall the equalities (2.2) and (2.3) that we have seen in Section 2.1:

$$d\boldsymbol{\Sigma} = J_{\rm s}\mathbb{F}_{\rm s}^{-T} d\boldsymbol{\Sigma}_* \tag{3.88a}$$

$$dV = J_{\rm s} dV_* \tag{3.88b}$$

Moreover,we will use the symbols $\nabla$ and $\nabla\cdot$ to denote the spatial gradient and spatial divergence, respectively, while Grad and Div will refer to the material gradient and divergence.

**Equation 3.80a** We integrate equation (3.80a) over the tumour domain $\Omega_{\rm t}^*$ and we obtain:

$$\int_{\Omega_{\rm t(t)}} \left[\frac{\partial \phi_{\rm s}}{\partial t} + \nabla\cdot(\phi_{\rm s}\mathbf{v}_{\rm s})\right] dV = \int_{\Omega_{\rm t(t)}} \Gamma_{\rm s} dV \tag{3.89}$$

Using Reynolds' transport theorem (2.5), which we have reported in Section 2.1, and recalling that the material interface $\partial\Omega_{\rm t}$ moves with the tumour cells, we obtain:

$$\frac{d}{dt}\int_{\Omega_{\rm t(t)}} \phi_{\rm s} dV = \int_{\Omega_{\rm t(t)}} \Gamma_{\rm s} dV \tag{3.90}$$

Then we write it in the reference configuration using (3.88b):

$$\frac{d}{dt}\int_{\Omega_{\rm t}^*} \phi_{\rm s} J_{\rm s} dV^* = \int_{\Omega_{\rm t}^*} \Gamma_{\rm s} J_{\rm s} dV^* \tag{3.91}$$

which locally becomes:

$$\dot{\overline{J_{\rm s}\phi_{\rm s}}} = J_{\rm s}\Gamma_{\rm s} \tag{3.92}$$

**Equation 3.80b** For what concerns equation (3.80b), integrating over the tumour domain leads to:

$$\int_{\Omega_{\rm t(t)}} [\partial_t\phi_\ell + \nabla\cdot(\phi_\ell\mathbf{v}_\ell)]\, dV = -\int_{\Omega_{\rm t(t)}} \Gamma_{\rm s} dV \tag{3.93}$$

Since the interface does not move with the fluid, we have to make use of the generalized Reynolds' transport theorem (2.6):

$$\frac{d}{dt}\int_{\Omega_{\rm t(t)}} \phi_\ell dV - \int_{\partial\Omega_{\rm t(t)}} \phi_\ell\,(\mathbf{v}_{\rm s} - \mathbf{v}_\ell)\cdot d\boldsymbol{\Sigma} = -\int_{\Omega_{\rm t(t)}} \Gamma_{\rm s} dV \tag{3.94}$$

Using (3.88a) and (3.88b), we obtain:

$$\frac{d}{dt}\int_{\Omega_{\mathrm{t}}^*} \phi_\ell J_{\mathrm{s}} dV^* - \int_{\partial\Omega_{\mathrm{t}}^*} \phi_\ell \left(\mathbf{v}_{\mathrm{s}} - \mathbf{v}_\ell\right) \cdot J_{\mathrm{s}} \mathbb{F}_{\mathrm{s}}^{-T} d\mathbf{\Sigma}^* = -\int_{\Omega_{\mathrm{t}}^*} \Gamma_{\mathrm{s}} J_{\mathrm{s}} dV^* \tag{3.95}$$

Using the divergence theorem:

$$\frac{d}{dt}\int_{\Omega_{\mathrm{t}}^*} \phi_\ell J_{\mathrm{s}} dV^* - \int_{\Omega_{\mathrm{t}}^*} \mathrm{Div}\left[J_{\mathrm{s}}\phi_\ell \mathbb{F}_{\mathrm{s}}^{-1}\left(\mathbf{v}_{\mathrm{s}} - \mathbf{v}_\ell\right)\right] dV^* = -\int_{\Omega_{\mathrm{t}}^*} \Gamma_{\mathrm{s}} J_{\mathrm{s}} dV^* \tag{3.96}$$

which locally becomes:

$$\dot{\overline{J_{\mathrm{s}}\phi_\ell}} + \mathrm{Div}\left[J_{\mathrm{s}}\phi_\ell \mathbb{F}_{\mathrm{s}}^{-1}\left(\mathbf{v}_\ell - \mathbf{v}_{\mathrm{s}}\right)\right] = -\Gamma_{\mathrm{s}} J_{\mathrm{s}} \tag{3.97}$$

**Equation 3.80d** As regards the momentum balance of the solid phase, if we integrate (3.80d) over the tumour domain and we remember that $\mathbb{T} = -p\mathbb{I} + \mathbb{T}_{\mathrm{s}}$ is the Cauchy stress tensor of the mixture, we obtain:

$$\int_{\Omega_{\mathrm{t}(t)}} \nabla \cdot \mathbb{T} dV = \mathbf{0} \tag{3.98}$$

Then we use the divergence theorem and we write the integral on the reference configuration:

$$\int_{\partial\Omega_t^*} J_{\mathrm{s}} \mathbb{T}\mathbb{F}_{\mathrm{s}}^{-T} d\mathbf{\Sigma}^* = \mathbf{0} \tag{3.99}$$

The integrand is know as the first Piola-Kirchhoff stress tensor $\mathbb{P} := J_{\mathrm{s}}\mathbb{T}\mathbb{F}_{\mathrm{s}}^{T}$ in continuum mechanics. Substituting $\mathbb{P}$ and using again the divergence theorem, we obtain:

$$\int_{\Omega_{\mathrm{t}}^*} \mathrm{Div}\, \mathbb{P} dV^* = \mathbf{0} \tag{3.100}$$

The local balance is then:

$$\mathrm{Div}\, \mathbb{P} = \mathbf{0} \tag{3.101}$$

**Equation 3.80e** In order to rewrite (3.80e) using the Lagrangian formulation, we integrate over a surface:

$$\int_S \phi_\ell \left(\mathbf{v}_\ell - \mathbf{v}_{\mathrm{s}}\right) \cdot d\mathbf{\Sigma} = -\int_S \frac{\mathbb{K}}{\mu} \nabla p \cdot d\mathbf{\Sigma} \tag{3.102}$$

Moving the integrals to the reference configuration, we get:

$$\int_{S^*} \left[\frac{\mathbb{K}}{\mu}\mathbb{F}_{\mathrm{s}}^{-T}\, \mathrm{Grad}\, p + \phi_\ell \left(\mathbf{v}_\ell - \mathbf{v}_{\mathrm{s}}\right)\right] \cdot J_{\mathrm{s}}\mathbb{F}_{\mathrm{s}}^{-T} d\mathbf{\Sigma}^* = \mathbf{0} \tag{3.103}$$

Let us assume that all the involved quantities are regular, we have then the local form:

$$J_{\mathrm{s}}\mathbb{F}_{\mathrm{s}}^{-1}\frac{\mathbb{K}}{\mu}\mathbb{F}_{\mathrm{s}}^{-T}\, \mathrm{Grad}\, p + \phi_\ell J_{\mathrm{s}}\mathbb{F}_{\mathrm{s}}^{-1}\left(\mathbf{v}_\ell - \mathbf{v}_{\mathrm{s}}\right) = \mathbf{0} \tag{3.104}$$

which is equivalent to:

$$\mathbb{F}_{\mathrm{s}}^{-1}\left(\mathbf{v}_\ell - \mathbf{v}_{\mathbf{s}}\right) = -\frac{1}{\mu\phi_\ell}\mathbb{F}_{\mathrm{s}}^{-1}\mathbb{K}\mathbb{F}_{\mathrm{s}}^{-T}\, \mathrm{Grad}\, p \tag{3.105}$$

and remembering (3.71), which leads to $\mathbb{K} = \mathbb{F}_{\mathrm{s}}\mathbb{K}_0\mathbb{F}_{\mathrm{s}}^T$ where $\mathbb{K}_0 = K(\phi_\ell)\mathbb{A}_0$, we have:

$$\mathbb{F}_{\mathrm{s}}^{-1}\left(\mathbf{v}_\ell - \mathbf{v_s}\right) = -\frac{1}{\mu\phi_\ell}\mathbb{K}_0 \operatorname{Grad} p \tag{3.106}$$

Finally, if we multiply both sides by $\mathbb{F}_{\mathrm{s}}$, we obtain:

$$\mathbf{v}_\ell - \mathbf{v_s} = -\mathbb{F}_{\mathrm{s}}\frac{\mathbb{K}_0}{\mu\phi_\ell} \operatorname{Grad} p \tag{3.107}$$

**Equation 3.80g** If we consider now nutrients balance equation and we integrate it over the tumour domain, recalling the closed mixture assumption, we obtain:

$$\begin{aligned}\int_{\Omega_{\mathrm{t}(t)}}\left[\frac{\partial\left(\phi_\ell c_n\right)}{\partial t} + \nabla\cdot\left(\phi_\ell c_n\mathbf{v}_\ell\right)\right]dV = \\ \int_{\Omega_{\mathrm{t}(t)}}\nabla\cdot\left(\phi_\ell\mathbb{D}\nabla c_n\right)dV - \int_{\Omega_{\mathrm{t}(t)}}\left(\Gamma_{\mathrm{s}}c_n - G_n\right)dV\end{aligned} \tag{3.108}$$

Then we use Reynolds transport theorem and Gauss theorem:

$$\begin{aligned}\frac{d}{dt}\int_{\Omega_{\mathrm{t}(t)}}\phi_\ell c_n dV - \int_{\partial\Omega_{\mathrm{t}(t)}}\phi_\ell c_n\left(\mathbf{v}_{\mathrm{s}} - \mathbf{v}_\ell\right)\cdot d\mathbf{\Sigma} = \\ \int_{\partial\Omega_{\mathrm{t}(t)}}\phi_\ell\mathbb{D}\nabla c_n\cdot d\mathbf{\Sigma} - \int_{\Omega_{\mathrm{t}(t)}}\left(\Gamma_{\mathrm{s}}c_n - G_n\right)dV\end{aligned} \tag{3.109}$$

Rewriting the integrals on the reference configuration:

$$\begin{aligned}\frac{d}{dt}\int_{\Omega_{\mathrm{t}}^*}\phi_\ell c_n J_{\mathrm{s}} dV^* - \int_{\partial\Omega_{\mathrm{t}}^*}\phi_\ell\left[c_n\left(\mathbf{v}_{\mathrm{s}} - \mathbf{v}_\ell\right) + \mathbb{D}\mathbb{F}_{\mathrm{s}}^{-T}\operatorname{Grad} c_n\right]\cdot J_{\mathrm{s}}\mathbb{F}_{\mathrm{s}}^{-T}d\mathbf{\Sigma}^* = \\ -\int_{\Omega_{\mathrm{t}}^*}\left(\Gamma_{\mathrm{s}}c_n J_{\mathrm{s}} - G_n J_{\mathrm{s}}\right)dV^*\end{aligned} \tag{3.110}$$

and in this way the local form becomes:

$$\begin{aligned}\overline{J_{\mathrm{s}}\phi_\ell c_n}^{\cdot} - \operatorname{Div}\left[J_{\mathrm{s}}\phi_\ell c_n\mathbb{F}_{\mathrm{s}}^{-1}\left(\mathbf{v}_{\mathrm{s}} - \mathbf{v}_\ell\right)\right] - \operatorname{Div}\left[J_{\mathrm{s}}\phi_\ell\mathbb{F}_{\mathrm{s}}^{-1}\mathbb{D}\mathbb{F}_{\mathrm{s}}^{-T}\operatorname{Grad} c_n\right] = \\ -\Gamma_{\mathrm{s}}c_n J_{\mathrm{s}} + G_n J_{\mathrm{s}}\end{aligned} \tag{3.111}$$

If we remember (3.66), we can rewrite it as:

$$\begin{aligned}\overline{J_{\mathrm{s}}\phi_\ell c_n}^{\cdot} - \operatorname{Div}\left[J_{\mathrm{s}}\phi_\ell c_n\mathbb{F}_{\mathrm{s}}^{-1}\left(\mathbf{v}_{\mathrm{s}} - \mathbf{v}_\ell\right)\right] - \operatorname{Div}\left[J_{\mathrm{s}}\phi_\ell\mathbb{D}_0\operatorname{Grad} c_n\right] = \\ -\Gamma_{\mathrm{s}}c_n J_{\mathrm{s}} + G_n J_{\mathrm{s}}\end{aligned} \tag{3.112}$$

In order to rephrase it, we recall the mass balance of the fluid phase (3.97) and so it becomes:

$$J_{\mathrm{s}}\phi_\ell\dot{c_n} + J_{\mathrm{s}}\phi_\ell\mathbb{F}_{\mathrm{s}}^{-1}\left(\mathbf{v}_\ell - \mathbf{v}_{\mathrm{s}}\right)\cdot\operatorname{Grad} c_n - \operatorname{Div}\left[J_{\mathrm{s}}\phi_\ell\mathbb{D}_0\operatorname{Grad} c_n\right] = G_n J_{\mathrm{s}} \tag{3.113}$$

which can be rephrased as:

$$\dot{c_n} + \mathbb{F}_{\mathrm{s}}^{-1}\left(\mathbf{v}_\ell - \mathbf{v}_{\mathrm{s}}\right)\cdot\operatorname{Grad} c_n - \frac{1}{J_{\mathrm{s}}\phi_\ell}\operatorname{Div}\left[J_{\mathrm{s}}\phi_\ell\mathbb{D}_0\operatorname{Grad} c_n\right] = \frac{G_n}{\phi_\ell} \tag{3.114}$$

**First Piola-Kirchhoff stress tensor $\mathbb{P}_{\rm s}$** To close the mathematical problem, we need to prescribe a constitutive equation for the elastic component of the first Piola-Kirchhoff stress tensor. We have:

$$\begin{aligned}
\mathbb{P}_{\rm s} &= J_{\rm s}\mathbb{T}_{\rm s}\mathbb{F}_{\rm s}^{-T} \\
&= 2J_{\rm s}J_{\rm e}^{-1}\left(\mathbb{F}_{\rm e}\frac{\partial\widehat{\mathcal{W}}_{\rm sn}}{\partial\mathbb{C}_{\rm e}}\mathbb{F}_{\rm e}^{T}\right)\mathbb{F}_{\rm s}^{-T} \\
&= 2J_{\rm g}J_{\rm e}J_{\rm e}^{-1}\mathbb{F}_{\rm e}\frac{\partial\widehat{\mathcal{W}}_{\rm sn}}{\partial\mathbb{C}_{\rm e}}\mathbb{F}_{\rm e}^{T}\left(\mathbb{F}_{\rm e}\mathbb{F}_{\rm g}\right)^{-T} \\
&= 2J_{\rm g}\mathbb{F}_{\rm e}\frac{\partial\widehat{\mathcal{W}}_{\rm sn}}{\partial\mathbb{C}_{\rm e}}\left(\left(\mathbb{F}_{\rm e}\mathbb{F}_{\rm g}\right)^{-1}\mathbb{F}_{\rm e}\right)^{T} \\
&= 2J_{\rm g}\mathbb{F}_{\rm e}\frac{\partial\widehat{\mathcal{W}}_{\rm sn}}{\partial\mathbb{C}_{\rm e}}\mathbb{F}_{\rm g}^{-T}
\end{aligned} \tag{3.115}$$

So, at the end, we have:

$$\mathbb{P}_{\rm s} = 2J_{\rm g}\mathbb{F}_{\rm s}\mathbb{F}_{\rm g}^{-1}\frac{\partial\widehat{\mathcal{W}}_{\rm sn}}{\partial\mathbb{C}_{\rm e}}\mathbb{F}_{\rm g}^{-T} = 2J_{\rm g}\mathbb{F}_{\rm s}\mathbb{F}_{\rm g}^{-1}\mathbb{W}\mathbb{F}_{\rm g}^{-T} \tag{3.116}$$

where the tensor $\mathbb{W}$ has the expression reported in (3.40).

### 3.3.1 The complete Lagrangian model

In conclusion, the set of equations in Lagrangian form on the tumour reference domain $\Omega_{\rm t}^{*}$ is:

$$\overset{\cdot}{\overline{J_{\rm s}\phi_{\rm s}}} = J_{\rm s}\Gamma_{\rm s} \tag{3.117a}$$

$$\overset{\cdot}{\overline{J_{\rm s}\phi_{\ell}}} + \mathrm{Div}\left[J_{\rm s}\phi_\ell\mathbb{F}_{\rm s}^{-1}\left(\mathbf{v}_\ell - \mathbf{v}_{\rm s}\right)\right] = -\Gamma_{\rm s}J_{\rm s} \tag{3.117b}$$

$$\phi_{\rm s} + \phi_\ell = 1 \tag{3.117c}$$

$$\mathrm{Div}\,\mathbb{P} = \mathbf{0} \tag{3.117d}$$

$$\mathbf{v}_\ell = \mathbf{v_s} - \mathbb{F}_{\rm s}\frac{\mathbb{K}_0}{\mu\phi_\ell}\,\mathrm{Grad}\,p \tag{3.117e}$$

$$\dot{c_n} + \mathbb{F}_{\rm s}^{-1}\left(\mathbf{v}_\ell - \mathbf{v}_{\rm s}\right)\cdot\mathrm{Grad}\,c_n - \frac{1}{J_{\rm s}\phi_\ell}\,\mathrm{Div}\left[J_{\rm s}\phi_\ell\mathbb{D}_0\,\mathrm{Grad}\,c_n\right] = \frac{G_n}{\phi_\ell} \tag{3.117f}$$

where

$$\mathbb{F}_{\rm e} = \mathbb{F}_{\rm s}\mathbb{F}_{\rm g}^{-1} \tag{3.118a}$$

$$\widehat{\mathcal{W}}_{\rm sn}\left(\overline{\mathbb{C}}_{\rm e}\right) = \frac{1}{2}\mu_{1\rm t}\left(\mathrm{I}_{\overline{\mathbb{C}}_{\rm e}} - 3\right) + \frac{1}{2}\mu_{2\rm t}\left(\mathrm{II}_{\overline{\mathbb{C}}_{\rm e}} - 3\right) \tag{3.118b}$$

$$\mathbb{P} = -p\mathbb{I} + \mathbb{P}_{\rm s}, \quad \mathbb{P}_{\rm s} = 2J_{\rm g}\mathbb{F}_{\rm e}\mathbb{W}\mathbb{F}_{\rm g}^{-T} \tag{3.118c}$$

$$\mathbb{K}_0 = K\left(\phi_\ell\right)\mathbb{A}_0 \tag{3.118d}$$

$$\Gamma_{\rm s} = \nu\phi_{\rm s}\left(\phi_{\rm max} - \phi_{\rm s}\right)\left(c_n - c_0\right)_+ \tag{3.118e}$$

$$G_n = -\zeta\phi_\ell\phi_{\rm s}c_n + S_n\phi_\ell\left(1 - c_n\right) \tag{3.118f}$$

and $\mathbb{D}_0$, $\mathbb{A}_0$ and $\mathbb{F}_{\rm g}$ are defined as in Section 3.2.4, $\mathbb{W}$ is defined as in(3.40) and the evolution of $g_1$, $g_2$ and $g_3$ is presented in (3.74), (3.75) and (3.76). Furthermore, we assume a constant expression for $K(\phi_\ell)$, i.e. $K(\phi_\ell) = k_p$.

A similar reasoning can be used to derive the Lagrangian equations in the healthy tissue reference domain $\Omega_{\mathrm{h}}^*$, starting from equations (3.82). At the end, we end up with the following set of equations in the healthy domain:

$$\dot{\overline{J_{\mathrm{s}}\phi_{\mathrm{s}}}} = 0 \tag{3.119a}$$

$$\dot{\overline{J_{\mathrm{s}}\phi_\ell}} + \operatorname{Div}\left[J_{\mathrm{s}}\phi_\ell \mathbb{F}_{\mathrm{s}}^{-1}\left(\mathbf{v}_\ell - \mathbf{v}_{\mathrm{s}}\right)\right] = 0 \tag{3.119b}$$

$$\phi_{\mathrm{s}} + \phi_\ell = 1 \tag{3.119c}$$

$$\operatorname{Div}\mathbb{P} = \mathbf{0} \tag{3.119d}$$

$$\mathbf{v}_\ell = \mathbf{v_s} - \mathbb{F}_{\mathrm{s}}\frac{\mathbb{K}_0}{\mu\phi_\ell}\operatorname{Grad} p \tag{3.119e}$$

$$\dot{c_n} + \mathbb{F}_{\mathrm{s}}^{-1}\left(\mathbf{v}_\ell - \mathbf{v}_{\mathrm{s}}\right)\cdot\operatorname{Grad} c_n - \frac{1}{J_{\mathrm{s}}\phi_\ell}\operatorname{Div}\left[J_{\mathrm{s}}\phi_\ell\mathbb{D}_0\operatorname{Grad} c_n\right] = 0 \tag{3.119f}$$

The constitutive assumptions (3.118) still hold, remembering that in the healthy region we assume $\mathbb{F}_{\mathrm{g}} = \mathbb{I}$, since there is no growth there, and we possibly change the material parameters in the constitutive equation, by considering $\mu_{1\mathrm{h}}$ and $\mu_{2\mathrm{h}}$:

$$\mathcal{W}_{\mathrm{sn}}\left(\overline{\mathbb{C}}_{\mathrm{e}}\right) = \left[\frac{1}{2}\mu_{1\mathrm{h}}\left(\mathrm{I}_{\overline{\mathbb{C}}_{\mathrm{e}}} - 3\right) + \frac{1}{2}\mu_{2\mathrm{h}}\left(\mathrm{II}_{\overline{\mathbb{C}}_{\mathrm{e}}} - 3\right)\right] \tag{3.120}$$

The effective unknowns of the problem are the volumetric fractions $\phi_{\mathrm{s}}$ and $\phi_\ell$, the scalar fields $g_1$, $g_2$, $g_3$, $c_n$ and $p$, the displacement field of the solid phase $\mathbf{u}_{\mathrm{s}}$ and the fluid velocity $\mathbf{v}_\ell$.

**Interface conditions** We need to provide appropriate conditions at the interface between the tumour and the host tissue. So, starting from (3.84), we have to consider them using a Lagrangian description of the motion. It is fundamental to remember:

$$\mathbf{n} = \mathbb{F}_{\mathrm{s}}^{-T}\mathbf{N} \tag{3.121a}$$

$$\mathbf{n}d\Sigma = J_{\mathrm{s}}\mathbb{F}_{\mathrm{s}}^{-T}\mathbf{N}d\Sigma_* \tag{3.121b}$$

$$dV = J_{\mathrm{s}}dV_* \tag{3.121c}$$

We have to integrate (3.84) and to apply the formulas (3.121), considering $\mathbf{N}$ to be the unit normal field pointing outward the tumour reference domain. In this way we obtain the following set of interface conditions:

$$[\![\mathbf{v}_{\mathrm{s}}\cdot\frac{\mathbb{F}_{\mathrm{s}}^{-T}\mathbf{N}}{|\mathbb{F}_{\mathrm{s}}^{-T}\mathbf{N}|}]\!]|_{\partial\Omega_t^*} = 0 \tag{3.122a}$$

$$[\![\phi_\ell J_{\mathrm{s}}\mathbb{F}_{\mathrm{s}}^{-1}\left(\mathbf{v}_{\mathrm{s}} - \mathbf{v}_\ell\right)\cdot\mathbf{N}d\Sigma_*]\!]|_{\partial\Omega_t^*} = 0 \tag{3.122b}$$

$$[\![\left(-J_{\mathrm{s}}p\mathbb{F}_{\mathrm{s}}^{-T} + \mathbb{P}_{\mathrm{s}}\right)\mathbf{N}d\Sigma_*]\!]|_{\partial\Omega_t^*} = \mathbf{0} \tag{3.122c}$$

$$[\![p]\!]|_{\partial\Omega_t^*} = \mathbf{0} \tag{3.122d}$$

$$[\![c_n]\!]|_{\partial\Omega_t^*} = \mathbf{0} \tag{3.122e}$$

$$[\![J_{\mathrm{s}}\phi_\ell c_n\mathbb{F}_{\mathrm{s}}^{-1}\left(\mathbf{v}_{\mathrm{s}} - \mathbf{v}_\ell\right)\cdot\mathbf{N}d\Sigma_* + J_{\mathrm{s}}\phi_\ell\mathbb{D}_0\operatorname{Grad} c_n\cdot\mathbf{N}d\Sigma_*]\!]|_{\partial\Omega_t^*} = 0 \tag{3.122f}$$

Remembering the further assumption (3.85), we obtained that the displacement field is continuous. This condition leads us to (3.86). In this way, using (3.86) and the Darcy's law (3.117e), the set of interface conditions (3.122) can be rephrased as:

$$[\![ J_{\mathrm{s}}\mathbb{F}_{\mathrm{s}}^{-T}\mathbf{N} ]\!]|_{\partial\Omega_t^*} = 0 \tag{3.123a}$$

$$[\![ J_{\mathrm{s}}\mathbb{K}_0 \,\mathrm{Grad}\, p \cdot \mathbf{N} ]\!]|_{\partial\Omega_t^*} = 0 \tag{3.123b}$$

$$[\![ \mathbb{P}_{\mathrm{s}}\mathbf{N} ]\!]|_{\partial\Omega_t^*} = \mathbf{0} \tag{3.123c}$$

$$[\![ p ]\!]|_{\partial\Omega_t^*} = \mathbf{0} \tag{3.123d}$$

$$[\![ c_n ]\!]|_{\partial\Omega_t^*} = \mathbf{0} \tag{3.123e}$$

$$[\![ J_{\mathrm{s}}\phi_\ell c_n \mathbb{F}_{\mathrm{s}}^{-1}(\mathbf{v}_{\mathrm{s}} - \mathbf{v}_\ell) \cdot \mathbf{N} + J_{\mathrm{s}}\phi_\ell \mathbb{D}_0 \,\mathrm{Grad}\, c_n \cdot \mathbf{N} ]\!]|_{\partial\Omega_t^*} = 0 \tag{3.123f}$$

We can modify (3.123f) remembering the Darcy's law (3.117e). In fact, by substituting, it becomes:

$$[\![ -J_{\mathrm{s}} c_n \frac{\mathbb{K}_0}{\mu} \,\mathrm{Grad}\, p \cdot \mathbf{N} + J_{\mathrm{s}}\phi_\ell \mathbb{D}_0 \,\mathrm{Grad}\, c_n \cdot \mathbf{N} ]\!]|_{\partial\Omega_t^*} = 0$$

and by (3.123b) and (3.123e), it is possible to conclude that (3.123f) can be rephrased as:

$$[\![ J_{\mathrm{s}}\phi_\ell \mathbb{D}_0 \,\mathrm{Grad}\, c_n \cdot \mathbf{N} ]\!]|_{\partial\Omega_t^*} = 0 \tag{3.123f}$$

# Chapter 4

# Numerical implementation

After having developed the mechanical model for Glioblastoma growth, the aim is to solve it through numerical simulation. In order to do this, we try to obtain a weak formulation of the Lagrangian model. Finally, we discretize in time and space the weak formulation and we prescribe boundary and initial conditions.

## 4.1 Summary of the Lagrangian model

In this section we simplify the Lagrangian model through some algebraic manipulation and we prescribe boundary and initial conditions. First of all, we sum up (3.117a) and (3.117b). Using the saturation condition and the closed mixture assumption, and substituting (3.117e), we obtain:

$$\dot{J}_{\mathrm{s}} = \mathrm{Div}\left[ J_{\mathrm{s}} \frac{\mathbb{K}_0}{\mu} \,\mathrm{Grad}\, p \right] \tag{4.1}$$

We obtain the same result in the healthy domain, by summing (3.119a) and (3.119b).
Then, if we recall the definition of $\phi_{\mathrm{sn}}$ and the fact that it is a constant quantity, we can rewrite the first equation of the model (3.117a) as:

$$J_{\mathrm{s}}\phi_{\mathrm{s}} = J_{\mathrm{g}}\phi_{\mathrm{sn}} \quad \Rightarrow \quad \phi_{\mathrm{s}} = \frac{J_{\mathrm{g}}}{J_{\mathrm{s}}}\phi_{\mathrm{sn}} \tag{4.2}$$

As regards the equation (3.117d), concerning the first Piola-Kirchhoff stress tensor $\mathbb{P}$, we remember that:

$$\mathbb{P} = J_{\mathrm{s}}\mathbb{T}\mathbb{F}_{\mathrm{s}}^{-T} = -J_{\mathrm{s}}p\mathbb{F}_{\mathrm{s}}^{-T} + \mathbb{P}_{\mathrm{s}} \tag{4.3}$$

where $\mathbb{P}_{\mathrm{s}}$ is the constitutive elastic part of the first Piola-Kirchhoff stress tensor. It follows that (3.117d) becomes:

$$\mathrm{Div}\left[ -J_{\mathrm{s}}p\mathbb{F}_{\mathrm{s}}^{-T} + \mathbb{P}_{\mathrm{s}} \right] = \mathbf{0} \tag{4.4}$$

Lastly, we can reformulate the equation for the nutrients (3.117f) using Darcy's Law in the reference configuration as follows:

$$J_{\mathrm{s}}\phi_\ell \dot{c}_n - J_{\mathrm{s}}\frac{\mathbb{K}_0}{\mu}\,\mathrm{Grad}\, p \cdot \mathrm{Grad}\, c_n - \mathrm{Div}\left[ J_{\mathrm{s}}\phi_\ell \mathbb{D}_0 \,\mathrm{Grad}\, c_n \right] = J_{\mathrm{s}} G_n \tag{4.5}$$

where $G_n$ is equal to zero in the healthy domain, as defined in (3.58).
To sum up, the equations we have to solve in the reference domain $\Omega^* = \Omega_{\mathrm{t}}^* \cup \Omega_{\mathrm{h}}^*$ are:

$$\dot{J}_{\mathrm{s}} = \mathrm{Div}\left[J_{\mathrm{s}} \frac{\mathbb{K}_0}{\mu} \,\mathrm{Grad}\, p\right] \tag{4.6a}$$

$$J_{\mathrm{s}}\phi_{\mathrm{s}} = J_{\mathrm{g}}\phi_{\mathrm{sn}} \tag{4.6b}$$

$$\mathbb{F}_{\mathrm{s}} = \mathbb{I} + \mathrm{Grad}\,\mathbf{u}_{\mathrm{s}} \tag{4.6c}$$

$$\phi_{\mathrm{s}} + \phi_\ell = 1 \tag{4.6d}$$

$$\mathrm{Div}\left[-J_{\mathrm{s}} p \mathbb{F}_{\mathrm{s}}^{-T} + \mathbb{P}_{\mathrm{s}}\right] = \mathbf{0} \tag{4.6e}$$

$$J_{\mathrm{s}}\phi_\ell \dot{c}_n - J_{\mathrm{s}} \frac{\mathbb{K}_0}{\mu} \,\mathrm{Grad}\, p \cdot \mathrm{Grad}\, c_n - \mathrm{Div}\left[J_{\mathrm{s}}\phi_\ell \mathbb{D}_0 \,\mathrm{Grad}\, c_n\right] = J_{\mathrm{s}} G_n \tag{4.6f}$$

remembering that we take $J_{\mathrm{g}} = 1$ and $\dot{J}_{\mathrm{g}} = 0$ in the healthy region $\Omega_{\mathrm{h}}^*$, while the evolution of $g_1$, $g_2$ and $g_3$ for the tumour region $\Omega_{\mathrm{t}}^*$ is presented in (3.74), (3.75) and (3.76).
This system allows to determine all the unknown fields, namely, the displacement field $\mathbf{u}_{\mathrm{s}}(\mathbf{X}, t)$ and the scalar fields $p(\mathbf{X}, t)$, $\phi_{\mathrm{s}}(\mathbf{X}, t)$, $\phi_\ell(\mathbf{X}, t)$, $g_1(t)$, $g_2(t)$, $g_3(t)$ and $c_n(\mathbf{X}, t)$, $\forall \mathbf{X} \in \Omega^* = \Omega_{\mathrm{t}}^* \cup \Omega_{\mathrm{t}}^*$ and $\forall t \in (0, T)$, if we provide proper initial and boundary conditions.

**Boundary conditions** Since in our simulations for Glioblastoma growth in the brain we will deal with the cranial skull as the boundary of our domain, we consider the following set of boundary conditions:

$$\mathbf{u}_{\mathrm{s}} = \mathbf{0} \qquad \text{on } \partial\Omega_{\mathrm{h}}^* \backslash \partial\Omega_{\mathrm{t}}^*, \forall t \in (0, T) \tag{4.7a}$$

$$p = 0 \qquad \text{on } \partial\Omega_{\mathrm{h}}^* \backslash \partial\Omega_{\mathrm{t}}^*, \forall t \in (0, T) \tag{4.7b}$$

$$c_n = 1 \qquad \text{on } \partial\Omega_{\mathrm{h}}^* \backslash \partial\Omega_{\mathrm{t}}^*, \forall t \in (0, T) \tag{4.7c}$$

We impose a null Dirichlet boundary condition for the displacement $\mathbf{u}_{\mathrm{s}}$ and for the pressure $p$, while for the nutrients concentration we suppose that the brain boundary is sufficiently far from the tumour and so we can assume that on the boundary the oxygen concentration is maintained constant at the physiological value of 1 by the vasculature.

**Initial conditions** At the beginning of the GBM growth process we assume that the displacement and the pressure are equal to zero. Furthermore, we take the scalar fields $g_1$, $g_2$ and $g_3$, related to the growth component of the deformation gradient, as equal to 1 everywhere in the domain at $t = 0$. We also assume that the volumetric fraction of the cell phase is initially equal to the constant volumetric fraction in the natural state $\phi_{\mathrm{sn}}$. Finally, in order to obtain the initial nutrients concentration $c_n^0(\mathbf{X})$, we solve the steady version of the nutrients governing equation, neglecting advection:

$$-\mathrm{Div}\left[J_{\mathrm{s}}\phi_\ell \mathbb{D}_0 \,\mathrm{Grad}\, c_n\right] = J_{\mathrm{s}} G_n \tag{4.8}$$

In conclusion, we have the following set of initial conditions:

$$\mathbf{u}_\mathrm{s}(\mathbf{X},0) = \mathbf{0} \qquad \forall \mathbf{X} \in \Omega^* \tag{4.9a}$$

$$p(\mathbf{X},0) = 0 \qquad \forall \mathbf{X} \in \Omega^* \tag{4.9b}$$

$$g_1(\mathbf{X},0) = 1,\ g_2(\mathbf{X},0) = 1,\ g_3(\mathbf{X},0) = 1 \qquad \forall \mathbf{X} \in \Omega^* \tag{4.9c}$$

$$\phi_\mathbf{s}(\mathbf{X},0) = \phi_\mathrm{sn} \qquad \forall \mathbf{X} \in \Omega^* \tag{4.9d}$$

$$c_n(\mathbf{X},0) = c_n^0(\mathbf{X}) \qquad \forall \mathbf{X} \in \Omega^* \tag{4.9e}$$

## 4.2 Weak formulation of the Lagrangian model

The weak form of a time-independent differential problem is:

$$\text{find } u \in V \quad : \quad a(u,v) = F(v) \quad \forall v \in V \tag{4.10}$$

where $V$ is a proper functional space, $a$ is a bilinear form and $F$ is a functional. In the same way, the weak form of a time-dependent differential problem can be written as:

$$\text{find } u(t) \in V \quad : \quad \left(\frac{\partial u}{\partial t}(t), v\right) + a(u(t),v) = F(v) \quad \forall v \in V \tag{4.11}$$

We will derive now a weak formulation of our Lagrangian model. We first write the weak form in each domain $\Omega_\mathrm{t}^*$ and $\Omega_\mathrm{h}^*$ separately and then we extend the weak form to the whole domain $\Omega^* = \Omega_\mathrm{t}^* \cup \Omega_\mathrm{h}^*$. It is important to remark that $\partial\Omega_\mathrm{h}^* = \partial\Omega_\mathrm{t}^* \cup \partial\Omega_\mathrm{out}^*$ is the boundary of the healthy domain that is composed by the interface with the tumour $\partial\Omega_\mathrm{t}^*$ and by the external boundary corresponding to the cranial skull $\Omega_\mathrm{out}^*$. At this point it is necessary to define the test functions space, that meets the Dirichlet conditions we impose on the external boundary for $p$ and $c_n$:

$$H^1_{0,\partial\Omega^*_\mathrm{out}}(\Omega^*) = \left\{q \in H^1(\Omega^*) \colon q = 0 \text{ on } \partial\Omega^*_\mathrm{out}\right\} \tag{4.12}$$

and the vector test functions space that that meets the Dirichlet conditions we impose on the external boundary for $\mathbf{u}_\mathrm{s}$:

$$\mathbf{H^1}_{0,\partial\Omega^*_\mathrm{out}}(\Omega^*) = \left\{q \in \mathbf{H^1}(\Omega^*) \colon q = 0 \text{ on } \partial\Omega^*_\mathrm{out}\right\} \tag{4.13}$$

In this way the weak form of our differential problem will take the form:

$$a(u,q) = (f,q) \quad \forall q \in H^1_{0,\partial\Omega^*_\mathrm{out}}(\Omega^*) \tag{4.14}$$

**Equation 4.6a** We multiply each side of (4.6a) by a test function $q_\mathrm{t} \in H^1_{0,\partial\Omega^*_\mathrm{out}}(\Omega^*)$ and then we integrate the whole equation over the Lagrangian tumour domain:

$$\int_{\Omega_\mathrm{t}^*} \dot{J}_\mathrm{s} q_\mathrm{t} dV^* = \int_{\Omega_\mathrm{t}^*} \operatorname{Div}\left[J_\mathrm{s}\frac{\mathbb{K}_0}{\mu}\operatorname{Grad} p\right] q_\mathrm{t} dV^* \tag{4.15}$$

Integrating by parts the second order derivatives:

$$\int_{\Omega_\mathrm{t}^*} \dot{J}_\mathrm{s} q_\mathrm{t} dV^* = -\int_{\Omega_\mathrm{t}^*} \operatorname{Grad} q_\mathrm{t} \cdot J_\mathrm{s}\frac{\mathbb{K}_0}{\mu}\operatorname{Grad} p \; dV^* + \int_{\partial\Omega_\mathrm{t}^*} \frac{q_\mathrm{t}}{\mu} J_\mathrm{s}\mathbb{K}_0 \operatorname{Grad} p \cdot \mathbf{N} d\Sigma^* \tag{4.16}$$

In the healthy domain we take as test function $q_{\mathrm{h}} \in H^1_{0,\partial\Omega^*_{\mathrm{out}}}(\Omega^*)$ and we obtain:

$$\int_{\Omega^*_{\mathrm{h}}} \dot{J}_{\mathrm{s}} q_{\mathrm{h}} dV^* = -\int_{\Omega^*_{\mathrm{h}}} \operatorname{Grad} q_{\mathrm{h}} \cdot J_{\mathrm{s}} \frac{\mathbb{K}_0}{\mu} \operatorname{Grad} p \; dV^* + \int_{\partial\Omega^*_{\mathrm{h}}} \frac{q_{\mathrm{h}}}{\mu} J_{\mathrm{s}} \mathbb{K}_0 \operatorname{Grad} p \cdot \mathbf{N} d\Sigma^* \tag{4.17}$$

Since the test function $q_{\mathrm{h}}$ is required to vanish on the boundary $\partial\Omega^*_{\mathrm{out}}$ because it belongs to $H^1_{0,\partial\Omega^*_{\mathrm{out}}}(\Omega^*)$:

$$\int_{\Omega^*_{\mathrm{h}}} \dot{J}_{\mathrm{s}} q_{\mathrm{h}} dV^* = -\int_{\Omega^*_{\mathrm{h}}} \operatorname{Grad} q_{\mathrm{h}} \cdot J_{\mathrm{s}} \frac{\mathbb{K}_0}{\mu} \operatorname{Grad} p \; dV^* + \int_{\partial\Omega^*_{\mathrm{t}}} \frac{q_{\mathrm{h}}}{\mu} J_{\mathrm{s}} \mathbb{K}_0 \operatorname{Grad} p \cdot \mathbf{N} d\Sigma^* \tag{4.18}$$

where $\mathbf{N}$ is the normal vector to the interface pointing outwards of the tumour domain $\Omega^*_{\mathrm{t}}$. If we sum up (4.16) and (4.18) and we take $q \in H^1_{0,\partial\Omega^*_{\mathrm{out}}}(\Omega^*)$, we obtain:

$$\int_{\Omega^*} \dot{J}_{\mathrm{s}} q dV^* = -\int_{\Omega^*} \operatorname{Grad} q \cdot J_{\mathrm{s}} \frac{\mathbb{K}_0}{\mu} \operatorname{Grad} p \; dV^* - \int_{\partial\Omega^*_{\mathrm{t}}} [\![ \frac{q}{\mu} J_{\mathrm{s}} \mathbb{K}_0 \operatorname{Grad} p ]\!] \cdot \mathbf{N} d\Sigma^* \tag{4.19}$$

that thanks to the interface condition (3.123b) can be rephrased as:

$$\int_{\Omega^*} \dot{J}_{\mathrm{s}} q dV^* = -\int_{\Omega^*} \operatorname{Grad} q \cdot J_{\mathrm{s}} \frac{\mathbb{K}_0}{\mu} \operatorname{Grad} p \; dV^* - \int_{\partial\Omega^*_{\mathrm{t}}} \frac{J_{\mathrm{s}}}{\mu} \mathbb{K}_0 \operatorname{Grad} p [\![ q ]\!] \cdot \mathbf{N} d\Sigma^* \tag{4.20}$$

Furthermore, since the test function $q$ belongs to $H^1_{0,\partial\Omega^*_{\mathrm{out}}}(\Omega^*)$ and so it is continuous inside the domain, we can rephrase the weak formulation of the first equation as:

$$\int_{\Omega^*} \dot{J}_{\mathrm{s}} q dV^* = -\int_{\Omega^*} \operatorname{Grad} q \cdot J_{\mathrm{s}} \frac{\mathbb{K}_0}{\mu} \operatorname{Grad} p \; dV^* \tag{4.21}$$

for all test functions $q \in H^1_{0,\partial\Omega^*_{\mathrm{out}}}(\Omega^*)$.
We introduce now a discretization of the time using the implicit Euler method:

$$\int_{\Omega^*} \frac{J_{\mathrm{s}}^{k+1}\left(\mathbf{u}_{\mathrm{s}}^{k+1}\right) - J_{\mathrm{s}}^{k}\left(\mathbf{u}_{\mathrm{s}}^{k}\right)}{\Delta t} q \; dV^* = -\int_{\Omega^*} \operatorname{Grad} q \cdot \frac{J_{\mathrm{s}}^{k+1}\left(\mathbf{u}_{\mathrm{s}}^{k+1}\right)\left(\mathbb{K}_0\right)^{k+1}}{\mu} \operatorname{Grad}\left(p^{k+1}\right) dV^* \tag{4.22}$$

where, given $N$ time steps on the interval $(0,T)$, $\Delta t := \frac{T}{N}$ is the time step and we use a superscript $k$ to denote the value of a quantity at time $t_k = k\Delta t$.
In order to simplify the notation, we will drop the superscript $k+1$ to denote the value of a quantity of interest at the next time step. Then, in order to write the weak formulation properly, we multiply both sides by $\Delta t$, isolating on the right-hand side all terms that involve only the test functions:

$$\int_{\Omega^*} J_{\mathrm{s}}\left(\mathbf{u}_{\mathrm{s}}\right) q \; dV^* + \Delta t \int_{\Omega^*} \operatorname{Grad} q \cdot \frac{J_{\mathrm{s}}\left(\mathbf{u}_{\mathrm{s}}\right)\mathbb{K}_0}{\mu} \operatorname{Grad} p \; dV^* = \int_{\Omega^*} J_{\mathrm{s}}^k(\mathbf{u}_{\mathrm{s}}^k) q \; dV^* \tag{4.23}$$

**Equation 4.6e** Considering (4.6e), we multiply it by a vector test function $\boldsymbol{q}_{\mathrm{t}} \in \mathbf{H^1}_{0,\partial\Omega^*_{\mathrm{out}}}(\Omega^*)$ and then we integrate over the tumour reference domain:

$$\int_{\Omega^*_{\mathrm{t}}} \operatorname{Div}\left[-J_{\mathrm{s}} p \mathbb{F}_{\mathrm{s}}^{-T} + \mathbb{P}_{\mathrm{s}}\right] \cdot \boldsymbol{q}_{\mathrm{t}} \; dV^* = 0 \tag{4.24}$$

Using tensor integration by parts, we get:

$$-\int_{\Omega_{\mathrm{t}}^*}\left(-J_{\mathrm{s}}p\mathbb{F}_{\mathrm{s}}^{-T}+\mathbb{P}_{\mathrm{s}}\right):\mathrm{Grad}\,\boldsymbol{q}_{\mathrm{t}}dV^*+\int_{\partial\Omega_{\mathrm{t}}^*}\left(-J_{\mathrm{s}}p\mathbb{F}_{\mathrm{s}}^{-T}+\mathbb{P}_{\mathrm{s}}\right)\mathbf{N}\cdot\boldsymbol{q}_{\mathrm{t}}d\Sigma^*=0 \quad (4.25)$$

Doing the same in the healthy domain and taking $\boldsymbol{q}_{\mathrm{h}}\in\mathbf{H^1}_{0,\partial\Omega_{\mathrm{out}}^*}(\Omega^*)$, the result is:

$$-\int_{\Omega_{\mathrm{h}}^*}\left(-J_{\mathrm{s}}p\mathbb{F}_{\mathrm{s}}^{-T}+\mathbb{P}_{\mathrm{s}}\right):\mathrm{Grad}\,\boldsymbol{q}_{\mathrm{h}}dV^*-\int_{\partial\Omega_{\mathrm{h}}^*}\left(-J_{\mathrm{s}}p\mathbb{F}_{\mathrm{s}}^{-T}+\mathbb{P}_{\mathrm{s}}\right)\mathbf{N}\cdot\boldsymbol{q}_{\mathrm{h}}d\Sigma^*=0 \quad (4.26)$$

As before, since the test function $\boldsymbol{q}_{\mathrm{h}}$ is required to vanish on $\partial\Omega_{\mathrm{out}}^*$:

$$-\int_{\Omega_{\mathrm{h}}^*}\left(-J_{\mathrm{s}}p\mathbb{F}_{\mathrm{s}}^{-T}+\mathbb{P}_{\mathrm{s}}\right):\mathrm{Grad}\,\boldsymbol{q}_{\mathrm{h}}dV^*-\int_{\partial\Omega_{\mathrm{t}}^*}\left(-J_{\mathrm{s}}p\mathbb{F}_{\mathrm{s}}^{-T}+\mathbb{P}_{\mathrm{s}}\right)\mathbf{N}\cdot\boldsymbol{q}_{\mathrm{h}}d\Sigma^*=0 \quad (4.27)$$

Summing the two equations (4.27) and (4.25) and being $\boldsymbol{q}\in\mathbf{H^1}_{0,\partial\Omega_{\mathrm{out}}^*}(\Omega^*)$, the weak formulation on the whole domain is:

$$-\int_{\Omega^*}\left(-J_{\mathrm{s}}p\mathbb{F}_{\mathrm{s}}^{-T}+\mathbb{P}_{\mathrm{s}}\right):\mathrm{Grad}\,\boldsymbol{q}\;dV^*-\int_{\partial\Omega_{\mathrm{t}}^*}[\![\left(-J_{\mathrm{s}}p\mathbb{F}_{\mathrm{s}}^{-T}+\mathbb{P}_{\mathrm{s}}\right)\mathbf{N}\cdot\boldsymbol{q}]\!]d\Sigma^*=0 \quad (4.28)$$

Looking at the interface conditions (3.123a), (3.123c) and (3.123d), it becomes:

$$-\int_{\Omega^*}\left(-J_{\mathrm{s}}p\mathbb{F}_{\mathrm{s}}^{-T}+\mathbb{P}_{\mathrm{s}}\right):\mathrm{Grad}\,\boldsymbol{q}\;dV^*-\int_{\partial\Omega_{\mathrm{t}}^*}\left(-J_{\mathrm{s}}p\mathbb{F}_{\mathrm{s}}^{-T}+\mathbb{P}_{\mathrm{s}}\right)\mathbf{N}\cdot[\![\boldsymbol{q}]\!]d\Sigma^*=0 \quad (4.29)$$

Furthermore, if we remember that $\boldsymbol{q}\in\mathbf{H^1}_{0,\partial\Omega_{\mathrm{out}}^*}(\Omega^*)$, the jump vanishes and we obtain:

$$-\int_{\Omega^*}\left(-J_{\mathrm{s}}p\mathbb{F}_{\mathrm{s}}^{-T}+\mathbb{P}_{\mathrm{s}}\right):\mathrm{Grad}\,\boldsymbol{q}\;dV^*=0 \quad (4.30)$$

**Union of the last two variational problems** The variational problems (4.21) and (4.30) are nonlinear and coupled: in view of the numerical implementation, it is convenient to rewrite them into a single nonlinear variational problem by summing them. If we do that, we obtain a discrete-time variational problem for the displacement and the pressure, i.e. find $(\mathbf{u}_{\mathrm{s}},p)\in\boldsymbol{H^1}(\Omega^*)\times H^1(\Omega^*)$ such that:

$$\left(J_{\mathrm{s}}(\mathbf{u}_{\mathrm{s}}),q_p\right)+\Delta t\left(\mathrm{Grad}\,q_p,J_{\mathrm{s}}(\mathbf{u}_{\mathrm{s}})\frac{\mathbb{K}_0}{\mu}\,\mathrm{Grad}\,p\right)+ \\ -\left(\mathbb{P}(\mathbf{u}_{\mathrm{s}},p),\mathrm{Grad}\,\boldsymbol{q}_u\right)=\left(J_{\mathrm{s}}^k(\mathbf{u}_{\mathrm{s}}^k),q_p\right) \quad (4.31)$$

**Equation 4.6f** We need a weak formulation for the equation of the nutrients. In order to do that, we multiply the equation for a test function $q_{\mathrm{t}}\in H^1_{0,\partial\Omega_{\mathrm{out}}^*}(\Omega^*)$:

$$\int_{\Omega_t^*}J_{\mathrm{s}}\phi_\ell\dot{c}_nq_{\mathrm{t}}dV^*-\int_{\Omega_{\mathrm{t}}^*}J_{\mathrm{s}}\frac{\mathbb{K}_0}{\mu}\,\mathrm{Grad}\,p\cdot\mathrm{Grad}\,c_nq_{\mathrm{t}}dV^*+ \\ -\int_{\Omega_{\mathrm{t}}^*}\mathrm{Div}\left[\phi_\ell J_{\mathrm{s}}\mathbb{D}_0\,\mathrm{Grad}\,c_n\right]q_{\mathrm{t}}dV^*=\int_{\Omega_{\mathrm{t}}^*}J_{\mathrm{s}}G_nq_{\mathrm{t}}dV^* \quad (4.32)$$

Integrating by parts, we obtain:

$$\int_{\Omega_t^*}\left(J_s\phi_\ell\dot{c}_n - J_s\frac{\mathbb{K}_0}{\mu}\operatorname{Grad}p\cdot\operatorname{Grad}c_n\right)q_t dV^* + \int_{\Omega_t^*}\phi_\ell\operatorname{Grad}q_t\cdot J_s\mathbb{D}_0\operatorname{Grad}c_n dV^* + \\ -\int_{\partial\Omega_t^*}q_t\phi_\ell J_s\mathbb{D}_0\operatorname{Grad}c_n\cdot\mathbf{N}d\Sigma^* = \int_{\Omega_t^*}J_s G_n q_t dV^* \quad (4.33)$$

We follow the same approach on the healthy domain and then we sum the two equations. Taking $q\in H^1_{0,\partial\Omega^*_{\text{out}}}(\Omega^*)$, the test function vanishes on that boundary and we finally have:

$$\int_{\Omega^*}\left(J_s\phi_\ell\dot{c}_n - J_s\frac{\mathbb{K}_0}{\mu}\operatorname{Grad}p\cdot\operatorname{Grad}c_n\right)q dV^* + \int_{\Omega^*}\phi_\ell\operatorname{Grad}q\cdot J_s\mathbb{D}_0\operatorname{Grad}c_n dV^* + \\ +\int_{\partial\Omega_t^*}[\![q\phi_\ell J_s\mathbb{D}_0\operatorname{Grad}c_n]\!]\cdot\mathbf{N}d\Sigma^* = \int_{\Omega^*}J_s G_n q dV^* \quad (4.34)$$

Also in this case, recalling the interface condition (3.123f), the previous formulation becomes:

$$\int_{\Omega^*}\left(J_s\phi_\ell\dot{c}_n - J_s\frac{\mathbb{K}_0}{\mu}\operatorname{Grad}p\cdot\operatorname{Grad}c_n\right)q dV^* + \int_{\Omega^*}\phi_\ell\operatorname{Grad}q\cdot J_s\mathbb{D}_0\operatorname{Grad}c_n dV^* + \\ +\int_{\partial\Omega_t^*}\phi_\ell J_s\mathbb{D}_0\operatorname{Grad}c_n[\![q]\!]\cdot\mathbf{N}d\Sigma^* = \int_{\Omega^*}J_s G_n q dV^* \quad (4.35)$$

Since $q\in H^1_{0,\partial\Omega^*_{\text{out}}}(\Omega^*)$ it becomes:

$$\int_{\Omega^*}\left(J_s\phi_\ell\dot{c}_n - J_s\frac{\mathbb{K}_0}{\mu}\operatorname{Grad}p\cdot\operatorname{Grad}c_n\right)q dV^* + \int_{\Omega^*}\phi_\ell\operatorname{Grad}q\cdot J_s\mathbb{D}_0\operatorname{Grad}c_n dV^* = \\ = \int_{\Omega^*}J_s G_n q dV^* \quad (4.36)$$

It is now important to introduce a time discretization of the previous equation. We use again the implicit Euler method, which leads to:

$$\int_{\Omega^*}\left[J_s^{k+1}\frac{c_n^{k+1}-c_n^k}{\Delta t} - J_s^{k+1}\frac{(\mathbb{K}_0)^{k+1}}{\mu\phi_\ell^{k+1}}\operatorname{Grad}\left(p^{k+1}\right)\cdot\operatorname{Grad}\left(c_n^{k+1}\right)\right]q dV^* + \\ +\int_{\Omega^*}\operatorname{Grad}q\cdot J_s^{k+1}(\mathbb{D}_0)^{k+1}\operatorname{Grad}\left(c_n^{k+1}\right)dV^* = \int_{\Omega^*}J_s^{k+1}\frac{G_n^{k+1}}{\phi_\ell^{k+1}}q dV^* \quad (4.37)$$

Multiplying by $\Delta t$, reordering the terms and dropping the superscript $k+1$ we obtain that for every $q\in H^1(\Omega^*)$:

$$\int_{\Omega^*}\left[J_s c_n q - \Delta t J_s\frac{\mathbb{K}_0}{\mu\phi_\ell}\operatorname{Grad}p\cdot\operatorname{Grad}c_n q + \Delta t\operatorname{Grad}q\cdot J_s\mathbb{D}_0\operatorname{Grad}c_n\right]dV^* = \\ = \int_{\Omega^*}\left(J_s c_n^k + \Delta t J_s\frac{G_n}{\phi_\ell}\right)q dV^* \quad (4.38)$$

We stress that, given the displacement $\mathbf{u}_s$ and the pressure $p$ obtained by solving (4.31), this one is a linear variational problem to be solved with respect to the unknown $c_n$.

**Initial conditions for nutrients** It remains to derive the variational formulazion of the equation which gives us the initial nutrients concentration $c_n^0(\mathbf{X})$, that means equation (4.8). Proceeding as made above, with identical passages, we obtain:

$$\int_{\Omega^*} \phi_\ell \operatorname{Grad} q \cdot J_{\mathrm{s}} \mathbb{D}_0 \operatorname{Grad} c_n dV^* = \int_{\Omega^*} J_{\mathrm{s}} G_n q dV^* \tag{4.39}$$

## 4.3 Discrete formulation of the continuous variational problems

We need now to introduce a spatially discrete formulation of the continuous variational problems (4.31) and (4.38). We make use of linear tetrahedron $\mathbb{P}_1$ elements, so we introduce the following finite element spaces:

$$\boldsymbol{V}_h := \left\{ \boldsymbol{q}_h \in \left[C^0\left(\overline{\Omega^*}\right)\right]^3 : \boldsymbol{q}_h|_K \in [\mathbb{P}_1(K)]^3 \ \forall K \in \mathcal{T}_h \right\} \subset \boldsymbol{H}^1\left(\Omega^*\right) \tag{4.40}$$

$$W_h := \left\{ q_h \in C^0\left(\overline{\Omega^*}\right) : q_h|_K \in \mathbb{P}_1(K) \ \forall K \in \mathcal{T}_h \right\} \subset H^1\left(\Omega^*\right) \tag{4.41}$$

where $\mathcal{T}_h$ is a decomposition of the domain $\Omega^*$ into tetrahedra $K$ conforming to the tumour boundary.
Furthermore, we define the discrete test functions spaces:

$$\overline{\boldsymbol{V}}_h := \{\boldsymbol{q}_h \in \boldsymbol{V}_h : \boldsymbol{q}_h = \boldsymbol{0} \text{ on } \partial\Omega^*_{\mathrm{out}}\} \tag{4.42}$$

$$\overline{W}_h := \{q_h \in W_h : q_h = 0 \text{ on } \partial\Omega^*_{\mathrm{out}}\} \tag{4.43}$$

Then, we can define the full discrete variational problem: for $k = 1, ..., N$, given $\left(\mathbf{u}_h^k, p_h^k, c_h^k\right) \in \boldsymbol{V}_h \times W_h \times W_h$ find $(\mathbf{u}_h, p_h, c_h) \in \boldsymbol{V}_h \times W_h \times W_h$ such that $\forall (\mathbf{v}_h, w_h, q_h) \in \overline{\boldsymbol{V}}_h \times \overline{W}_h \times \overline{W}_h$ it holds:

$$\begin{aligned} \left(J_{\mathrm{s}}\left(\mathbf{u}_h\right), w_h\right) + \Delta t \left(\operatorname{Grad} w_h, J_{\mathrm{s}}\left(\mathbf{u}_h\right) \frac{\mathbb{K}_0}{\mu} \operatorname{Grad} p_h\right) + & \\ - \left(\mathbb{P}\left(\mathbf{u}_h, p_h\right), \operatorname{Grad} \boldsymbol{v}_h\right) = \left(J_{\mathrm{s}}^k\left(\mathbf{u}_h^k\right), w_h\right) & \end{aligned} \tag{4.44}$$

$$\begin{aligned} \left(J_{\mathrm{s}}\left(\mathbf{u}_h\right) c_h, q_h\right) - \Delta t \left(J_{\mathrm{s}}\left(\mathbf{u}_h\right) \frac{\mathbb{K}_0}{\mu\phi_\ell} \operatorname{Grad} p_h \cdot \operatorname{Grad} c_h, q_h\right) + & \\ \Delta t \left(\operatorname{Grad} q_h, J_{\mathrm{s}}\left(\mathbf{u}_h\right) \mathbb{D}_0 \operatorname{Grad} c_h\right) = \left(J_{\mathrm{s}}\left(\mathbf{u}_h\right) c_h^k, q_h\right) + \Delta t \left(J_{\mathrm{s}}\left(\mathbf{u}_h\right) \frac{G_n\left(c_h\right)}{\phi_\ell}, q_h\right) & \end{aligned} \tag{4.45}$$

where we we have denoted by $(\cdot,\cdot)$ the standard scalar product on $L^2(\Omega^*)$.

## 4.4 Discretization of the other equations involved

The last step is to introduce a proper discretization of the other equations involved, namely the ordinary differential equation for $g_1$ (3.74), $g_2$ (3.75) and $g_3$ (3.76), the saturation condition (4.6d) and the relation (4.6b).
Regarding (3.74), it can be easily discretized in time using a semi-implicit Euler method, made only in the cells which belongs to the tumour domain $\Omega^*_{\mathrm{t}}$:

$$\frac{g_1^{k+1} - g_1^k}{\Delta t} = g_1^{k+1} \frac{\lambda_1 a_1(r)}{\lambda_1 a_1(r) + \lambda_2 a_2(r) + \lambda_3 a_3(r)} \frac{\Gamma_{\mathrm{s}}^{k+1}}{\phi_{\mathrm{s}}^{k+1}} \tag{4.46}$$

which can be immediately rephrased as:

$$g_1^{k+1} = g_1^k \left(1 - \Delta t \frac{\lambda_1 a_1(r)}{\lambda_1 a_1(r) + \lambda_2 a_2(r) + \lambda_3 a_3(r)} \frac{\Gamma_{\mathrm{s}}^{k+1}}{\phi_{\mathrm{s}}^{k+1}}\right)^{-1} \tag{4.47}$$

Similarly for (3.75) and (3.76):

$$g_2^{k+1} = g_2^k \left(1 - \Delta t \frac{\lambda_2 a_2(r)}{\lambda_1 a_1(r) + \lambda_2 a_2(r) + \lambda_3 a_3(r)} \frac{\Gamma_{\mathrm{s}}^{k+1}}{\phi_{\mathrm{s}}^{k+1}}\right)^{-1} \tag{4.48}$$

$$g_3^{k+1} = g_3^k \left(1 - \Delta t \frac{\lambda_3 a_3(r)}{\lambda_1 a_1(r) + \lambda_2 a_2(r) + \lambda_3 a_3(r)} \frac{\Gamma_{\mathrm{s}}^{k+1}}{\phi_{\mathrm{s}}^{k+1}}\right)^{-1} \tag{4.49}$$

Equation (4.6b) is discretized as follows:

$$J_{\mathrm{s}}^{k+1} \phi_{\mathrm{s}}^{k+1} = J_{\mathrm{g}}^{k+1} \phi_{\mathrm{sn}} \quad \Rightarrow \quad \phi_{\mathrm{s}}^{k+1} = \frac{J_{\mathrm{g}}^{k+1}}{J_{\mathrm{s}}^{k+1}} \phi_{\mathrm{sn}} \tag{4.50}$$

Once we have computed $\phi_{\mathrm{s}}^{k+1}$, we can derive $\phi_{\ell}^{k+1}$ using the saturation condition:

$$\phi_{\ell}^{k+1} = 1 - \phi_{\mathrm{s}}^{k+1} \tag{4.51}$$

It is important to underline that $g_1$, $g_2$, $g_3$, $\phi_{\mathrm{s}}$ and $\phi_{\ell}$ are approximated by piecewise-constant functions.

## 4.5 Parameters estimation

We have now to assess the values of the parameters that appear in the system. It is important to underline that the choice of the parameters is fundamental to have a realistic and reliable outcome. On the other hand, when working in the field of mathematical biomedicine, accurate estimations of the parameters are often difficult to obtain. Since we cannot conduce experiments, we review the literature in order to assign a value, or at least a range of values, to the parameters introduced in our model. We will use, when possible, the same values proposed in [**63**].

- Firstly, we deal with the material parameters $\mu_{1\mathrm{h}}$ and $\mu_{2\mathrm{h}}$ that appear in the Mooney-Rivlin energy density for healthy tissue. In the article of Balbi et al. [**72**], they consider a Mooney-Rivlin-type energy, for which they propose as a mean value for the shear modulus of $\mu = 2(\mu_{1\mathrm{h}} + \mu_{2\mathrm{h}}) = 900 \pm 312\ Pa$ and for the second Mooney–Rivlin parameter $\mu_{2\mathrm{h}} = 297 \pm 189\ Pa$. Since we will deal with units of the order of millimeters, we have to convert them into $MPa$. Choosing the mean values within the range, we get $\mu_{1\mathrm{h}} = 1.53 \cdot 10^{-4}\ MPa$ and $\mu_{2\mathrm{h}} = 2.97 \cdot 10^{-4}\ MPa$.
  For what concerns the Mooney-Rivlin parameters in the diseased tissue, we will consider them ten times stiffer than the healthy ones, that means $\mu_{1\mathrm{t}} = 1.53 \cdot 10^{-3}\ MPa$ and $\mu_{2\mathrm{t}} = 2.97 \cdot 10^{-3}\ MPa$.
- Then, we have to estimate the values of the parameters involved in the growth rate $\Gamma_{\mathrm{s}}$ proposed in (3.62). The cell proliferation constant $\nu$ is taken as the inverse of typical doubling times for in vitro glioma cells, that vary from 24 to 48 hours: for this reason, a range $0.5 - 1\ day^{-1}$ can be considered appropriate for $\nu$. As underlined in [**63**, **66**], since proliferation depends

significantly on nutrients availability, also smaller values seem however admissible. Having said that, in the following we will consider the minimum value inside the mentioned interval, i.e. $\nu = 0.5\ day^{-1}$.

- The hypoxia threshold $c_0$ is estimated in the literature [**67**, **73**, **74**, **75**] as ranging from 0.15 to 0.5. We will consider $c_0 = 0.30$ in simulations, as done by Agosti et al. in [**67**].

- Concerning the nutrients consumption rate $\zeta$ that appears in (3.58), we follow the approach by Colombo et al. [**66**] and so we know it can be estimated indirectly through biological measurements of the oxygen diffusion coefficient in the human brain $D_n$ and the distance covered by an oxygen molecule before it is uptake by a cancer cell $l_n$. The mean value for $D_n$ reported in the literature is $D_n = 86.4\ mm^2/day$ [**66**, **74**], while $l_n$ is estimated to be about $l_n = 100\ \mu m = 10^{-1}\ mm$ [**74**]. Hence, we can take a value of $\zeta = \frac{D_n}{l_n^2} = 8640\ 1/day$.

- The nutrients supply rate $S_n$ that appears in (3.58) is quite difficult to estimate: as done in [**66**, **67**] we refer to the value of $10^4\ 1/day$ proposed in [**76**].

- Finally, as mean diffusion coefficient of the nutrients, we consider the same $D_n$ previously mentioned, recalling that we consider oxygen as the main source of nourishment for the cells.

- We need then to give an estimate of the cell volumetric fraction in the natural state $\phi_{\mathrm{sn}}$. We have proved that on growth process it is a constant, so we can assume that it is given from the outset. Different values appear in the literature: Colombo et al. [**66**] and Agosti et al. [**67**] considered a value of $\phi_{\mathrm{sn}} = 0.39$, which they derived as the complementary value of the extra-cellular space studied in [**77**] and amounting at up to 61%. Differently, in their tumour growth model, Mascheroni et al [**29**] employed a quite high value of $\phi_{\mathrm{sn}} = 0.8$. We considered the value proposed by Agosti and Ciarletta [**78**], which is $\phi_{\mathrm{sn}} = 0.3$.

- It remains to estimate the value $k_p$ which appears in the permeability tensor expression: in the literature it is often estimated the ratio $k := \frac{k_p}{\mu}$, where $\mu$ is the dynamic viscosity of the fluid phase. Given its definition and the spatial and temporal scale we employ in our model, such a ratio has units $mm^2/(MPa \cdot day)$. Values found in the literature cover quite a wide range: for example, Mascheroni et al. [**29**] consider a value $k = 4.875 \cdot 10^{-13}\ m^2/(Pa \cdot s)$; a conversion to our framework results in a value of $k = 5.5 \cdot 10^2\ mm^2/(MPa \cdot day)$. Moreover, in their dimensional analysis, Giverso et al. [**27**] consider a range of $10^{-15} - 10^{-13}\ m^2/(Pa \cdot s)$, which corresponds to an interval of $10^0 - 10^2\ mm^2/(MPa \cdot day)$. We consider an higher value, that corresponds to $k = 2.17 \cdot 10^5\ mm^2/(MPa \cdot day)$

For the sake of completeness we report below the complete list of all the used parameters:

| Parameter | Description | Value |
|---|---|---|
| $\mu_{1\mathrm{h}}$ | Mooney-Rivlin material parameter | $1.53 \cdot 10^{-4}\ MPa$ |
| $\mu_{2\mathrm{h}}$ | Mooney-Rivlin material parameter | $2.97 \cdot 10^{-4}\ MPa$ |
| $\mu_{1\mathrm{t}}$ | Mooney-Rivlin material parameter | $1.53 \cdot 10^{-3}\ MPa$ |
| $\mu_{2\mathrm{t}}$ | Mooney-Rivlin material parameter | $2.97 \cdot 10^{-3}\ MPa$ |
| $\nu$ | Cell proliferation constant | $0.5\ day^{-1}$ |
| $c_0$ | Hypoxia threshold | 0.30 |
| $\zeta$ | Nutrients consumption rate | $8640\ day^{-1}$ |
| $S_n$ | Nutrients supply rate | $10^4\ day^{-1}$ |
| $\phi_{\mathrm{sn}}$ | Cell volume fraction in the natural state | 0.30 |
| $\phi_{\max}$ | Maximum cell volume fraction | 0.85 |
| $D_n$ | Mean nutrients diffusion coefficient | $86.4\ mm^2 \cdot day^{-1}$ |
| $k$ | Hydraulic conductivity | $2.17 \cdot 10^5\ mm^2 \cdot MPa^{-1} \cdot day^{-1}$ |

## 4.6 Mesh preparation

The last step before starting with the numerical simulations is to discuss how we get the computational brain mesh and the mesh containing the values of $\mathbb{D}_0$.
For what concern the brain mesh, it is constructed from DTI (Diffusion Tensor Imaging) and MRI (Magnetic Resonance Imaging) data, collected from patients of the Istituto Neurologico Carlo Besta in Milan. Having available the nodes and faces of the brain contour, the mesh was constructed using the program *Tetgen* [**79**], which is able to generate tetrahedral meshes of any 3D polyhedral domains. Furthermore, we have constructed a tumour-conformal mesh, in order to be able to clearly separate the healthy domain to the tumour domain. The tumour domain was considered as a sphere of radius 5 $cm$. Finally, the mesh has been refined along the the tumour, as it is around it that the results of the simulations have the greatest variations.

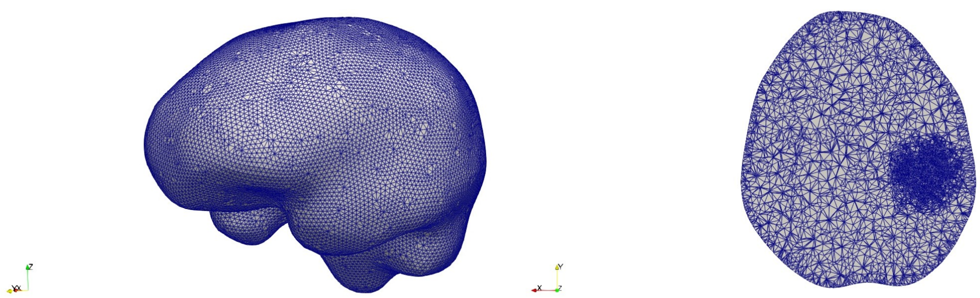

Figure 4.1: External computational brain mesh and refinement

For what concern the six independent component of the tensor $\mathbb{D}_0$, we employ data from DTI imaging. First of all, the six images coming from DTI medical exams need to be aligned with the ones from MRI, since in general they are not. This can be done thanks to automated tools. Once all the images are aligned, one can create six different meshes, in which a diffusion value for the coefficient $D_{ij}$ is assigned to each cell. Doing so, diffusion data can be integrated into the computational mesh. Furthermore, we treat the input diffusion images with a particular model called multi-compartment. The fundamental hypothesis is that, from medical MRI images, you can extract different types of images regarding the water diffusion. In particular, the multi-compartment model tries to isolate free water to give more weight to the one whose motion is affected by the fibers. For this reason, initial data are 6 diffusion images, concerning only the non-free water, and an image containing free water weights for each voxel. At the end, the diffusion tensor should be calculated as follows:

$$\mathbb{D}_{tot} = p_{FW}\mathbb{D}_{FW} + (1 - p_{FW})\,\mathbb{D}_0$$

where $\mathbb{D}_{FW}$, which represents the free water diffusion at $37°$, is the identity tensor multiplied by $0.003\ mm^2/s = 259.2\ mm^2/day$ (the diffusivity of the water under those conditions), while $p_{FW}$ and the tensor $\mathbb{D}_0$ are obtained directly from DTI images as described above. The tensor $\mathbb{D}_{tot}$ is used as Lagrangian diffusion tensor for the nutrients, which diffuse in both fibers and free water, while the tensor $\mathbb{D}_0$ is used to calculate $\mathbb{A}$ and $\mathbb{F}_g$ as discussed in Section 3.2.4.
A Z-normal slice of each DTI mesh, representing an independent component of $\mathbb{D}_0$ extracted from DTI images, is reported in Figure 4.2.

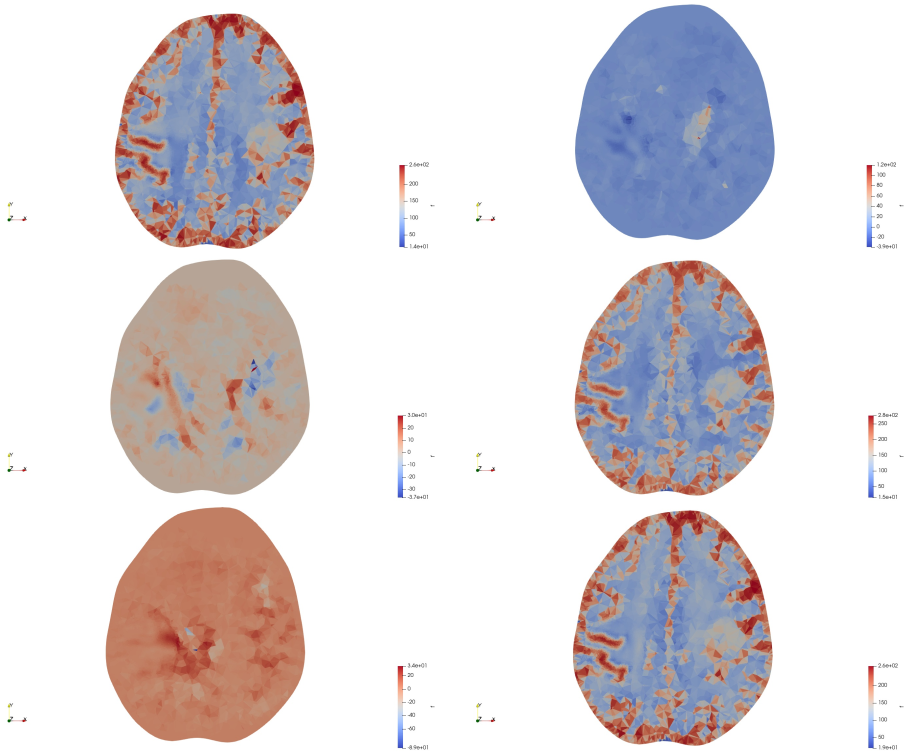

Figure 4.2: Components of the diffusion tensor $\mathbb{D}_0$ reconstructed from DTI imaging data of a patient. Starting from the top: $D_{xx}$, $D_{xy}$, $D_{xz}$, $D_{yy}$, $D_{yz}$ and $D_{zz}$

# Chapter 5

# Numerical simulations

In this chapter, we simulate the progression of Glioblastoma Multiforme. Firstly, we implement our model in a simplified geometry, i.e. a cube of side 50 mm. After, we focus on the real brain since our aim is to investigate the mechanical behaviour of Glioblastoma Multiforme in the surrounding brain tissue.

## 5.1 Numerical tests in a simplified geometry

After creating the mesh of a cube with side length of 50 mm, we want to simulate Glioblastoma Multiforme progression in order to test the reliability of our code in this simplified setting. The tumour is considered as a sphere of radious 5 mm. Firstly, the tumour region is separated from the healthy tissue by a mollification of the indicator function, as done in [**63**]. In this first case the mesh is not conformal to the material host-tumour interface but it is refined along tumour boundary in the Lagrangian reference domain. The fields $\mathbf{u}_s$, $p$, $c_n$, $g_1$, $g_2$, $g_3$ and $\phi_s$ are considered as continuous between the two zones. We take into account the parameters values discussed in Section 4.5. At the beginning, the healthy and the tumour tissue are considered identical from the mechanical viewpoint. This means that the Mooney-Rivlin elastic parameters in the two regions are taken equal with the values $\mu_{1h}$ and $\mu_{2h}$ reported in Section 4.5. Afterwards we distinguish the two tissues, using the values $\mu_{1h}$ and $\mu_{2h}$ for the healthy one and $\mu_{1t}$ and $\mu_{2t}$ for the tumour zone. We choose as time step $\Delta t = 0.1$ days, which is nearly equal to 2 hours and a half. Furthermore, we use boundary and initial conditions described in (4.7) and (4.9).
In this setting, we run two simulations: in the first one we consider isotropic diffusion and permeability, the second one has instead an artificial anisotropic behaviour.

- In the isotropic case, we take both the diffusion tensor $\mathbb{D}_0$ and the permeability tensor $\mathbb{K}_0$ as multiples of the identity tensor:

$$\begin{aligned} \mathbb{D}_0 &= D_n \mathbb{I} \\ \mu^{-1}\mathbb{K}_0 &= k\mathbb{I} \end{aligned}$$

  where $D_n$ and $k$ are reported in Section 4.5.

- In the anisotropic simulation, we vary the diffusion tensor and the permeability tensor. In this simplified setting, we do not consider data obtained from DTI imaging yet. Instead, we impose a forced anisotropic diffusion along the Y-axis, taking the diffusion tensor as

$$\mathbb{D}_0 = D_n \cdot \mathrm{diag}(0.9, 1.2, 0.9)$$

We observe that we preserve the same trace of the isotropic simulation. After that, we construct the tensor of preferential directions $\mathbb{A}_0$ and the anisotropic growth tensor $\mathbb{F}_{\mathrm{g}}$ as discussed in Section 3.2.4, using the eigenvalues and the eigenvectors of $\mathbb{D}_0$. Consequently, in this simulation we expect to observe enhanced diffusion, fluid motion and displacement induced by GBM proliferation along the Y-direction.

In Table 5.1 a comparison between the two simulations after a period of 20 days is reported.

<table>
<tr><th></th><th>Isotropic simulation</th><th>Anisotropic simulation</th></tr>
<tr><td>$\|\mathbf{u}_s\|$</td><td>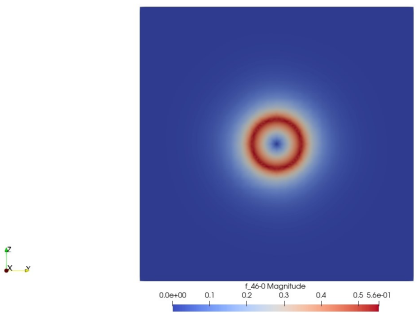</td><td>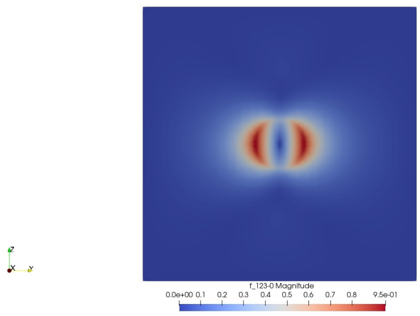</td></tr>
<tr><td>$p$</td><td>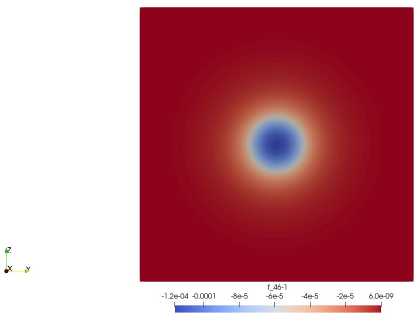</td><td>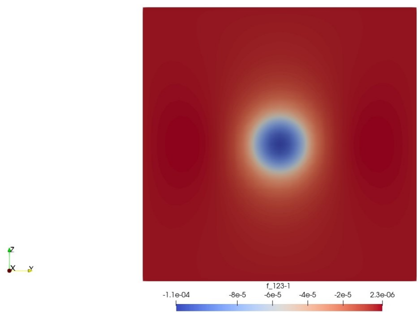</td></tr>
<tr><td>$\phi_{\mathrm{s}}$</td><td>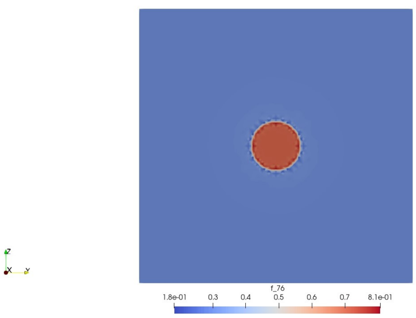</td><td>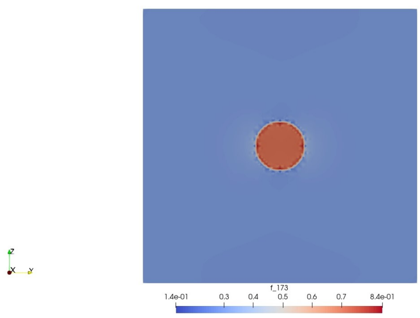</td></tr>
</table>

*Table 5.1: continued overleaf*

*Table 5.1: continued from preceding page*

| | Isotropic simulation | Anisotropic simulation |
|---|---|---|
| $g/g_1$ | 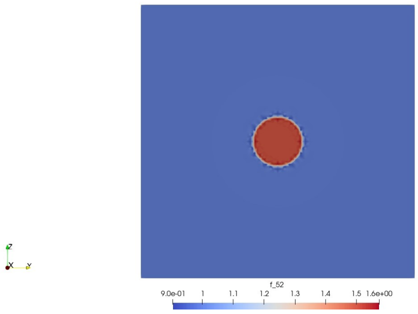 | 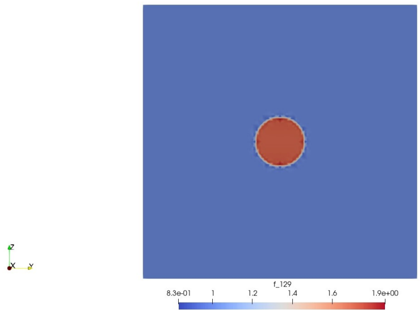 |
| $J_s$ | 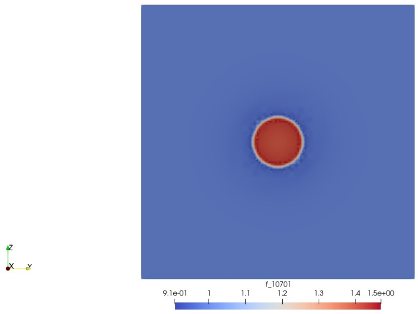 | 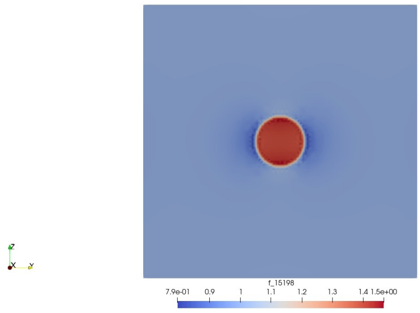 |
| $c_n$ | 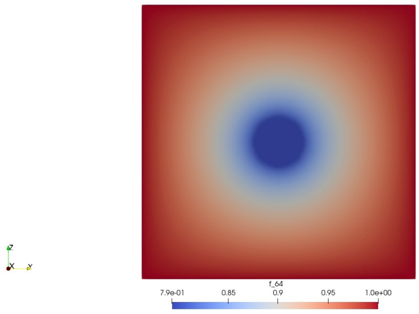 | 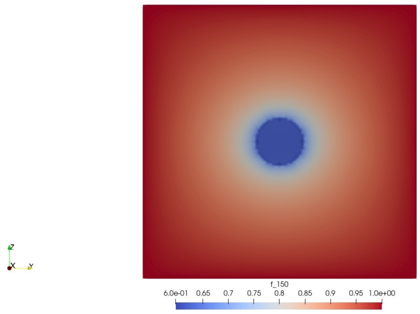 |

Table 5.1: Comparison between displacement magnitude, pressure, $J_s$, the fraction of solid particles $\phi_s$, nutrients concentration $c_n$ and $g$ in isotropic case and in the anisotropic case, at time $t = 20$ days, in the YZ-plane.

The presence of anisotropy in diffusion and conductivity causes the tumour to grow preferentially along the Y direction. In the isotropic case there is a uniform induced displacement in a circular region around the growing Glioblastoma, while the introduction of anisotropy forces GBM to acquire a more elongated shape. Furthermore, it is also intersting to make a comparison between displacement Y- and Z-components in the isotropic case and in the anisotropic case after a time of 20 days, reported in Table 5.2. It results that the displacement of the anisotropic case is greater than the isotropic one along the preferential direction (about 0.95 mm instead of 0.54 mm) and reduced on the other two directions (about 0.33 mm each).
For what concerns all the other variables, both in the isotropic and in the anisotropic case, the concentration of nutrients is reduced in the tumour region at the center of the cube, since the tumour is consuming oxygen and other nutrients to sustain

its own proliferation; at the same time, the presence of an incremented cell volume in the tumour core provokes a decrease in fluid pressure. Finally, the solid particles fraction is equal to $\phi_{\text{sn}} = 0.3$ outside the diseased zone and it increases inside it due to tumour proliferation.

| | **Isotropic simulation** | **Anisotropic simulation** |
|---|---|---|
| $(\mathbf{u}_s)_Y$ | 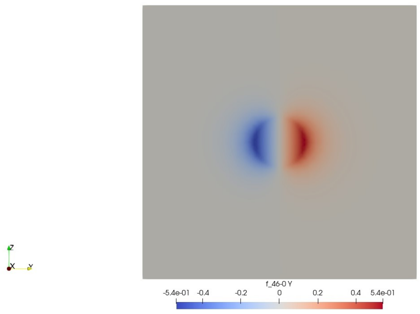 | 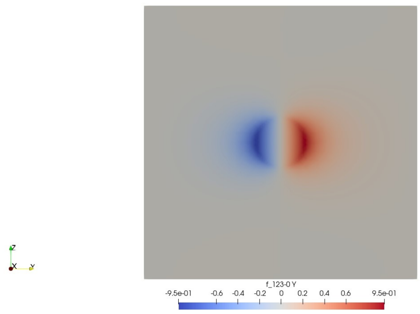 |
| $(\mathbf{u}_s)_Z$ | 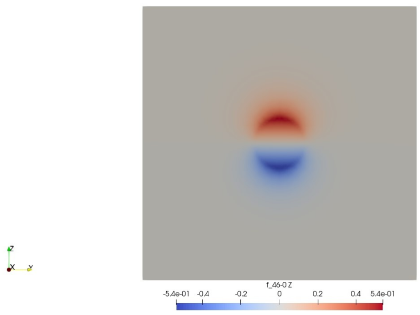 | 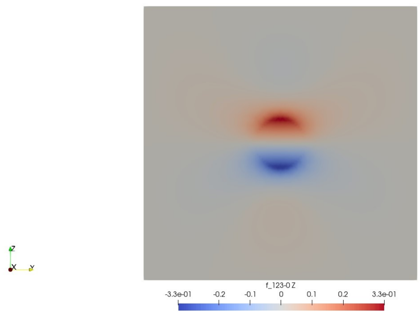 |

Table 5.2: Comparison between displacement components in isotropic case and in the anisotropic case, at time $t = 20$ days, in the YZ-plane.

We run other simulations, both in the isotropic setting and in the anisotropic one, distinguishing the material parameters between the tumour zone and the healthy one. We use $\mu_{1h}$ and $\mu_{2h}$ as the parameters for the healthy zone, while we use $\mu_{1t}$ and $\mu_{2t}$ in the tumour zone.
The results we obtain in the isotropic case after 20 days are reported in Table 5.3. The results are compared with the ones using constant material parameters. Focusing on the displacement magnitude $\|\mathbf{u}_s\|$, we observe that in every direction it is almost 5 times greater than the case where the material parameters were supposed constant. This means that the tumour tissue is stiffer than the surrounding tissue and it can expand more easily. There is a remarkable difference also between the other quantities, especially there is more nutrients consumption and the variable $g$ has a stronger growth.
If we run the same simulation in the anisotropic case we obtain the results reported in Table 5.4, considered always after a period of 20 days. In this case the magnitude of displacement along the preferential direction is four times greater than the constant parameters case. As in the isotropic case, there is also a clear difference between the other variables: the fluid pressure has a stronger decrease, the variable $g_1$ has greater growth while there is an increased consumption of nutrients in tumour zone.

| | Constant material parameters | Nonconstant material parameters |
|---|---|---|
| $\Vert\mathbf{u}_s\Vert$ | 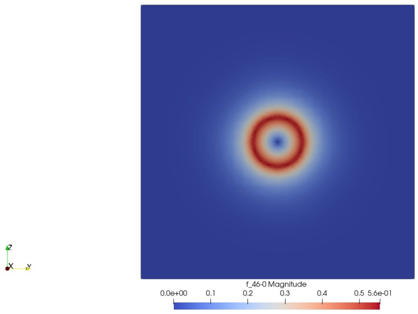 | 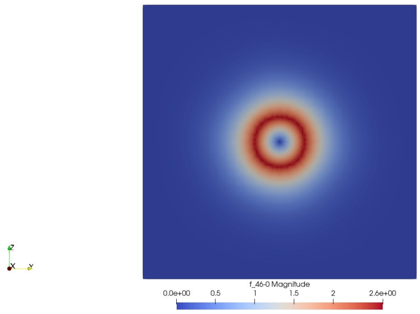 |
| $p$ | 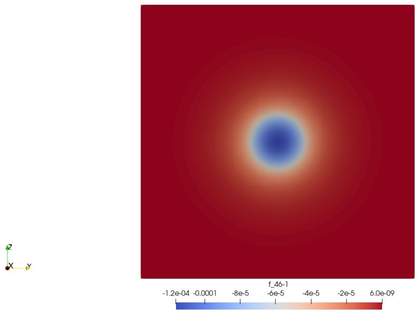 | 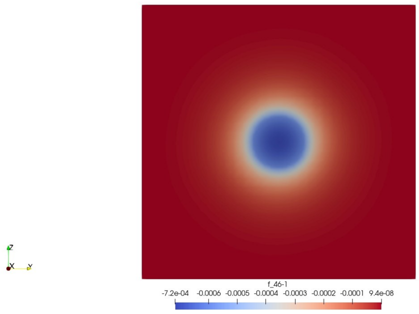 |
| $\phi_s$ | 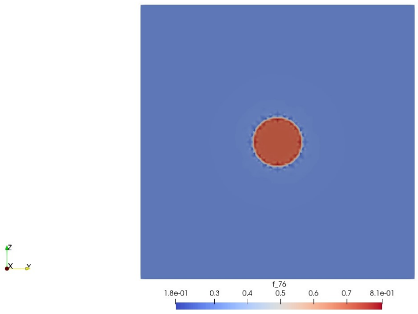 | 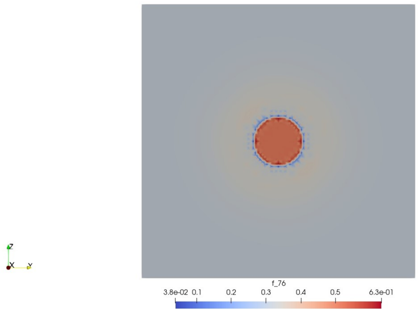 |
| $g$ | 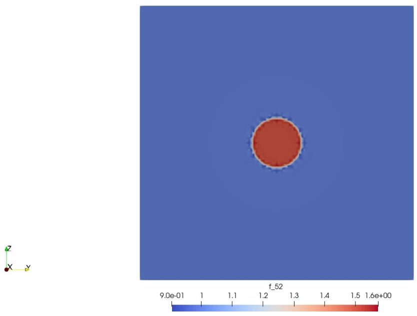 | 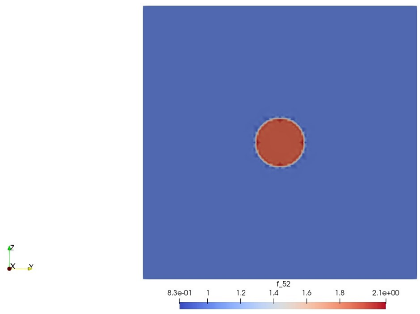 |

*Table 5.3: continued overleaf*

*Table 5.3: continued from preceding page*

| | **Constant material parameters** | **Nonconstant material parameters** |
| --- | --- | --- |
| $J_s$ | 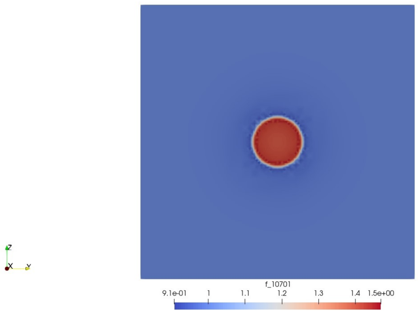 | 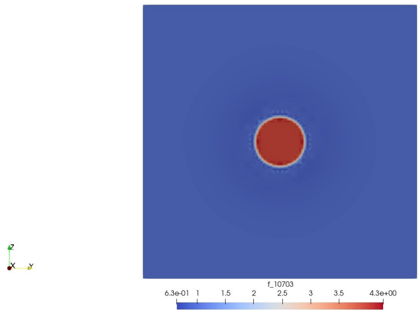 |
| $c_n$ | 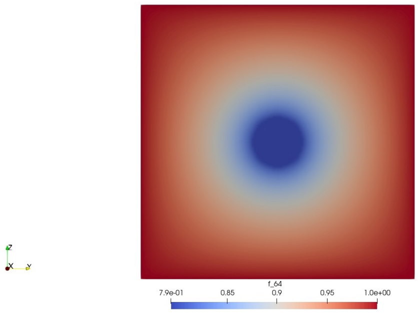 | 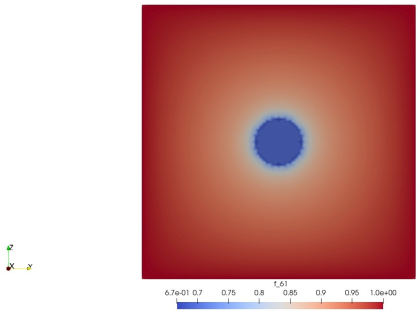 |

Table 5.3: Comparison between constant and nocostant parameters after 20 days in the isotropic case: magnitude of displacement $\|\mathbf{u}_s\|$, pressure $p$, the fraction of solid particles $\phi_s$, $g$, $J_s$ and nutrients concentration $c_n$.

| | **Constant material parameters** | **Nonconstant material parameters** |
| --- | --- | --- |
| $\|\mathbf{u}_s\|$ | 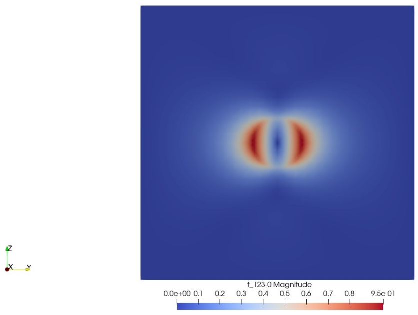 | 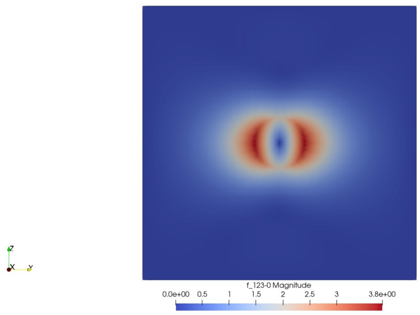 |
| $p$ | 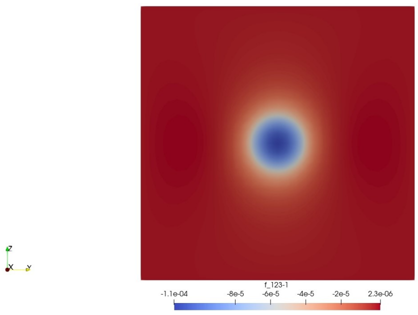 | 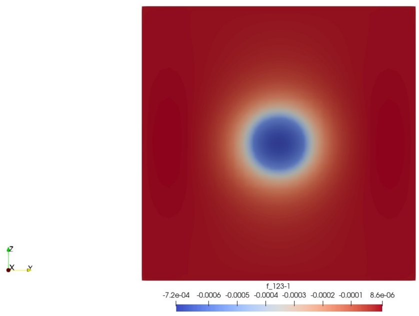 |

*Table 5.4: continued overleaf*

*Table 5.4: continued from preceding page*

| | Constant material parameters | Nonconstant material parameters |
|---|---|---|
| $\phi_s$ | 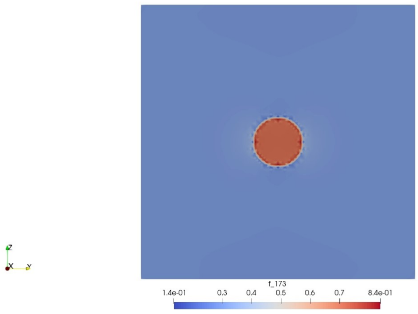 | 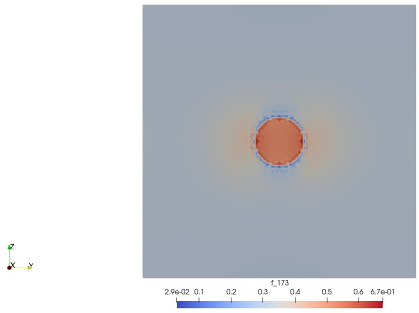 |
| $g_1$ | 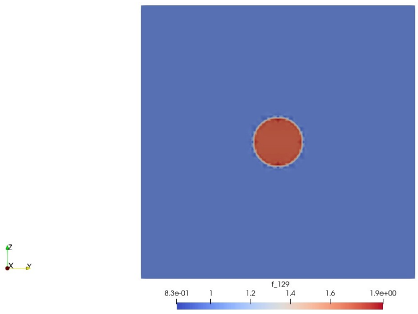 | 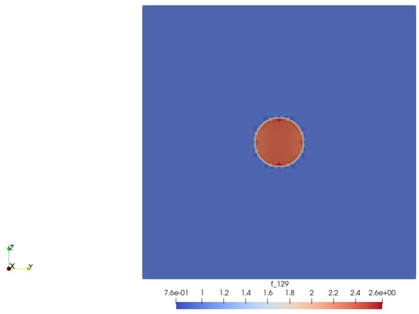 |
| $J_s$ | 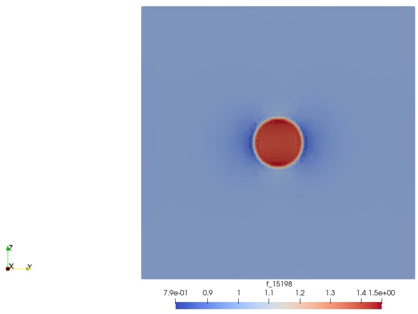 | 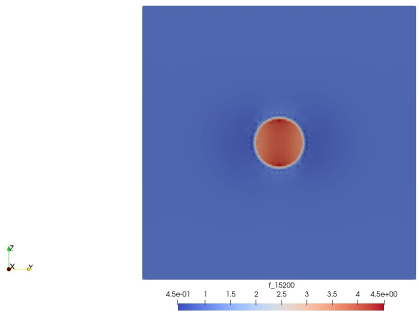 |
| $c_n$ | 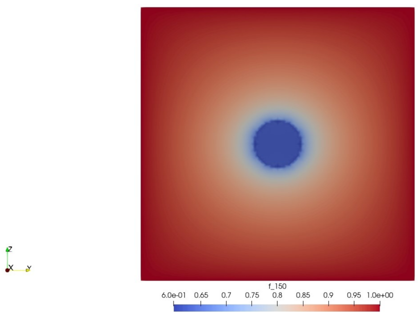 | 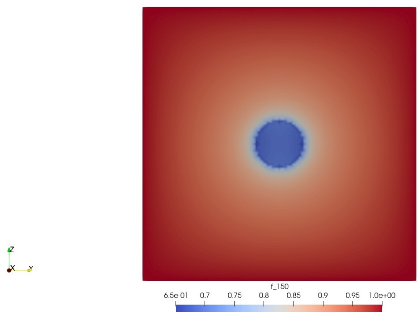 |

Table 5.4: Comparison between constant and nocostant parameters after 20 days in the anisotropic case: magnitude of displacement $\|\mathbf{u}_s\|$, pressure $p$, the fraction of solid particles $\phi_s$, $g_1$, $J_s$ and nutrients concentration $c_n$.

It is possible to notice that little irregularities appears along the boundary of the tumour in all previous simulations. This is due to the choice of a steep mollification of the indicator function and to the fact that all variables are forced to be continuous across the interface. To fix this problem we try to use a mesh conforming to the material host-tumour interface which manages to distinguish which cells belong to the tumour and which are part of the healthy tissue. In this way we manage to construct a real indicator function of the tumour. The difference between the two meshes is shown in Figure 5.1, where the red part highlight the tetrahedra which belong to the tumour zone.

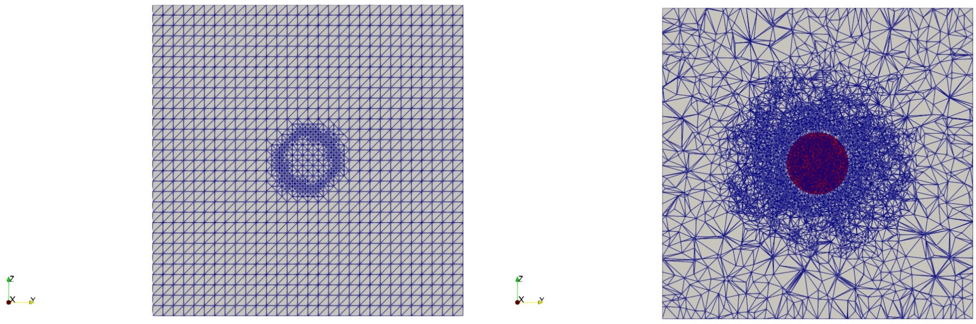

Figure 5.1: Difference between the two cube meshes

We run two simulations with this last mesh. In the first one we consider constant material parameters equal everywhere to $\mu_{1h}$ and $\mu_{2h}$. The last simulation we run in this setting is the one using different parameters between the healthy and the diseased zone, i.e. using $\mu_{1h}$ and $\mu_{2h}$ for the healthy zone and $\mu_{1t}$ and $\mu_{2t}$ for the tumour one. The results are compared in Table 5.5.

| | **Constant material parameters** | **Nonconstant material parameters** |
|---|---|---|
| $\|\mathbf{u}_s\|$ | 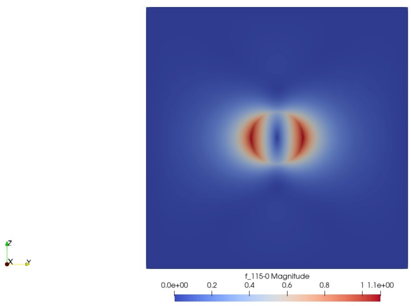 | 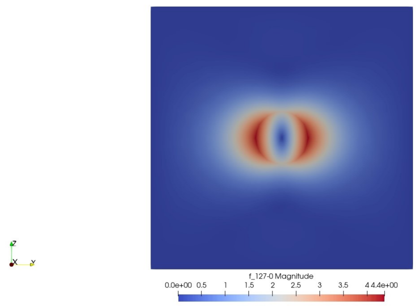 |
| $p$ | 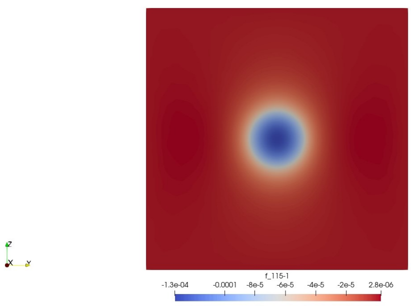 | 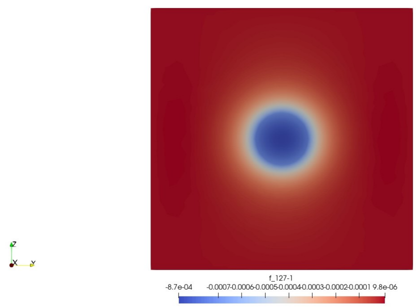 |

*Table 5.5: continued overleaf*

*Table 5.5: continued from preceding page*

| | Constant material parameters | Nonconstant material parameters |
|---|---|---|
| $\phi_s$ | 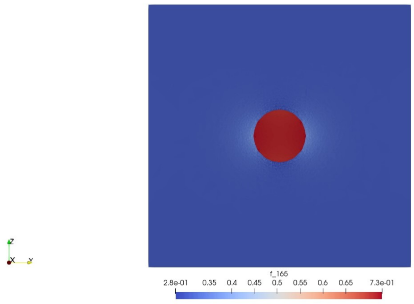 | 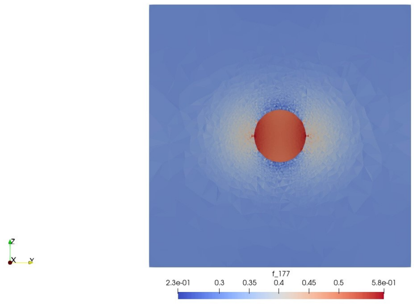 |
| $g_1$ | 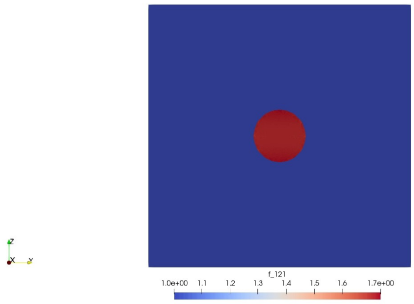 | 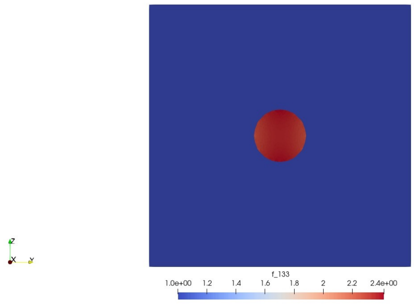 |
| $J_s$ | 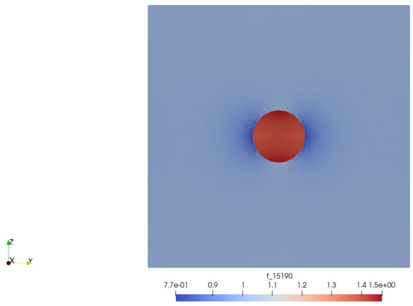 | 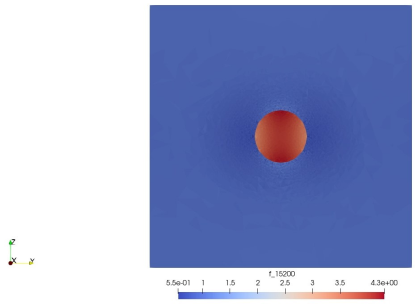 |
| $c_n$ | 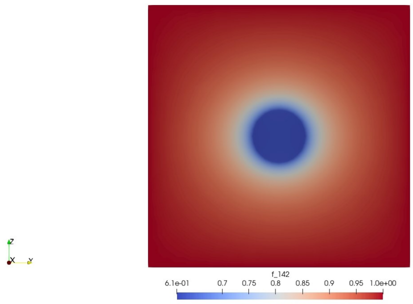 | 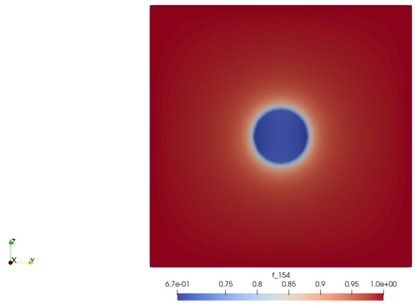 |

Table 5.5: Comparison between constant and nocostant parameters after 20 days in the anisotropic case: magnitude of displacement $\|\mathbf{u}_s\|$, pressure $p$, the fraction of solid particles $\phi_s$, $g_1$, $J_s$ and nutrients concentration $c_n$.

It is important to notice that the irregularities which were present in the previous simulations are not there anymore. Furthermore, in the simulations with the mollification function, we found some numerical problems that made the simulations stop after a certain number of iterations. Using the mesh conforming to the material host-tumour interface they have been solved. For this reason in the brain simulations we will use this last framework.

## 5.2 Numerica tests in the brain

At this point, we run simulations about GBM progression on a realistic brain geometry, obtained from DTI and MRI data. The preparation of the mesh have been described in Section 4.6. In this case the mesh was constructed conformal to the material host-tumour interface and for this reason we can use a real indicator function of the tumour, which distinguishes between cells that belong to the tumour and cells in the healthy tissue. Differently from the cubical case, the diffusion tensor and the permeability tensor have been constructed through medical data, so as to build a realistic geometry. In this simulation we consider the material parameters which appear in the Mooney-Rivlin constitutive equation equal to $\mu_{1h}$ and $\mu_{2h}$ in the healthy tissue whereas we take $\mu_{1t}$ and $\mu_{2t}$ in the diseased zone. The results we obtain after a simulation of 36 days are reported in Table 5.6.

| Variable | XY | XZ | YZ |
|---|---|---|---|
| $\lVert \mathbf{u}_s \rVert$ | 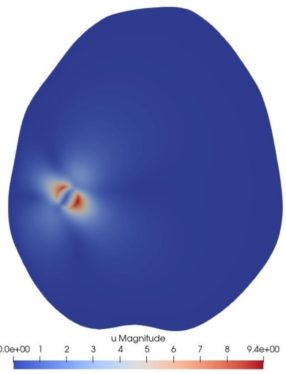 | 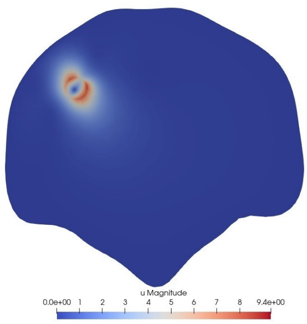 | 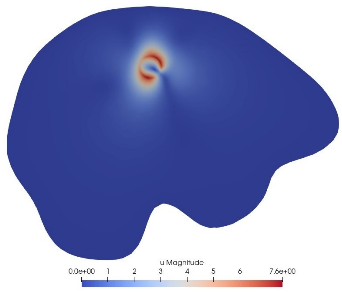 |
| $p$ | 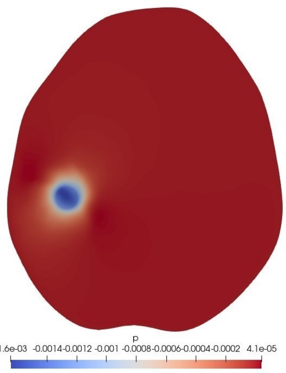 | 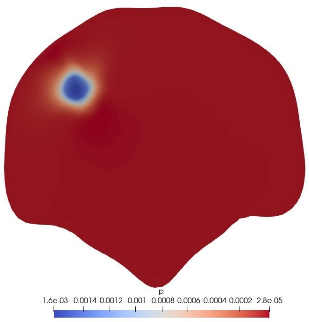 | 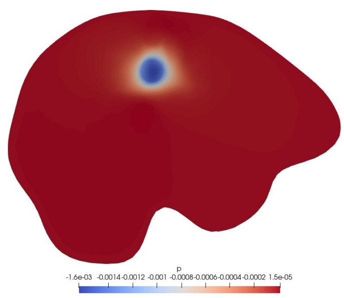 |

*Table 5.6: continued overleaf*

*Table 5.6: continued from preceding page*

| Variable | XY | XZ | YZ |
|---|---|---|---|
| $g_1$ | 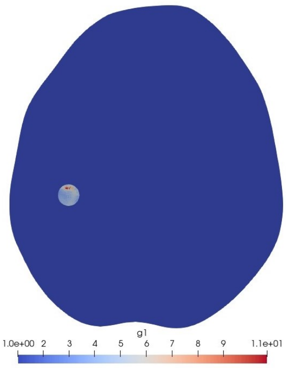  | 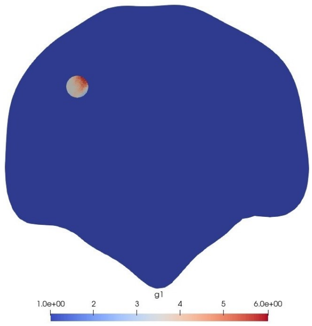  | 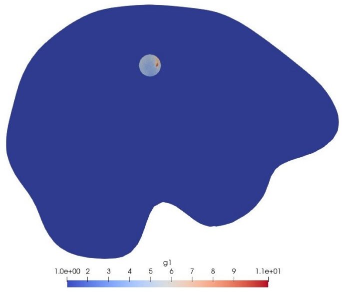  |
| $\phi_s$ | 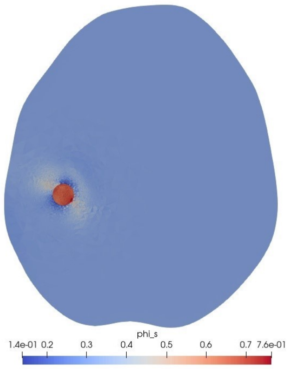  | 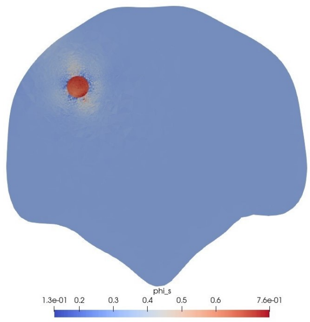  | 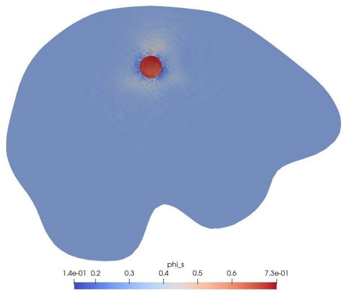  |
| $c_n$ | 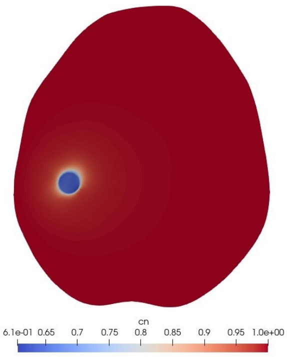  | 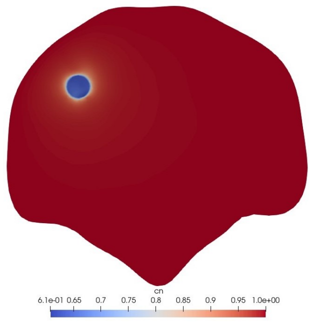  | 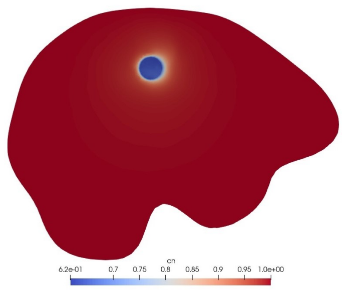  |

*Table 5.6: continued overleaf*

*Table 5.6: continued from preceding page*

| **Variable** | **XY** | **XZ** | **YZ** |
|---|---|---|---|
| $J_s$ | 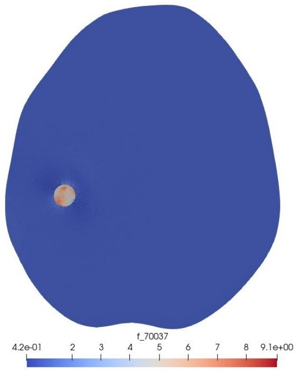 | 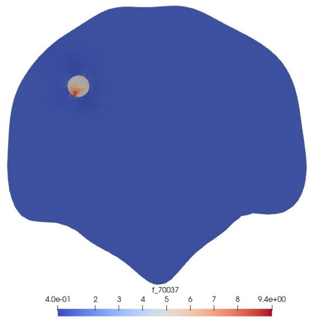 | 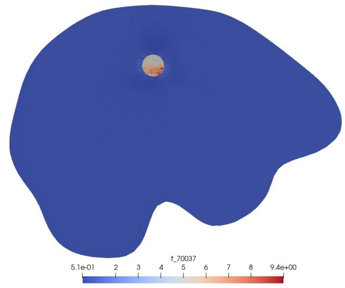 |
| $J_g$ | 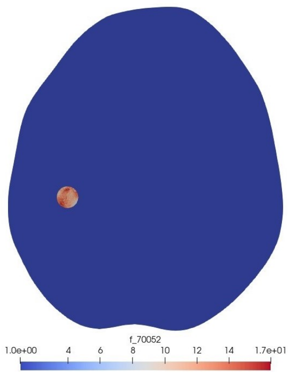 | 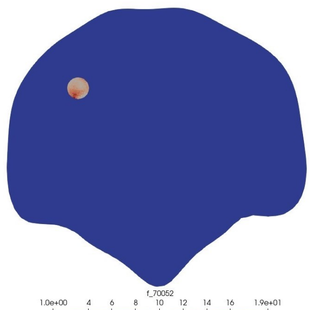 | 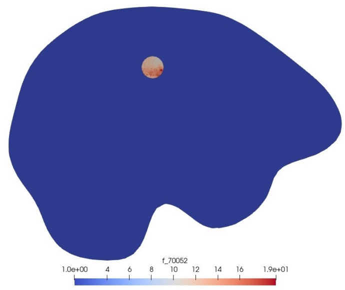 |

Table 5.6: Comparison between variables during GBM growth in the brain, clipped along three different planes, at time $t = 36$ days.

The results of all the variables are in agreement with tumour proliferation: we have a negative pressure in the tumour zone, where the volumetric fraction of the cell phase $\phi_s$ increases and the concentration of nutrients $c_n$ decreases. It is important to notice the anisotropic behaviour of all this variables, in agreement with the typical anisotropy of white matter tracts.
For what concerns the displacement, it is clearly anisotropic and the maximum of its magnitude reaches 9.4 mm. It is evident that it is quite big and it cannot be neglected. In Table 5.7 we collect the maximum and minimum values of the components of the displacement vector.

| | **X** | **Y** | **Z** |
|---|---|---|---|
| **Min** | -6.85 mm | -4.99 mm | -6.62 mm |
| **Max** | 5.61 mm | 4.41 mm | 6.27 mm |

Table 5.7: Maximum and minimum displacement values along each direction at time $t = 36$ days

# Conclusions and future developments

Glioblastoma multiforme (GBM) is an extremely aggressive and malignant type of brain tumour. This means that there is a great interest in the scientific community to analise its progression, with the purpose of understanding what is the most appropriate strategy to fight it. For this reason many mathematical models were developed, in order to predict future tumour shape and volume and to quantify its aggressiveness. Recently, many efforts have been aimed to improve the comprehension of the mechanics involved in its progression. Remaining in this field, we have developed a multiphase model based on the framework of Continuum Mechanics and mixture theory. Our aim was to include in our model constitutive properties of brain tissue, the role of stress and deformations exerted by the growing tumour on the surrounding environment and on the alignment of white matter tracts and the influence of anisotropy on tumour growth. Both the healthy and the diseased regions are treated as a saturated biphasic mixture, comprising a solid and a fluid phase. With this assumptions, using mass and momentum balance laws, we obtained a Lagrangian model including seven equations, accompanied by the constitutive definition of the hyperelastic energy and by the multiplicative decomposition of the deformation gradient, to distinguish the elastic contribution from the inelastic one due to growth.
Once the model has been obtained, we solved it numerically using Finite Elements Method. In order to do so, we derived a weak formulation of our Lagrangian model and we implemented its discretized version using the open source computing platform FEniCS, which provides a high-level Python and C++ interface. First of all, we tested our code in a simplified geometry, i.e. a cube of side 50 mm, both in isotropic and anisotropic conditions. At the beginning we used a mollified version of the indicator function. Then, in order to solve some irregularities that we noticed on the boundary of the tumour, we construct a mesh conformal to the material host-tumour interface and for this reason it is not necessary any mollification of the indicator function. In this way, we observe an improvement of the results, especially on the boundary of the tumor. All this simulations were made comparing the case where the material parameters are taken constant in all the domain and the case where the tumour tissue is considered ten times stiffer than the healthy one. We observe huge differences also between these cases. In fact, to give an example, the displacement magnitude is more than four times bigger in the second than the first one. This result highlights the importance of considering the correct mechanical material parameters in predicting cancer growth. Then, we performed a simulation on a brain geometry to verify the outcome of our model when applied to a realistic setting: we included medical data from DTI

and MRI into the computational mesh, to account for real diffusion patterns and for anisotropy of the fibers inside the brain. We observed how the growth of a tumour inside the brain has a mechanical impact on the surrounding healthy tissue, causing a deformation and a subsequent displacement magnitude quantified in about 9.4 mm after 36 days. The displacements turn out to be quite big and for this reason it cannot be neglected.
However, there are some other issues that have to be addressed in future research developments. A possible improvement of the proposed model concerns the simulation of therapies and resection. First of all, it would be interesting to model chemotherapy and radiotherapy, in order to evaluate their effectiveness in the treatment of this brain tumour. Furthermore, it would be important to highlight deformations and displacements that happen after surgical removal of Glioblastoma tumour mass. With regard to this, plastic reorganization could be included in the model, to reproduce the mechanical behaviour of the brain as much realistically as possible.

# Appendix A

# Code documentation

In the following, we report the complete Python code that has been used for numerical simulations of the model in the brain. In our simulations we rely on an open source software named the FEniCS project through a Python interface. We import the mesh, previously constructed using the program *Tetgen* and then converted from the .mesh format to the .xdmf format, which is supported by FEniCS. The conversion was made using meshio with the following code:

```
import meshio

msh = meshio.read("dominio.2.mesh")

def create_mesh(mesh, cell_type, prune_z=False):
    cells = mesh.get_cells_type(cell_type)
    cell_data = mesh.get_cell_data("medit:ref", cell_type)
    out_mesh = meshio.Mesh(points=mesh.points, \
        ...         cells ={cell_type: cells}, \
        ...         cell_data={"name_to_read": [cell_data]})
    if prune_z:
        out_mesh.prune_z_0()
    return out_mesh

tetra_mesh = create_mesh(msh, "tetra")
meshio.write("dominio2.xdmf", tetra_mesh)
```

Furthermore, we take as input the diffusion images. Input data are 6 diffusion images Fwij.nii.gz, concerning only the non-free water, and an image Fraction_fw.nii.gz containing free water weights for each voxel. At the end, the diffusion tensor will be calculated as described in Section 4.6

The code we used to simulate the model is reported in the following. After importing the libraries DOLFIN and FEniCS, we define all the useful kinematic variables that appear in the variational formulations (lines 1-109). Then, we upload the mesh and we introduce the tumour indicator function using the mesh labels (lines 111-130). After, we focus on the construction of the diffusion tensor, the tensor of preferential directions and the growth tensor, obtained from patient-specific data (lines 130-573). We then define the finite elements, the parameters, the model variables, initial and boundary conditions (lines 574-751). Finally, we construct the variational problems (lines 752-802) and the output files where the results and data will be stored (lines 803-865). At the end, all the equations are solved inside the time loop (lines 866-991).

```python
import dolfin
from dolfin import *
from fenics import *
import numpy
from numpy import linalg as LA

#set_log_level(LogLevel.PROGRESS)

#Form compiler options
dolfin.parameters["form_compiler"]["cpp_optimize"] = True
dolfin.parameters["form_compiler"]["representation"] = "uflacs"
dolfin.parameters["form_compiler"]["quadrature_degree"] = 4

### USEFUL KINEMATICS VARIABLES ###

# Renaming grad to Grad
from ufl import grad as ufl_grad
def Grad(v):
    return ufl_grad(v)

# Second order identity tensor
def SecondOrderIdentity(u):
    d = u.geometric_dimension()
    return variable(Identity(d))

# Deformation gradient
def DeformationGradient(u):
    I = SecondOrderIdentity(u)
    return variable(I + Grad(u))

# Determinant of the deformation gradient
def Jacobian(u):
    F = DeformationGradient(u)
    return variable(det(F))

# Right Cauchy-Green tensor
def RightCauchyGreen(u):
    F = DeformationGradient(u)
    return variable(F.T*F)

# Left Cauchy-Green tensor
def LeftCauchyGreen(u):
    F = DeformationGradient(u)
    return variable(F*F.T)

# Invariants of an arbitrary tensor, A
def Invariants(A):
    I1 = tr(A)
    I2 = 0.5*(tr(A)**2 - tr(A*A))
    I3 = det(A)
    return [variable(I1), variable(I2), variable(I3)]

# Invariants of the (right/left) Cauchy-Green tensor
def CauchyGreenInvariants(u):
    C = RightCauchyGreen(u)
```

```python
    [I1, I2, I3] = Invariants(C)
    return [variable(I1), variable(I2), variable(I3)]

# Anisotropic growth tensor in the multiplicative decomposition
def AnisotropicGrowthTensor(u,g1,g2,g3,eig_1,eig_2,eig_3):
    return variable(g1*outer(eig_1,eig_1)+g2*outer(eig_2,eig_2)+g3*outer(eig_3, eig_3))

# Elastic part of the deformation gradient
def ElasticPart(u, g1,g2,g3, eig_1, eig_2, eig_3):
    F = DeformationGradient(u)
    F_g = AnisotropicGrowthTensor(u, g1, g2, g3, eig_1, eig_2, eig_3)
    return variable(F*inv(F_g))

# Right Cauchy-Green tensor of the elastic part
def ElasticRCG(u, g1, g2, g3, eig_1, eig_2, eig_3):
    F_e = ElasticPart(u, g1, g2, g3, eig_1, eig_2, eig_3)
    return variable(F_e.T*F_e)

# Determinant of the growth tensor
def Jg(u, g1, g2, g3, eig_1, eig_2, eig_3):
    F_g = AnisotropicGrowthTensor(u, g1, g2, g3, eig_1, eig_2, eig_3)
    return variable(det(F_g))

# Determinant of the elastic part
def Je(u, g1, g2, g3, eig_1, eig_2, eig_3):
    F_e = ElasticPart(u, g1, g2, g3, eig_1, eig_2, eig_3)
    return variable(det(F_e))

def ElasticCbar(u, g1, g2, g3, eig_1, eig_2, eig_3):
    C_e = ElasticRCG(u, g1, g2, g3, eig_1, eig_2, eig_3)
    J_e = Je(u, g1, g2, g3, eig_1, eig_2, eig_3)
    return variable(pow(J_e,-2.0/3)*C_e)

def Pk(u, p, g1, g2, g3, eig_1, eig_2, eig_3, mu1, mu2):
    J_g = Jg(u, g1, g2, g3, eig_1, eig_2, eig_3)
    J_e = Je(u, g1, g2, g3, eig_1, eig_2, eig_3)
    F = DeformationGradient(u)
    J = Jacobian(u)
    I = SecondOrderIdentity(u)
    C_e = ElasticRCG(u, g1, g2, g3, eig_1, eig_2, eig_3)
    C_ebar = ElasticCbar(u, g1, g2, g3, eig_1, eig_2, eig_3)
    F_g = AnisotropicGrowthTensor(u, g1, g2, g3, eig_1, eig_2, eig_3)
    F_e = ElasticPart(u, g1, g2, g3, eig_1, eig_2, eig_3)
    Ice, IIce, IIIce = Invariants(C_e)
    Icbar, IIcbar, IIIcbar = Invariants(C_ebar)

    #Strain Energy using C_e bar
    psi = (mu1/2)*(Icbar - 3) + (mu2/2)*(IIcbar - 3)
    gamma1 = diff(psi, Icbar) + Icbar*diff(psi, IIcbar)
    gamma2 = -diff(psi, IIcbar)

    P_s = 2*J_g*F_e*pow(J_e, -2/3)*(gamma1*I + gamma2*C_ebar - 1/3*gamma1*Ice*inv(C_e) - 1/3*gamma2*inner(C_e,C_e)*inv(C_e))*inv(F_g).T #Piola tensor using C_ebar
    return variable(P_s - J*p*inv(F).T)
```

```
# --- Define mesh and tumour indicator function ---#

# Brain simulations
mesh = Mesh()

#Creazione MeshFunction che indica le celle col tumore

mvc = MeshValueCollection("size_t", mesh, mesh.topology().dim())
with XDMFFile("dominio2.xdmf") as infile:
    infile .read(mesh)
    infile .read(mvc, "name_to_read")

mf = cpp.mesh.MeshFunctionSizet(mesh, mvc)

mfc = MeshFunction("int", mesh, mesh.topology().dim())
mfc.set_all(0)
for cell in cells (mesh):
    if (mf.array()[ cell .index()] == 1):
        mfc[cell ] = 1

#- Diffusion tensor and the permeability tensor construction -#

mvc_Pfw = MeshValueCollection("double", mesh, "meshpFW.xml")
meshf_Pfw = MeshFunction("double", mesh, mvc_Pfw)
values_Pfw = meshf_Pfw.array()

mvc_FWxx = MeshValueCollection("double", mesh, "meshFWxx.xml")
meshf_FWxx = MeshFunction("double", mesh, mvc_FWxx)
values_Dxx = meshf_FWxx.array()

mvc_FWyy = MeshValueCollection("double", mesh, "meshFWyy.xml")
meshf_FWyy = MeshFunction("double", mesh, mvc_FWyy)
values_Dyy = meshf_FWyy.array()

mvc_FWzz = MeshValueCollection("double", mesh, "meshFWzz.xml")
meshf_FWzz = MeshFunction("double", mesh, mvc_FWzz)
values_Dzz = meshf_FWzz.array()

mvc_FWxy = MeshValueCollection("double", mesh, "meshFWxy.xml")
meshf_FWxy = MeshFunction("double", mesh, mvc_FWxy)
values_Dxy = meshf_FWxy.array()

mvc_FWxz = MeshValueCollection("double", mesh, "meshFWxz.xml")
meshf_FWxz = MeshFunction("double", mesh, mvc_FWxz)
values_Dxz = meshf_FWxz.array()

mvc_FWyz = MeshValueCollection("double", mesh, "meshFWyz.xml")
meshf_FWyz = MeshFunction("double", mesh, mvc_FWyz)
values_Dyz = meshf_FWyz.array()

## Preparazione variabili

n = len(values_Dzz) # n = ncells!
 ncells = mesh.num_cells()
numtrDnull = 0
```

```
numtrdnull = 0
numtrdnull_fisici = 0
numtrdnull_non_fisici = 0
numPfwnull = 0
epsilon = (1e-6)/3.0
r = 3 #r>1 do' piu' peso all'anisotropia
dFW = 259.2 #0.003*86400 mm^2/day
numtrTnull = 0

print("Lunghezza array: ", n)
print("Numero di celle: ", ncells)

D11 = MeshFunction("double",mesh,3)
D22 = MeshFunction("double",mesh,3)
D33 = MeshFunction("double",mesh,3)
D12 = MeshFunction("double",mesh,3)
D13 = MeshFunction("double",mesh,3)
D23 = MeshFunction("double",mesh,3)

d11 = MeshFunction("double",mesh,3)
d22 = MeshFunction("double",mesh,3)
d33 = MeshFunction("double",mesh,3)
d12 = MeshFunction("double",mesh,3)
d13 = MeshFunction("double",mesh,3)
d23 = MeshFunction("double",mesh,3)

t11 = MeshFunction("double",mesh,3)
t22 = MeshFunction("double",mesh,3)
t33 = MeshFunction("double",mesh,3)
t12 = MeshFunction("double",mesh,3)
t13 = MeshFunction("double",mesh,3)
t23 = MeshFunction("double",mesh,3)

L1 = MeshFunction("double",mesh,3)
L2 = MeshFunction("double",mesh,3)
L3 = MeshFunction("double",mesh,3)

trace_d = MeshFunction("double",mesh,3)
trace_D = MeshFunction("double",mesh,3)
MD_d = MeshFunction("double",mesh,3)
MD_D = MeshFunction("double",mesh,3)
FA = MeshFunction("double",mesh,3)

E0 = MeshFunction("double",mesh,3)
E1 = MeshFunction("double",mesh,3)
E2 = MeshFunction("double",mesh,3)
E3 = MeshFunction("double",mesh,3)
E4 = MeshFunction("double",mesh,3)
E5 = MeshFunction("double",mesh,3)
E6 = MeshFunction("double",mesh,3)
E7 = MeshFunction("double",mesh,3)
E8 = MeshFunction("double",mesh,3)
coef1=MeshFunction("double",mesh,3)
coef2=MeshFunction("double",mesh,3)
coef3=MeshFunction("double",mesh,3)

```

```
## Copia o correzione della matrice D - Calcolo della matrice T

for i in range (0,n):

  #questa matrice "ricomposta" viene usata solo per il nutriente
  D11[i] = (1-values_Pfw[i])*values_Dxx[i] + values_Pfw[i]*dFW
  D22[i] = (1-values_Pfw[i])*values_Dyy[i] + values_Pfw[i]*dFW
  D33[i] = (1-values_Pfw[i])*values_Dzz[i] + values_Pfw[i]*dFW
  D12[i] = (1-values_Pfw[i])*values_Dxy[i]
  D13[i] = (1-values_Pfw[i])*values_Dxz[i]
  D23[i] = (1-values_Pfw[i])*values_Dyz[i]

  #qui finiscono i dati presi dalle immagini fornite da Aymeric (valori SENZA free water) -> da qui calcoliamo matT
  d11[i] = values_Dxx[i]
  d22[i] = values_Dyy[i]
  d33[i] = values_Dzz[i]
  d12[i] = values_Dxy[i]
  d13[i] = values_Dxz[i]
  d23[i] = values_Dyz[i]

  trace_d[i] = d11[i] + d22[i] + d33[i]
  MD_d[i] = trace_d[i]/3.0
  trace_D[i] = D11[i] + D22[i] + D33[i]
  MD_D[i] = trace_D[i]/3.0

  if trace_D[i] == 0: #tr_D = (1-p_FW)*tr_d + 3*p_FW*dFW
    numtrDnull = numtrDnull + 1
    if values_Pfw[i] == 0:
      numPfwnull = numPfwnull + 1 #tr_D=0 e p_FW=0 => tr_d=0
    #else: tr_d=3*p_FW*dFW/(p_FW-1) con 0 < p_FW < 1
    #il caso p_FW=1 e' escluso: non potrebbe essere che tr_D=0


  if trace_d[i] != 0:
    matD = numpy.matrix([[d11[i], d12[i], d13[i]], [d12[i], d22[i], d23[i]], [d13[i], d23[i], d33[i]]])
    egvl, egvc = LA.eigh(matD)

    #egvl e' un array di tre elementi con indici 0,1,2 ordinati in ordine crescente, lambda1 e' il piu' grande
    #egvc e' una matrice dove gli elementi hanno indici 0,1,2 (prima riga) 3,4,5 (seconda riga) 6,7,8 (terza riga);
    #ogni colonna e' un autovettore, la prima relativa all'autovalore piu' piccolo, poi in ordine crescente

    lambda1 = egvl.item(2)
    lambda2 = egvl.item(1)
    lambda3 = egvl.item(0)

    if lambda3 < 0:
      lambda3 = 1e-6

    L1[i] = lambda1
    L2[i] = lambda2
    L3[i] = lambda3
```

```
    e1 = numpy.array([egvc.item(2), egvc.item(5), egvc.item(8)])
    e2 = numpy.array([egvc.item(1), egvc.item(4), egvc.item(7)])
    e3 = numpy.array([egvc.item(0), egvc.item(3), egvc.item(6)])

    E0[i]=egvc.item(0)
    E1[i]=egvc.item(1)
    E2[i]=egvc.item(2)
    E3[i]=egvc.item(3)
    E4[i]=egvc.item(4)
    E5[i]=egvc.item(5)
    E6[i]=egvc.item(6)
    E7[i]=egvc.item(7)
    E8[i]=egvc.item(8)

    c_l = (lambda1-lambda2)/(lambda1 + lambda2 + lambda3)
    c_p = 2*(lambda2-lambda3)/(lambda1 + lambda2 + lambda3)
    c_s = 3*lambda3/(lambda1 + lambda2 + lambda3)

    FA[i] = numpy.sqrt(((lambda1-lambda2)**2+(lambda2-lambda3)**2+(
     lambda3-lambda1)**2)/(2*(lambda1**2+lambda2**2+lambda3**2)))

    matR = numpy.matrix([[r, r, 1], [1, r, 1], [1, 1, 1]])
    vecC = numpy.array([c_l, c_p, c_s])
    vecA = numpy.dot(matR, vecC)

    matT = vecA.item(0)*lambda1*numpy.outer(e1,e1) + vecA.item(1)*lambda2*
     numpy.outer(e2,e2) + vecA.item(2)*lambda3*numpy.outer(e3,e3)
    matT = matT*3/(vecA.item(0)*lambda1 + vecA.item(1)*lambda2 + vecA.item
     (2)*lambda3)

    t11[i] = matT.item(0)   # T_index = [0 1 2
    t22[i] = matT.item(4)   #            3 4 5
    t33[i] = matT.item(8)   #            6 7 8]
    t12[i] = matT.item(1)
    t13[i] = matT.item(2)
    t23[i] = matT.item(5)

    coef1[i]=(lambda1*vecA.item(0))/(vecA.item(0)*lambda1+vecA.item(1)*
     lambda2+vecA.item(2)*lambda3)
    coef2[i]=(lambda2*vecA.item(1))/(vecA.item(0)*lambda1+vecA.item(1)*
     lambda2+vecA.item(2)*lambda3)
    coef3[i]=(lambda3*vecA.item(2))/(vecA.item(0)*lambda1+vecA.item(1)*
     lambda2+vecA.item(2)*lambda3)

    if t11[i] == 0 and t22[i] != 0 and t33[i] != 0:
      Tmin = numpy.minimum(t22[i],t33[i])

      if Tmin <= epsilon:
        epsilon = Tmin/2.0

      t11[i] = epsilon
      t22[i] = t22[i] - epsilon
      t33[i] = t33[i] - epsilon

    if t11[i] != 0 and t22[i] == 0 and t33[i] != 0:
```

```
            Tmin = numpy.minimum(t11[i],t33[i])

            if Tmin <= epsilon:
                epsilon = Tmin/2.0

            t11[i] = t11[i] - epsilon
            t22[i] = epsilon
            t33[i] = t33[i] - epsilon

        if t11[i] != 0 and t22[i] != 0 and t33[i] == 0:
            Tmin = numpy.minimum(t11[i],t22[i])

            if Tmin <= epsilon:
                epsilon = Tmin/2.0

            t11[i] = t11[i] - epsilon
            t22[i] = t22[i] - epsilon
            t33[i] = epsilon

        if t11[i] - 3.0 == 0:
            t11[i] = t11[i] - epsilon
            t22[i] = epsilon
            t33[i] = epsilon

        if t22[i] - 3.0 == 0:
            t11[i] = epsilon
            t22[i] = t22[i] - epsilon
            t33[i] = epsilon

        if t33[i] - 3.0 == 0:
            t11[i] = epsilon
            t22[i] = epsilon
            t33[i] = t33[i] - epsilon

        if t11[i] == 0 or t22[i] == 0 or t33[i] == 0:
            if t11[i] - 3.0 == 0:
                t11[i] = t11[i] - epsilon
                t22[i] = epsilon
                t33[i] = epsilon

            if t22[i] - 3.0 == 0:
                t11[i] = epsilon
                t22[i] = t22[i] - epsilon
                t33[i] = epsilon

            if t33[i] - 3.0 == 0:
                t11[i] = epsilon
                t22[i] = epsilon
                t33[i] = t33[i] - epsilon


    #nelle immagini fornite da Aymeric e' stata tolta la free water -> i valori nulli possono essere dovuti a errori
    # di registrazione (Pfw != 1, non fisici) oppure al fatto che in quel voxel c'e' solo free water (Pfw = 1, fisici)
    if trace_d[i] == 0:
```

```
numtrdnull = numtrdnull + 1

if values_Pfw[i] == 1: #voxel con solo free water
    numtrdnull_fisici = numtrdnull_fisici + 1

    lambda1 = d11[i] #qui viene messo 0
    lambda2 = d22[i]
    lambda3 = d33[i]
    L1[i] = lambda1
    L2[i] = lambda2
    L3[i] = lambda3
    FA[i] = 0.0


if values_Pfw[i] != 1: #voxel da correggere
    numtrdnull_non_fisici = numtrdnull_non_fisici + 1

    d11[i] = numpy.mean(values_Dxx)
    d22[i] = numpy.mean(values_Dyy)
    d33[i] = numpy.mean(values_Dzz)
    d12[i] = 0.0
    d13[i] = 0.0
    d23[i] = 0.0

    lambda1 = d11[i] #qui viene messa la media
    lambda2 = d22[i]
    lambda3 = d33[i]
    L1[i] = lambda1
    L2[i] = lambda2
    L3[i] = lambda3
    FA[i] = numpy.sqrt( ((lambda1-lambda2)**2 + (lambda2-lambda3)**2 + (lambda3-lambda1)**2) / (2*(lambda1**2 + lambda2**2 + lambda3**2)) )


D11[i] = (1-values_Pfw[i])*d11[i] + values_Pfw[i]*dFW
D22[i] = (1-values_Pfw[i])*d22[i] + values_Pfw[i]*dFW
D33[i] = (1-values_Pfw[i])*d33[i] + values_Pfw[i]*dFW
D12[i] = 0
D13[i] = 0
D23[i] = 0

t11[i] = 1.0
t22[i] = 1.0
t33[i] = 1.0
t12[i] = 0
t13[i] = 0
t23[i] = 0

E0[i]=1
E1[i]=0
E2[i]=0
E3[i]=0
E4[i]=1
E5[i]=0
E6[i]=0
E7[i]=0
```

```
    E8[i]=1

    coef1[i]=1/3
    coef2[i]=1/3
    coef3[i]=1/3

# Code for construction of tensor D and T

defineMatrix_code = """

#include <pybind11/pybind11.h>
#include <pybind11/eigen.h>
namespace py = pybind11;

#include <dolfin/function/Expression.h>
#include <dolfin/mesh/MeshFunction.h>

 class Components_DT_D : public dolfin::Expression

{
public:

      // Create expression with 6 components
      Components_DT_D() : dolfin::Expression(6) {}

      // Function for evaluating expression on each cell
      void eval(Eigen::Ref<Eigen::VectorXd> values, Eigen::Ref<const Eigen::VectorXd> x, const ufc::cell& cell) const override
     {
      const uint topDim = cell.topological_dimension;
      const uint cell_index = cell.index;
      values[0] = (*d11)[cell_index];
      values[1] = (*d12)[cell_index];
      values[2] = (*d13)[cell_index];
      values[3] = (*d22)[cell_index];
      values[4] = (*d23)[cell_index];
      values[5] = (*d33)[cell_index];
     }

     // The data stored in mesh functions
     std::shared_ptr<dolfin::MeshFunction<double> > d11;
     std::shared_ptr<dolfin::MeshFunction<double> > d12;
     std::shared_ptr<dolfin::MeshFunction<double> > d13;
     std::shared_ptr<dolfin::MeshFunction<double> > d22;
     std::shared_ptr<dolfin::MeshFunction<double> > d23;
     std::shared_ptr<dolfin::MeshFunction<double> > d33;

};

PYBIND11_MODULE(SIGNATURE, m)
{
    py::class_<Components_DT_D, std::shared_ptr<Components_DT_D>, dolfin::Expression>
      (m, "Components_DT_D")
      .def(py::init<>())
      .def_readwrite("d11", &Components_DT_D::d11)
```

```
        .def_readwrite("d12", &Components_DT_D::d12)
        .def_readwrite("d13", &Components_DT_D::d13)
            .def_readwrite("d22", &Components_DT_D::d22)
            .def_readwrite("d23", &Components_DT_D::d23)
            .def_readwrite("d33", &Components_DT_D::d33);
}

"""

d = CompiledExpression(compile_cpp_code(defineMatrix_code).Components_DT_D(), d11 = D11, d12 = D12, d13 = D13, d22 = D22, d23 = D23, d33 = D33, degree=2)
D0 = as_matrix([ [d[0], d[1], d[2]], [d[1], d[3], d[4]], [d[2], d[4], d[5]] ])

tmat = CompiledExpression(compile_cpp_code(defineMatrix_code).Components_DT_D(), d11 = t11, d12 = t12, d13 = t13, d22 = t22, d23 = t23, d33 = t33, degree=2)
mat_T = as_matrix([ [tmat[0], tmat[1], tmat[2]], [tmat[1], tmat[3], tmat[4]], [tmat[2], tmat[4], tmat[5]] ])

# Code for the construction of the eigenvectors
defineVector_code = """

#include <pybind11/pybind11.h>
#include <pybind11/eigen.h>
namespace py = pybind11;

#include <dolfin/function/Expression.h>
#include <dolfin/mesh/MeshFunction.h>

class Components_DT_e : public dolfin::Expression
{
public:

    // Create expression with 3 components
    Components_DT_e() : Expression(3) {}

    // Function for evaluating expression on each cell
    void eval(Eigen::Ref<Eigen::VectorXd> values, Eigen::Ref<const Eigen::VectorXd> x, const ufc::cell& cell) const override
    {
    const uint topDim = cell.topological_dimension;
    const uint cell_index = cell.index;
    values[0] = (*C1)[cell_index];
    values[1] = (*C2)[cell_index];
    values[2] = (*C3)[cell_index];
    }

    // The data stored in mesh functions
    std::shared_ptr<dolfin::MeshFunction<double> > C1;
    std::shared_ptr<dolfin::MeshFunction<double> > C2;
    std::shared_ptr<dolfin::MeshFunction<double> > C3;

};

PYBIND11_MODULE(SIGNATURE, m)
```

```
{
    py::class_<Components_DT_e, std::shared_ptr<Components_DT_e>, dolfin::Expression>
      (m, "Components_DT_e")
      .def(py::init<>())
      .def_readwrite("C1", &Components_DT_e::C1)
      .def_readwrite("C2", &Components_DT_e::C2)
      .def_readwrite("C3", &Components_DT_e::C3);
}

"""

e1v = CompiledExpression(compile_cpp_code(defineVector_code).
    Components_DT_e(), C1 = E2, C2 = E5, C3 = E8, degree=2)
eig_1 = as_vector([e1v[0], e1v[1], e1v[2]])

e2v = CompiledExpression(compile_cpp_code(defineVector_code).
    Components_DT_e(), C1 = E1, C2 = E4, C3 = E7, degree=2)
eig_2 = as_vector([e2v[0], e2v[1], e2v[2]])

e3v = CompiledExpression(compile_cpp_code(defineVector_code).
    Components_DT_e(), C1 = E0, C2 = E3, C3 = E6, degree=2)
eig_3 = as_vector([e3v[0], e3v[1], e3v[2]])

coe = CompiledExpression(compile_cpp_code(defineVector_code).
    Components_DT_e(), C1 = coef1, C2 = coef2, C3 = coef3, degree=2)
coeff = as_vector([coe[0], coe[1], coe[2]])

# Salvataggio dati

D11_file_pvd = File("D11.pvd")
D22_file_pvd = File("D22.pvd")
D33_file_pvd = File("D33.pvd")
D12_file_pvd = File("D12.pvd")
D13_file_pvd = File("D13.pvd")
D23_file_pvd = File("D23.pvd")

D11_file_pvd << D11
D22_file_pvd << D22
D33_file_pvd << D33
D12_file_pvd << D12
D13_file_pvd << D13
D23_file_pvd << D23

#--- Define finite elements and function spaces ---#

P2 = VectorElement("Lagrange", mesh.ufl_cell(), 1) # displacement u
P1 = FiniteElement("Lagrange", mesh.ufl_cell(), 1) # pressure p, concentration c_n
TH = MixedElement([P2, P1])
DGe = FiniteElement("Discontinuous Lagrange", mesh.ufl_cell(), 0)

V = FunctionSpace(mesh, TH) #(u,p)
W = FunctionSpace(mesh, P1) # c_n
U2 = FunctionSpace(mesh, P2)
DG = FunctionSpace(mesh, DGe) #g1, g2, g3, fraction phi_s

```

```
#--- Parameters definition ---#

class Tumor(UserExpression):
    def __init__(self, mfc, t_zone, h_zone, **kwargs):
        super().__init__(**kwargs)
        self._mfc = mfc
        self._t_zone = t_zone
        self._h_zone = h_zone

    def eval_cell(self, values, x, cell):
            if self._mfc.array()[cell.index] == 0:
                values[0] = self._h_zone
            else:
                values[0] = self._t_zone

    def value_shape(self):
         return ()

sharp_tumour_indicator = Tumor(mfc, 1, 0, degree=0)

# Initial and boundary values
c = Constant(1.0)
u0 = Constant((0.0, 0.0, 0.0))
pp = Constant(0.0)

# Simulation time and time step
t = float(0)

T = 90 #90 days
sudd_day = 10
num_steps = T*sudd_day #900 steps
dt = T / num_steps #1e-01 days --> 2,4 hours

phi_sn = Constant(0.3)
nu = 0.5 # day^-1
k = Constant(2.17e05) #(mm^2) / (MPa day)
K0 = k*mat_T
cn0 = Constant(0.3) # Hypoxia Threshold (dimensionless)
zeta = Constant(8640) # Nutrients consumption rate (1/day)
Sn = Constant(1e04) # Nutrients supply rate (1/day)
phimax = Constant(0.85)

mu1 = Function(DG)
mu2 = Function(DG)

mu1t = Constant(1.53e-03)
mu2t = Constant(2.97e-03)
mu1h = Constant(1.53e-04)
mu2h = Constant(2.97e-04)

mu1_e = Tumor(mfc, mu1t, mu1h, degree=0)
mu2_e = Tumor(mfc, mu2t, mu2h, degree=0)

mu1.interpolate(mu1_e)
mu2.interpolate(mu2_e)
#--- Define Dirichlet boundary conditions for u, p, c ---#
```

```
def boundary(x, on_boundary):
    return on_boundary

bcu = DirichletBC(V.sub(0), u0, boundary)
bcp = DirichletBC(V.sub(1), pp, boundary)
bcn = DirichletBC(W, c, boundary)

bcs = [bcu, bcp]

#--- Define functions for variational problems ---#

# Incremental displacement and pressure
dup = TrialFunction(V)
(du, dp) = split(dup)

# Test functions for displacement and pressure
u_, p_ = TestFunctions(V)

# Displacement and pressure (current value)
up = Function(V)
(u, p) = split(up)

# Displacement and pressure (previous iteration)
up_prev = Function(V)
(u_prev, p_prev) = split(up_prev)

# Functions for scalar field g1
g1 = Function(DG)
dg1 = TrialFunction(DG)
g1_prev = Function(DG)
q = TestFunction(DG)

# Functions for scalar field g2
g2 = Function(DG)
dg2 = TrialFunction(DG)
g2_prev = Function(DG)

# Functions for scalar field g3
g3 = Function(DG)
dg3 = TrialFunction(DG)
g3_prev = Function(DG)

# Functions for phi_s
phi_s = Function(DG)
dphi = TrialFunction(DG)
eta = TestFunction(DG)

# Functions for c_n
cn = Function(W)
dcn = TrialFunction(W)
qcn = TestFunction(W)
cn_prev = Function(W)

#--- Define initial conditions ---#
# Initial condition for u and p
up_init = Expression( ("0.0", "0.0", "0.0", "0.0"), degree=1)
```

```
up_prev = interpolate(up_init, V)

#u_init = Function(U2,"out_u.xml")
#p_init = Function(W,"out_p.xml")
#assign(up_prev, [u_init, p_init])

# Initial conditions for g and phi_s
g1_prev = interpolate(Constant(1.0), DG)
#g1_prev = Function(DG, "out_g1.xml")
g2_prev = interpolate(Constant(1.0), DG)
#g2_prev = Function(DG, "out_g2.xml")
g3_prev = interpolate(Constant(1.0), DG)
#g3_prev = Function(DG, "out_g3.xml")

phi_s = interpolate(Constant(0.3), DG)
#phi_s = Function(DG, "out_phi_s.xml")

#--- Definition of model variables ---#

# Gamma_s: tumour growth term
cn_g = Expression("cc > c0 ? (cc-c0) : 0", cc = cn_prev, c0 = cn0, degree=1)

def Gamma_s(phi_s, cn_g):
    return variable(nu*phi_s*(phimax-phi_s)*cn_g)

# Gn: source term for nutrients
### NOTA: non e' presente phi_l perche' qua si intende quello che nella tesi risulta essere Gn/phi_l
def Gn_l(phi_s, cn):
    return variable(-zeta*phi_s*cn + Sn*(1-cn))

Gn = Gn_l(phi_s, dcn)

# Kinematics
d = len(u)
I = SecondOrderIdentity(u) # Identity tensor
F = DeformationGradient(u) # Deformation gradient F_s
C = RightCauchyGreen(u) # Right Cauchy-Green tensor of F_s

# Growth part of F_s
F_g = AnisotropicGrowthTensor(u, g1, g2, g3, eig_1, eig_2, eig_3)
# Elastic part of F_s
F_e = ElasticPart(u, g1, g2, g3, eig_1, eig_2, eig_3)
# Elastic right Cauchy-Green
C_e = ElasticRCG(u, g1, g2, g3, eig_1, eig_2, eig_3)

Ic, IIc, IIIc = CauchyGreenInvariants(u)
Ice, IIce, IIIce = Invariants(C_e) # Invariants of elastic RCG
J = Jacobian(u)
F_k = DeformationGradient(u_prev)
J_k = Jacobian(u_prev)
J_g = Jg(u, g1, g2, g3, eig_1, eig_2, eig_3)
J_e = Je(u, g1, g2, g3, eig_1, eig_2, eig_3)
P = Pk(u, p, g1, g2, g3, eig_1, eig_2, eig_3, mu1, mu2)

#--- Variational problem for u and p ---#
```

```
deltat = Constant(dt)
L = J*p_*dx + deltat*inner(Grad(p_), J*K0*Grad(p))*dx - inner(P, Grad(u_))*dx - J_k*p_*dx
j = derivative(L, up, dup)
problem = NonlinearVariationalProblem(L, up, bcs, J=j)
solver = NonlinearVariationalSolver(problem)

prm = solver.parameters
#info(prm, True)

prm['nonlinear_solver'] = 'snes'
prm['snes_solver']['line_search'] = 'bt'

#prm['snes_solver']['absolute_tolerance'] = 1E-8
#prm['snes_solver']['relative_tolerance'] = 1E-7
prm['snes_solver']['maximum_iterations'] = 100
#prm['snes_solver']['relaxation_parameter'] = 1.0

prm['snes_solver']['linear_solver'] = 'mumps'
#prm['snes_solver']['linear_solver'] = 'gmres'

prm['snes_solver']['error_on_nonconvergence'] = False

#prm['snes_solver']['preconditioner'] = 'hypre_amg'
#prm['snes_solver']['krylov_solver']['absolute_tolerance'] = 1E-9
#prm['snes_solver']['krylov_solver']['relative_tolerance'] = 1E-7
#prm['newton_solver']['krylov_solver']['maximum_iterations'] = 1000
prm['snes_solver']['krylov_solver']['monitor_convergence'] = True
#prm['newton_solver']['krylov_solver']['nonzero_initial_guess'] = True
#prm['newton_solver']['krylov_solver']['gmres']['restart'] = 40
#prm['newton_solver']['krylov_solver']['preconditioner']['ilu']['fill_level'] = 0

#--- Variational problem for nutrients ---#
# Steady state solution to derive initial condition
dcn_staz = TrialFunction(W)
cn_staz = Function(W)
ac_staz = inner(Grad(qcn), J_k*D0*Grad(dcn_staz))*dx + J_k*sharp_tumour_indicator*zeta*phi_s*dcn_staz*qcn*dx + J_k*sharp_tumour_indicator*Sn*dcn_staz*qcn*dx
Lc_staz = J_k*sharp_tumour_indicator*Sn*qcn*dx

solve(ac_staz == Lc_staz, cn_staz, bcn)
cn_prev.assign(cn_staz)

#cn_prev = Function(W, "out_cn.xml")

# Variational problem
Fcn = J*dcn*qcn*dx - deltat*(1/(1-phi_s))*inner(J*K0*Grad(p), Grad(dcn))*qcn*dx + deltat*inner(Grad(qcn), J*D0*Grad(dcn))*dx - J*cn_prev*qcn*dx - deltat*J*sharp_tumour_indicator*Gn*qcn*dx

ac = lhs(Fcn)

Lc = rhs(Fcn)

#--- Files for data storing ---#
```

```

Jp_k = project(J_k, DG)
Jg_k = project(J_g, DG)
Je_k = project(J_e, DG)

(uu, pp) = up_prev.split()

uu.rename("u", "")
pp.rename("p", "")
phi_s.rename("phi_s", "")
g1_prev.rename("g1", "")
g2_prev.rename("g2", "")
g3_prev.rename("g3", "")
cn_prev.rename("cn", "")

### Salvataggio in file diversi pvd

displacement_file = File("u.pvd")
pressure_file  = File("p.pvd")
phi_s_file = File("phi_s.pvd")
g1_file  = File("g1.pvd")
g2_file  = File("g2.pvd")
g3_file  = File("g3.pvd")
cn_file  = File("cn.pvd")
Js_file  = File("Js.pvd")
Jg_file  = File("Jg.pvd")
Je_file  = File("Je.pvd")

displacement_file << (uu, t)
pressure_file  << (pp, t)
phi_s_file << (phi_s, t)
g1_file  << (g1_prev, t)
g2_file  << (g2_prev, t)
g3_file  << (g3_prev, t)
cn_file  << (cn_prev, t)
Js_file  << (Jp_k, t)
Jg_file  << (Jg_k, t)
Je_file  << (Je_k, t)

#--- Salvataggio xml ---#

out_g1 = Function(DG)
out_g1_file = File("out_g1.xml")

out_g2 = Function(DG)
out_g2_file = File("out_g2.xml")

out_g3 = Function(DG)
out_g3_file = File("out_g3.xml")

out_cn = Function(W)
out_cn_file = File("out_cn.xml")

out_phi_s = Function(DG)
out_phi_s_file = File("out_phi_s.xml")

```

```
out_p = Function(W)
out_p_file = File("out_p.xml")

out_u = Function(U2)
out_u_file = File("out_u.xml")

#--- Loop for time stepping ---#
n = 1
d = 0 #dimezzamenti nel tempo

while(t <= T):
        t+= dt
        print("Iterazione", n, "-esima", "Tempo", t)

        # Solution for g1
        ag = dg1*(1-coeff[0]*deltat*(Gamma_s(phi_s, cn_g)*
       sharp_tumour_indicator/(phi_s)))*q*dx
        Lg = g1_prev*q*dx
        solve(ag == Lg, g1)

        # Solution for g2
        ag = dg2*(1-coeff[1]*deltat*(Gamma_s(phi_s, cn_g)*
       sharp_tumour_indicator/(phi_s)))*q*dx
        Lg = g2_prev*q*dx
        solve(ag == Lg, g2)

        # Solution for g3
        ag = dg3*(1-coeff[2]*deltat*(Gamma_s(phi_s, cn_g)*
       sharp_tumour_indicator/(phi_s)))*q*dx
        Lg = g3_prev*q*dx
        solve(ag == Lg, g3)

        # Solution of nonlinear variational problem for u and p
        (num_iter, conv) = solver.solve()

        #Caso in cui il metodo non converge
        if conv == 0:
            while(conv == 0 and d < 10):
                d = d+1
                print("Tempo dimezzato")
                dt = 0.5*dt
                t = t-dt
                deltat = Constant(dt)
                print("Dimezzamento", d, "-esimo", "Tempo", t)

                # Solution for g1
                ag = dg1*(1-coeff[0]*deltat*(Gamma_s(phi_s, cn_g)*
       sharp_tumour_indicator/(phi_s)))*q*dx
                Lg = g1_prev*q*dx
                solve(ag == Lg, g1)

                # Solution for g2
                ag = dg2*(1-coeff[1]*deltat*(Gamma_s(phi_s, cn_g)*
       sharp_tumour_indicator/(phi_s)))*q*dx
                Lg = g2_prev*q*dx
                solve(ag == Lg, g2)
```

```
            # Solution for g3
            ag = dg3*(1-coeff[2]*deltat*(Gamma_s(phi_s, cn_g)*
    sharp_tumour_indicator/(phi_s)))*q*dx
            Lg = g3_prev*q*dx
            solve(ag == Lg, g3)

            # Solution of nonlinear variational problem for u and p
            (num_iter, conv ) = solver.solve()

            if conv == 0 & d == 10:
                print("Non si riesce a convergere")
                exit()

    #Caso in cui il metodo converge
    if conv == 1:

        (u, p) = up.split()
        Jp = project(Jacobian(u),DG)
        Jg_k = project(J_g, DG)
        Je_k = project(J_e, DG)

        # Solution for phi_s

        aphi = Jp*dphi*eta*dx
        Lphi = J_g*phi_sn*eta*dx
        solve(aphi == Lphi, phi_s)

        # Solution of linear variational problem for cn

        solve(ac == Lc, cn, bcn)

        ### Salvataggio su file

        u.rename("u", "")
        p.rename("p", "")
        g1.rename("g1", "")
        g2.rename("g2", "")
        g3.rename("g3", "")
        cn.rename("cn", "")

        if (t % 1 <= 1e-5) or (t % 1 > 0.999):
            g1_file << (g1, t)
            assign(out_g1, g1)
            out_g1_file << out_g1

            g2_file << (g2, t)
            assign(out_g2, g2)
            out_g2_file << out_g2

            g3_file << (g3, t)
            assign(out_g3, g3)
            out_g3_file << out_g3

            displacement_file << (u, t)
            pressure_file << (p, t)
```

```
            Js_file  << (Jp, t)
            Jg_file  << (Jg_k, t)
            Je_file  << (Je_k, t)
            assign(out_p, p)
            out_p_file << out_p
            assign(out_u, u)
            out_u_file << out_u

            phi_s_file << (phi_s, t)
            assign(out_phi_s, phi_s)
            out_phi_s_file << out_phi_s

            cn_file  << (cn, t)
            assign(out_cn, cn)
            out_cn_file << out_cn

        # Assegnazione variabili tempo precedente

        g1_prev.assign(g1)
        g2_prev.assign(g2)
        g3_prev.assign(g3)
        up_prev.assign(up)
        cn_prev.assign(cn)


    n = n+1
```

# Bibliography


[1] Cancer.Net (08/2019). 'What is Cancer?'.
*https://www.cancer.net/navigating-cancer-care/cancer-basics/what-cancer*

[2] R. A. Weinberg, 'How Cancer Arises'.
*Scientific American*, 275(3):62–70, 1996

[3] R.A. Weinberg. 'The Biology of Cancer' (2nd Edition).
*Garland Science*, 2014.

[4] Kitos Biotech (March 6, 2019). '3D Spheroids for Cancer Research'
*https://www.labsexplorer.com/news/3d-spheroids-for-cancer-research_ 707*

[5] P. Carmeliet. 'Mechanisms of Angiogenesis and Arteriogenesis'.
*Nature Medicine*, 6:389–395, 2000.

[6] L.A. Hapach, J.A. Mosier, W. Wang et al. 'Engineered models to parse apart the metastatic cascade'.
*npj Precis. Onc. 3*, 20 (2019).

[7] D. Hanahan and R.A. Weinberg, 'The Hallmarks of Cancer'.
*Cell*, 100:57–70, 2000.

[8] D. Hanahan and R.A. Weinberg, 'Hallmarks of Cancer: The Next Generation.'
*Cell*, 144:646–674, 2011.

[9] M. Hoffman, 'Picture of the Brain'
*Human Anatomy*

[10] D. Purves, G.J. Augustine, D. Fitzpatrick, W.C. Hall, A.-S. LaMantia, J.O. McNamara, S.M. Williams. 'Neuroscience'.
*Sinauer Associates*, 3rd edition, 2004.

[11] F. Bray, J. Ferlay, I. Soerjomataram, R.L. Siegel, L.A. Torre, and A. Jemal. 'Global cancer statistics 2018: Globocan estimates of incidence and mortality worldwide for 36 cancers in 185 countries.'
*CA: A Cancer Journal for Clinicians*, 68:394-424, 2018.

[12] C. Lu-Emerson, A.F. Eichler. 'Brain metastases'.
*Continuum (Minneap Minn).* 2012 Apr; 18(2):295-311.

[13] D.W. Parsons, S. Jones, X. Zhang, J.C. Lin, R.J. Leary et al. 'An Integrated Genomic Analysis of Human Glioblastoma Multiforme'.
*Science*. 2008 Sep 26;321(5897):1807-12.

[14] F. B. Furnari, T. Fenton, R. M. Bachoo, A. Mukasa, J. M. Stommel, A. Stegh, W.C. Hahn, K. L. Ligon, D. N. Louis, C. Brennan, L. Chin, R. A. DePinho, W. K. Cavenee, 'Malignant astrocytic glioma: genetics, biology, and paths to treatment'.
*Genes & Development*, vol. 21 (2007); pp. 2683-2710

[15] R.M. Young, A. Jamshidi, G. Davis and J.H. Sherman. 'Current trends in the surgical management and treatment of adult glioblastoma'.
*Annals of Translational Medicine*, 3(9):1–15, 2015.

[16] G.S. Stoyanov, D.L. Dzhenkov. 'On the Concepts and History of Glioblastoma Multiforme - Morphology, Genetics and Epigenetics'.
*Folia Med (Plovdiv)*, 2018 Mar 1;60(1):48-66.

[17] R.K. Hobbie and B.J. Roth. 'Intermediate Physics for Medicine and Biology.'
*Springer*, 4th edition, 2007.

[18] S. Mori. 'Introduction to Diffusion Tensor Imaging'.
*Elsevier*, 2007.

[19] E.O. Stejskal and J.E. Tanner. 'Spin Diffusion Measurements: Spin Echoes in the Presence of a Time-Dependent Field Gradient'.
*The Journal of Chemical Physics*, 42:288–292, 1965.

[20] S. S. Dutta. 'Rappresentazione del tensore di diffusione (DTI) spiegata'.
*News-Medical*. 24 September 2021.

[21] M.E. Gurtin, E. Fried, and L. Anand. 'The Mechanics and Thermodynamics of Continua.'
*Cambridge University Press*, 2010.

[22] S. Forte, L. Preziosi and M.Vianello 'Meccanica dei continui'
*Springer*, 2019

[23] K. R. Rajagopal and L. Tao. 'Mechanics of mixtures'
*World Scientific Publishing Co Pte Ltd*, 1995

[24] D. Ambrosi and L. Preziosi. 'On the Closure of Mass Balance Models for Tumor Growth.'
*Mathematical Models and Methods in Applied Sciences*, 12(5):737–754, 2002.

[25] D. Ambrosi and F. Mollica. 'On the mechanics of a growing tumor.'
*International Journal of Engineering Science*, 40:1297–1316, 2002.

[26] R. de Rooij and E. Kuhl. 'Constitutive Modeling of Brain Tissue: Current Perspectives.'
*Applied Mechanics Reviews*, 68:1–16, 2016.

[27] C. Giverso, M. Scianna, and A. Grillo. 'Growing avascular tumours as elasto-plastic bodies by the theory of evolving natural configurations'.
*Mechanics Research Communications*, 68:31–39, 2015.

[28] D. Ambrosi and F. Mollica. 'The role of stress in the growth of a multicell spheroid.'
*Journal of Mathematical Biology*, 48:477–499, 2004.

[29] P. Mascheroni, M. Carfagna, A. Grillo, D.P. Boso, and B.A. Schrefler. 'An avascular tumor growth model based on porous media mechanics and evolving natural states.'
*Mathematics and Mechanics of Solids*, 23:686–712, 2018.

[30] V.A. Lubarda. 'Constitutive theories based on the multiplicative decomposition of deformation gradient: Thermoelasticity, elastoplasticity, and biomechanics.'
*Applied Mechanics Reviews*, 57:95–108, 2004.

[31] A. Goriely, M.G.D. Geers, G.A. Holzapfel, J. Jayamohan, A. Jérusalem, S. Sivaloganathan, W. Squier, J.A.W. van Dommelen, S. Waters and E. Kuhl 'Mechanics of the brain: perspectives, challenges, and opportunities.'
*Biomechanics and Modeling in Mechanobiology*, 14:931–965, 2015.

[32] S. Budday, G. Sommer, C. Birkl, C. Langkammer, J. Haybaeck, J. Kohnert, M. Bauer, F. Paulsen, P. Steinmann, E. Kuhl and G.A. Holzapfel . 'Mechanical characterization of human brain tissue.'
*Acta Biomaterialia*, 48:319–340, 2017.

[33] B.R. Donnelly and J. Medige. 'Shear properties of human brain tissue.'
*J Biomech Eng* 119(4) (1997) 423–32

[34] S. K. Kyriacou, A. Mohamed, K. Miller and S. Neff. 'Brain mechanics for neurosurgery: modeling issues.'
*Biomechan Model Mechanobiol 1*, 151–164, Springer-Verlag 2002

[35] B. Rashid, M. Destrade, and M.D. Gilchrist. 'Mechanical characterization of brain tissue in compression at dynamic strain rates.'
*Journal of the Mechanical Behavior of Biomedical Materials*, 10:23–38, 2012.

[36] B. Rashid, M. Destrade, and M.D. Gilchrist. 'Mechanical characterization of brain tissue in simple shear at dynamic strain rates.'
*Journal of the Mechanical Behavior of Biomedical* Materials, 28:71–85, 2013.

[37] B. Rashid, M. Destrade, and M.D. Gilchrist. 'Mechanical characterization of brain tissue in tension at dynamic strain rates.'
*Journal of the Mechanical Behavior of Biomedical Materials*, 33:43–54, 2014.

[38] K. Miller and K. Chinzei. 'Constitutive modelling of brain tissue; experiment and theory.'
*Journal of Biomechanics*, 30:1112–1115, 1997.

[39] K. Miller. 'Constitutive model of brain tissue suitable for finite element analysis of surgical procedures.'
*Journal of Biomechanics*, 32:531–537, 1999.

[40] K. Miller, K. Chinzei, G. Orssengo, and P. Bednarz. 'Mechanical properties of brain tissue in-vivo: experiment and computer simulation.'
*Journal of Biomechanics*, 33:1369–1376, 2000.

[41] R.W. Ogden. 'Large deformation isotropic elasticity - on the correlation of theory and experiment for incompressible rubberlike solids.'
*Proceedings of the Royal Society of London* A, 326:565–584, 1972.

[42] L.A. Mihai, L.A. Mihai, S. Budday, G.A. Holzapfel, E. Kuhl and A. Goriely, 'A family of hyperelastic models for human brain tissue.'
*Journal of the Mechanics and Physics of Solids*, 106:60–79, 2017.

[43] A. Elazab, A. M. Anter, H. Bai, Q. Hu, Z. Hussain, D. Ni, T. Wang and B. Lei. 'An optimized generic cerebral tumor growth modeling framework by coupling biomechanical and diffusive models with treatment effects.'
*Applied Soft Computing*, 80 (2019) 617-627

[44] H. Hatzikirou, A. Deutsch, C. Schaller, M. Simon, and K. Swanson. 'Mathematical Modelling of Glioblastoma Tumour Development: a review.'
*Mathematical Models and Methods in Applied Sciences*, 15(11):1779–1794, 2005.

[45] J.C.L. Alfonso, K. Talkenberger, M. Seifert, B. Klink, A. Hawkins-Daarud, K.R. Swanson, H. Hatzikirou, and A. Deutsch. 'The biology and mathematical modelling of glioma invasion: a review.'
*Journal of the Royal Society Interface*, 14:1–20, 2017.

[46] L. M. Sander and T. S. Deisboeck. 'Growth patterns of microscopic brain tumours'.
*Phys. Rev.* E66 (2002) 051901.

[47] A. R. Kansal, S. Torquato, G. R. Harsh IV, E. A. Chiocca and T. S. Deisboeck. 'Simulated brain tumor growth dynamics using a three-dimensional cellular automaton'.
*J. Theor. Biol.* 203 (2000) 367–382.

[48] Y. Mansury and T. S. Deisboeck. 'Modelling tumours as complex biosystems: An agent-based approach, in Complex Systems Science: The Emergence of a New Approach in BioMedicine'.
*Kluwer* (2004).

[49] M. Wurzel, C. Schaller, M. Simon and A. Deutsch. 'Cancer cell invasion of normal brain tissue: Guided by Prepattern'.
*J. Theor. Med.* (2005)

[50] M. Aubert, M. Badoual, S. Fereol, C. Christov and B. Grammaticos. 'A cellular automaton model for the migration of glioma cells.'
*Phys. Biol.* 3,93 – 100

[51] M. Aubert, M. Badoual, C. Christov and B. Grammaticos. 'A model for glioma cell migration on collagen and astrocytes.'
*J. R. Soc. Interface* 5, 75 – 83.

[52] A. Szabò, K. Varga, T. Garay, B. Hegedus and A. Cziròk. 'Invasion from a cell aggregate –the roles of active cell motion and mechanical equilibrium.'
*Phys. Biol.* 9, 016010.

[53] K.R. Swanson, E.C. Alvord Jr., and J.D. Murray. 'A quantitative model for differential motility of gliomas in grey and white matter.'
*Cell Proliferation*, 33:317–329, 2000.

[54] K.R. Swanson, C. Bridge, J.D. Murray, and E.C. Alvord Jr. 'Virtual and real brain tumors: using mathematical modeling to quantify glioma growth and invasion.'
*Journal of the Neurological Sciences*, 216:1–10, 2003.

[55] K.R. Swanson, E.C. Alvord Jr., and J.D. Murray. 'Virtual brain tumours (gliomas) enhance the reality of medical imaging and highlight inadequacies of current therapy'.
*British Journal of Cancer*, 86:14–18, 2002.

[56] J.D.Murray. 'Mathematical Biology I: An Introduction.'
*Interdisciplinary Applied Mathematics*, vol. 17, Springer, New York, NY, USA, 2002.

[57] S. Jbabdi, E. Mandonnet, H. Duffau, L. Capelle, K.R. Swanson, M. Pélégrini-Issac, R. Guillevin, and H. Benali. 'Simulation of anisotropic growth of low-grade gliomas using diffusion tensor imaging'.
*Magnetic Resonance in Medicine*, 54:616–624, 2005.

[58] S. Banerjee, S. Khajanchi and S. Chaudhuri. 'A mathematical model to elucidate brain tumor abrogation by immunotherapy with T11 Target Structure'.
*PLoS ONE* 10(5): e0123611. doi:10.1371/journal.pone.0123611

[59] D. Ambrosi and L. Preziosi. 'On the Closure of Mass Balance Models for Tumor Growth.'
*Mathematical Models and Methods in Applied Sciences*, 12(5):737–754, 2002.

[60] H. Byrne and L. Preziosi. 'Modelling solid tumour growth using the theory of mixtures.'
*Mathematical Medicine and Biology*, 20:341–366, 2003.

[61] S. Angeli and T. Stylianopoulos. 'Biphasic modeling of brain tumor biomechanics and response to radiation treatment.'
*Journal of Biomechanics*, 49:1524–1531, 2016.

[62] S. Angeli, K.E. Emblem, P. Due-Tonnessen, and T. Stylianopoulos. 'Towards patientspecific modeling of brain tumor growth and formation of secondary nodes guided by dti-mri.'
*NeuroImage: Clinical*, 20:664–673, 2018.

[63] G. Lucci 'The role of brain hyperelasticity in growth and proliferation of Glioblastoma Multiforme'
*Tesi di laurea magistrale, Politecnico di Torino*

[64] J.W. Cahn and J.E. Hilliard. 'Free energy of a nonuniform system. I. interfacial free energy.'
*The Journal of Chemical Physics*, 28:258–267, 1958.

[65] Y. Chen and J.S. Lowengrub. 'Tumor growth in complex, evolving microenvironmental geometries: a diffuse domain approach.' *Journal of Theoretical Biology*, 361:14–30, 2014.

[66] M.C. Colombo, C. Giverso, E. Faggiano, C. Boffano, F. Acerbi, and P. Ciarletta. 'Towards the personalized treatment of Glioblastoma: Integrating

patient-specific clinical data in a continuous mechanical model.'
*PLoS ONE*, 10:e0132887, 2015.

[67] A. Agosti, C. Cattaneo, C. Giverso, D. Ambrosi, and P. Ciarletta. 'A computational framework for the personalized clinical treatment of glioblastoma multiforme.'
*ZAMM*, pages 1–21, 2018.

[68] A. Agosti, C. Giverso, E. Faggiano, A. Stamm, and P. Ciarletta. 'A personalized mathematical tool for neuro-oncology: a clinical case study.'
*International Journal of Non-Linear Mechanics*, 107:170–181, 2018.

[69] M.H. Holmes, V.C. Mow, 'The nonlinear characteristics of soft gels and hydrated connective tissues in ultrafiltration',
*J. Biomech.* 23 (11) (1990) 1145–1156.

[70] S. Di Stefano, M. Carfagna, M.M M. Knodel, K. Hashlamoun, S. Federico, A. Grillo, 'Anelastic reorganisation of fibre-reinforced biological tissues'
*Computing and Visualization in Science* (2019) 20:95–109

[71] C. Giverso, L. Preziosi, 'Influence of the mechanical properties of the necrotic core on the growth and remodelling of tumour spheroids'
*International Journal of Non-Linear Mechanics*, Volume 108, January 2019, Pages 20-32

[72] V. Balbi, A. Trotta, M. Destrade, A. Annaidh, 'Poynting effect of brain matter in torsion'.
*Soft Matter*, 10.1039/C9SM00131J

[73] P. Gerlee and A.R.A. Anderson. 'An evolutionary hybrid cellular automaton model of solid tumour growth.'
*Journal of Theoretical Biology*, 246:583–603, 2007.

[74] H.B. Frieboes, J.S. Lowengrub, S. Wise, X. Zheng, P. Macklin, E.L. Bearer, and V. Cristini. 'Computer simulations of glioma growth and morphology.'
*NeuroImage*, 37:S59–S70, 2007.

[75] M.L. Tanaka, W. Debinski, and I.K. Puri. 'Hybrid mathematical model of glioma progression.'
*Cell Proliferation*, 42:637–646, 2009

[76] C. Chatelain, T. Balois, P. Ciarletta, and M. Ben Amar. 'Emergence of microstructural patterns in skin cancer: a phase separation analysis in a binary mixture.'
*New Journal of Physics*, 13:115013, 2011.

[77] M. Bruehlmeier, U. Roelcke, P. Blauenstein, J. Missimer, P.A. Schubiger, J.T. Locher, R. Pellikka, and S.M. Ametamey. 'Measurement of the extracellular space in brain tumors using 76br-bromide and pet.'
*Journal of Nuclear Medicine*, 44:1210–1218, 2003.

[78] A. Agosti, P. Ciarletta, H. Garcke, M. Hinze. 'Learning patient-specific parameters for a diffuse interface glioblastoma model from neuroimaging data'.
*Mathematical Methods in the Applied Sciences*, 43 (15), 8945-8979.(2020)

[79] H. Si. Hang, 'TetGen, a Delaunay-Based Quality Tetrahedral Mesh Generator'.
*Association for Computing Machinery*, 41 (2) 0098-3500, January 2015